Journal of Oncology

Innovations in Imaging for the Diagnosis and Treatment of Liver Lesions

Lead Guest Editor: Roberto Iezzi
Guest Editors: Tiago Bilhim, Abdul-Naser Elzouki, Jaak Janssens, and György Kovacs

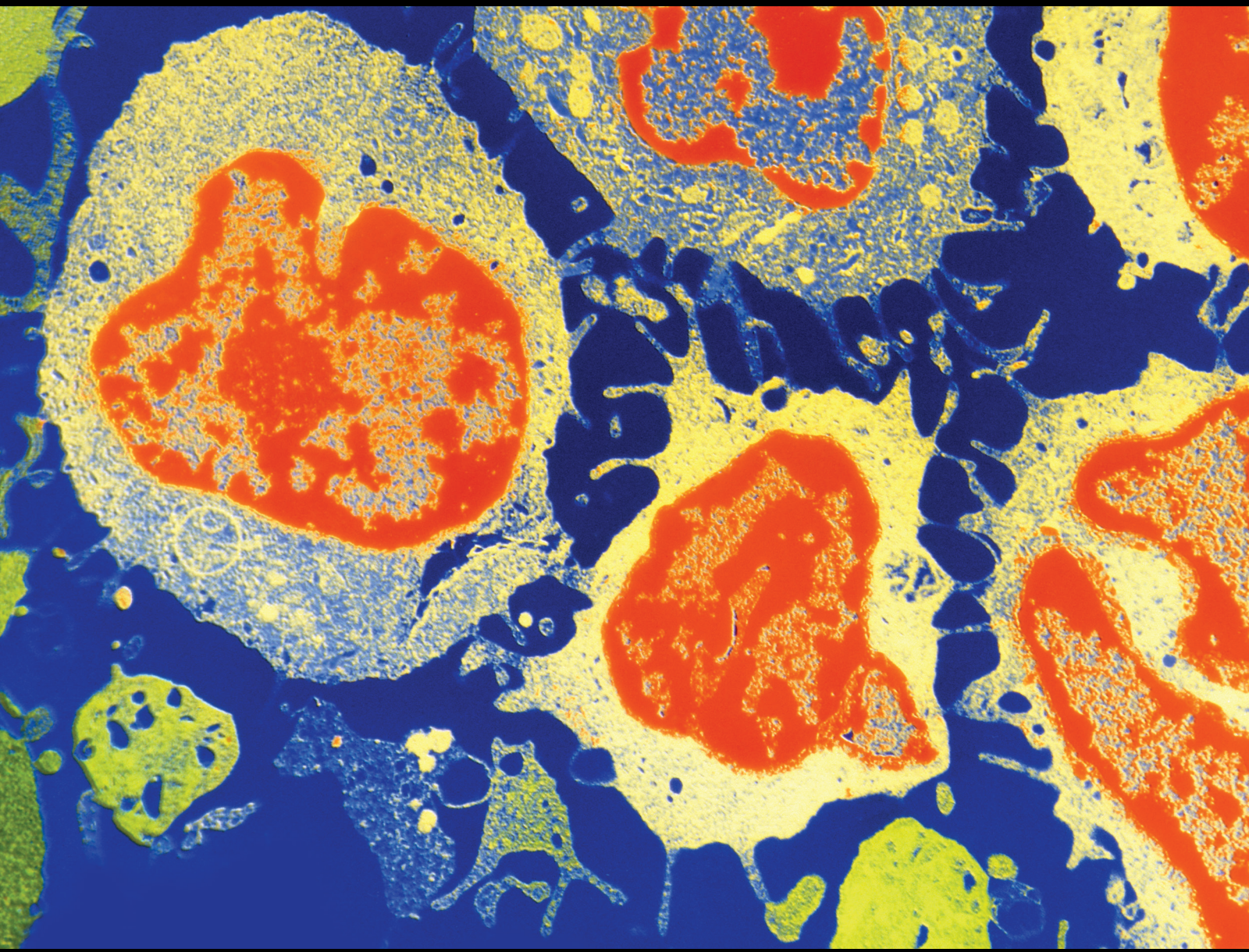

Innovations in Imaging for the Diagnosis and Treatment of Liver Lesions

Journal of Oncology

Innovations in Imaging for the Diagnosis and Treatment of Liver Lesions

Lead Guest Editor: Roberto Iezzi
Guest Editors: Tiago Bilhim, Abdul-Naser Elzouki, Jaak Janssens, and György Kovacs

Contents

Hindawi
Journal of Oncology
Volume 2019, Article ID 6153041, 5 pages
https://doi.org/10.1155/2019/6153041

Review Article

Artificial Intelligence in Interventional Radiology: A Literature Review and Future Perspectives

Roberto Iezzi,[1,2] **S. N. Goldberg**,[3] **B. Merlino**,[1,2] **A. Posa**,[4] **V. Valentini**,[5,6] **and R. Manfredi**[1,2]

[1]*Fondazione Policlinico Universitario A. Gemelli IRCCS, UOC di Radiologia, Dipartimento di Diagnostica per Immagini, Radioterapia Oncologica ed Ematologia, Roma, Italy*
[2]*Università Cattolica del Sacro Cuore, Istituto di Radiologia, Roma, Italy*
[3]*Department of Radiology, Hadassah Hebrew University Medical Center, Jerusalem, Israel*
[4]*Department of Radiology, AFaR-IRCCS Fatebenefratelli Hospital Foundation for Health Research and Education, via di Ponte Quattro Capi 39, 00186 Roma, Italy*
[5]*Fondazione Policlinico Universitario A. Gemelli IRCCS, UOC di Radioterapia Oncologica, Dipartimento di Diagnostica per Immagini, Radioterapia Oncologica ed Ematologia, Roma, Italy*
[6]*Università Cattolica del Sacro Cuore, Istituto di Radioterapia Oncologica, Roma, Italy*

Correspondence should be addressed to Roberto Iezzi; roberto.iezzi.md@gmail.com

Received 18 May 2019; Revised 22 September 2019; Accepted 1 October 2019; Published 3 November 2019

Academic Editor: Francesca De Felice

The term "artificial intelligence" (AI) includes computational algorithms that can perform tasks considered typical of human intelligence, with partial to complete autonomy, to produce new beneficial outputs from specific inputs. The development of AI is largely based on the introduction of artificial neural networks (ANN) that allowed the introduction of the concepts of "computational learning models," machine learning (ML) and deep learning (DL). AI applications appear promising for radiology scenarios potentially improving lesion detection, segmentation, and interpretation with a recent application also for interventional radiology (IR) practice, including the ability of AI to offer prognostic information to both patients and physicians about interventional oncology procedures. This article integrates evidence-reported literature and experience-based perceptions to assist not only residents and fellows who are training in interventional radiology but also practicing colleagues who are approaching to locoregional mini-invasive treatments.

1. Introduction

The term "artificial intelligence" (AI) includes computational algorithms that can perform tasks considered typical of human intelligence, with partial to complete autonomy, to produce new beneficial outputs from specific inputs [1]. Although premises to the development of AI were achieved in the early era of computers, it has only been with the introduction of new powerful computational hardware, in association with the capability of collecting and storing huge amounts of data, that it has become feasible to explore its potential in tasks most relevant to the field of radiology such as pattern recognition, pattern identification, planning, language comprehension, object and sound recognition, problem solving, prognosticating diseases, and deciding when and whether therapy is not needed or of limited use or in offering patients and physicians prognostic data on treatment outcomes. Indeed, although healthcare represents a challenging field for AI application, medical imaging is currently one of the most promising areas to apply this technology [2].

From the beginning, it has been quite clear that computers could be potentially useful in assisting the radiologist in the routine tasks of detection and diagnosis. The idea fostering the use of the so-called computer-aided detection/diagnosis (CAD) systems, precursors of modern AI, was to provide radiologists with the assistance in the detection and interpretations of potential lesions (especially in mammography and chest or musculoskeletal radiography) in order to discriminate between benign and malignant lesions, reduce false negatives, and boost radiologists' productivity,

especially in terms of discovery and identification of significant findings requiring a prompt human validation [3]. Main limitations of CAD systems were their task-specific orientation which is suited to only one particular given task in a corresponding specific imaging modality and, moreover, their reliability and the risk of false positive results implied mandatory validation by a trained radiologist [3]. Since then, ever-increasing attempts have been made to improve upon the diagnostic performance of AI and facilitate the help it could provide in daily clinical practice.

The development of AI is largely based on the introduction of artificial neural networks (ANN) in the early 1950s [4] and their subsequent further evolution (from single to multilayer ANN), introducing the concepts of "computational learning models," machine learning (ML) and deep learning (DL).

ML is based upon the so-called "reverse training" method, in which computer systems focus on specific pathological features identified during a training period [5]. Thus, ML applications require a set of data on a specific pathology on which the computer can train itself, and those data must necessarily contain the desired outcome that needs to be predicted (e.g., nodules or emphysema on chest X-rays, focal liver lesions, hemorrhage in head CT, and so on). Big data is the type of data that may be supplied into the analytical system so that an ML model could learn, improving the accuracy of its predictions. Once trained, the computer can apply this information even to new cases never seen before [6, 7]. ML can be supervised or unsupervised, depending, respectively, on the "labeled" input previously selected by human experts, or directly extracted by the machine using several computational methods [6, 8]. Among the evaluated features, the ideal ML model should include those most relevant to the outcome and the most generic ones which can be applied to the general population, even though it may not be possible to identify these features beforehand. Typical ML tasks in radiology are the *identification* of specific patterns/conditions or *image segmentation*, which can be defined as the representation through partitioning of the digital image into meaningful parts (i.e., pixels or segments) for interpretation. Both have been successfully applied over a wide range of clinical settings including for the detection of fatty liver using ultrasound [9], CT carotid plaque characterization [10], and prediction of lesion-specific ischaemia from quantitative coronary CT angiography [11].

A significant step forward is represented by deep learning (DL), which is based on the implementation of a large number of ANN layers, allowing determination of more complex relationships (similar to neuronal networks) and a more sophisticated performance, attributes particularly suited for imaging. More important, DL is able to perform higher level classification tasks and to automatically extract and learn features, which is valuable when managing the information content of digital images that are only partially detectable and usable by a human reader. This concept unveils the extraordinary potential of DL in comparison with conventional imaging management.

The presence of numerous neural layers between input and output and the use of several techniques (most commonly called convolutional neural networks—CNN) contribute to the plasticity of DL and offer the potential to mimic human brain mechanisms in the training process. Crucial to success of the method is the exposure of CNN to data, in particular images, which can be processed during "training" (supervised or unsupervised). If data are unlabeled, the learning process is based on the automatic clustering of image findings according to their natural variability. Hybrid learning models that include some human guidance are most often used, due to the difficulty of successfully achieving truly unsupervised training. DL represents a hot topic in research, literally exploding in the last years.

Matching ML/DL image processing with clinical and when available pathological/histological data, to correlate intrinsic diagnostic patterns and features of a CT or MRI scan to a specific pathology and histological subtype, has opened a new window in research establishing so-called radiomics [12–14]. In this setting, CAD can also be taken to a higher performance level. ML-based CAD can be taught on the intrinsic differences of a population and then detect and/or diagnose the variations of a single lesion, allowing the identification of common as well as uncommon cases [15].

Supervised and unsupervised learning are largely based on statistical algorithms [16], with important differences between them. Supervised learning deals primarily with classification (i.e., identification of categories for new observations using the same collected on labelled training data sets) and regression (i.e., predictions on continued variables for new observations inferred on training sets). Unsupervised learning cannot take advantage on the labelling process and manages unclassified data; therefore, recognition of latent patterns is performed by applying clustering (aimed to define groups within data) and dimensionality reduction [16]. The sense of such a classification needs a subsequent validation to assess its utility.

Whichever the ML technique used, each approach presents advantages and disadvantages. General pros have to be considered for ML ability to process large volumes of data, to identify trends and patterns only partly detectable by humans, to face with complexity (multidimensionality of data), and to perform high computational tasks.

These advantages are not without cons. First, huge data sets are necessary to train ML machines, whose collection has been limited for a long time in healthcare (although the development of large databases in the era of the so-called "big data" is going to be more widespread). But even when available, the "quality" of data is a major challenge both for the supervised training (due to the large amount of effort needed for labelling data) and the unsupervised training (process of selection and validation).

Moreover, ML assessment represents a critical aspect in terms of statistical power definition (sensitivity, specificity, error susceptibility, and so on) of ML within the task (especially in clinical settings), often in the absence of "disclosure" about "how and why" machines elaborate their tasks, which raises problems when ML applications are introduced in routine medical activity [1, 2, 6, 8, 16].

The aim of this article is to integrate evidence-reported literature and experience-based perceptions, while attempting to make the information easy to access, assisting not only residents and fellows who are training in interventional radiology, but also practicing colleagues who are attempting to gain further expertise with these locoregional mini-invasive treatments.

2. AI and Interventional Radiology

2.1. Treatment Response. AI applications appear promising for radiology scenarios, as they naturally affect and potentially improve upon lesion detection, segmentation, and interpretation of imaging—prerequisites for good interventional radiology (IR) practice [17]. Moreover, advantages are foreseen even in areas previously not addressed.

One of the biggest challenges of interventional radiology is to estimate/forecast the outcomes and/or the benefits of a treatment before actually performing it [18]. The identification of an accurate method to predict the success rate of a specific treatment in a specific patient could reduce unnecessary and useless procedures and interventions, reducing healthcare costs and dramatically decreasing the risk for the patient. It should also be useful to investigate how a patient's demographic and pathologic characteristics before the treatment can influence treatment efficacy, which can then be measured with posttreatment evaluations.

This type of challenge can be readily taken up using AI and DL, using a computer which autoimproves itself by learning from given inputted data. A patient's baseline diagnostic images, clinical data, and characteristics and outcomes of the planned intervention can be retrospectively applied to a cohort of patients to teach the computer to construct and work on a model that can correlate and "learn" the relationship between those model variables and procedural results. The resultant refined model would then allow the prediction of the procedural outcome in future new patients even before performing the procedure, assuming the characteristics of the intervention are specified. Classification of patients as a responder (complete or partial) or nonresponder could potentially be used in daily clinical practice as an indicator to decide whether or not a specific intervention should be performed [19]. DL-based prediction models can assist interventional radiologists in making decisions as to what procedure will offer the best outcome for each patient. Obviously, these prediction models would require a continuous evaluation and validation to limit or even eliminate possible errors and improve performance in both terms of diagnostic and therapeutic efficiencies.

The field of interventional oncology could greatly benefit from AI, given the great variety of data on which the prediction for daily clinical practice can be made, even though there is the need for more data to help implement ML in the best way [18]. A robust and trustworthy perspective on procedural outcomes could give interventional radiologist more and more solid data upon which to recommend a particular and specific treatment to each patient. In particular, Abajan et al. evaluated the capacity of artificial intelligence to predict chemoembolization outcomes in patients with hepatocellular carcinoma, based on baseline magnetic resonance imaging, dividing patients into responders and nonresponders. They obtained a very good negative predictive value (88.5%) based upon the ML models that relied upon the two features of tumour signal intensity and the presence or absence of cirrhosis [19]. In another anatomic site, the brain, Asadi et al. performed studies on prediction of procedural outcome in stroke and brain arteriovenous malformations patients and successfully individualized treatment based on predicting features [20, 21]. Nonetheless, even if AI can provide information on disease and treatment correlation, it does not necessarily provide an insight on causality and pathophysiology; this information can be, however, obtained from randomized controlled trials, making these two approaches complementary to each other, to design the best treatment strategy.

2.2. Procedural Guidance and Support. Owing to the evolution of ML/DL, we are currently surrounded by technology to such an extent that it can assist us, among other tasks, to overcome distances and grant access to extensive knowledge. Touch and touchless devices are everywhere, simplifying our life in many ways, from phone and home assistants to intelligent lights or thermostats, to smart-locks and navigators, and with the introduction of sharing platforms and networks, streaming channels, and live-chat channels as well, our world can be seen as a great, unique web of people.

In an operating room setting, and more specifically in the interventional radiology suite, one of the most important things in procedural planning is the assessment of the patient's anatomy and its pathophysiologic changes. There is also much other valuable information archived in online databases or literature, ranging from (1) individual patient characteristics such as those on tumour characteristics and behaviour which are useful in the specific field of oncological interventions; (2) evidence to support or overcome a particular and unforeseen problem or finding; and (3) local hospital information on angio suite supplies, on the availability of specific devices such as a microcatheter, guidewire, or metallic coils. Currently, however, in large part but not exclusively due to sterility issues, procedural information must be collected beforehand, in the preprocedural planning, whereas, during the procedure, the interaction between the operator and the great amount of patient, literature, and supply data can only be achieved through sterile covers, or indirectly made by other team members, which implies a certain amount of distraction, errors, and time consumption. Nevertheless, these obstacles could be overcome with the implementation, in medical clinical practice, and particularly in operatory theaters and angio suites, of touchless interaction devices, ranging from eye-tracking systems to inertial sensors, to cameras or webcams, to voice-driven smart assistants [22].

Gesture-capture camera systems, with or without utilization of inertial sensors, have been experimented with defining and associating specific actions to a variety of gestures to control medical image viewers while in surgical scrub [23–25]. Indeed, voice recognition interfaces have

been demonstrated to enable significant time sparing when dealing with switching on and off operating room components [26]. Navigation systems constructed using inertial sensors worn under sterile gloves have been tried for needle insertion path planning, with a claimed gesture-recognition rate of 100% for 3/4 gestures [27]. Augmented reality devices, such as glasses, which interactively display to the operator the whole variety of relevant information or diagnostic images have also been tested [28, 29].

A group of researchers from the University of California, San Francisco, tested the possibility to question a smart assistant—previously instructed with a large database of information on sheath sizes and compatibility—to obtain suggestions as to which sheath is likely to be most appropriate for the deployment of a particular endovascular stent, during a specific interventional procedure, without removing the sterile surgical scrub, with good results both in terms of time sparing and accuracy [30].

As in the above-mentioned case, questions regarding the correct size of a device or on the time-consuming task of assess for the availability of a particular device or instrument according to the hospital stocks could be directly and instantaneously answered by the smart computer. Questions to the smart assistant could also imply a cost analysis, allowing the operator to choose between two devices not only assessing their dimensions but also their expensiveness in relation to outcome data, providing to all angio-suite staff the perception of the real global cost of a procedure, which must not be taken lightly, minimizing the waste and the inappropriate utilization of guidewires, catheters, coils, and other devices [18].

3. Future Perspectives

Most researchers agree that the future of AI lies in enhancing and assisting interventional radiology, not taking over from interventionalists.

Augmented reality, in which additional information about the patient can be provided to the operator in real time during the operation, is another technology already being put into practice. When this is combined with machine learning, the algorithm could help the radiologist to make more rapid proper and accurate decisions in terms of diagnosis, treatment management, and planning. Earlier diagnosis through quicker, more accurate reading of scans might enable cancer to be detected earlier, enabling treatment at an earlier stage, with less need for invasive standard surgical approaches. Collaboration between computer algorithms—with their ability to synthesize and spot patterns in vast data sets—and skilled operators—who are able to make sense of the "messiness" of the human body by arriving at correct conclusions despite the multiplicity and complexity of the situation—could raise the standard of IR across the board. Yet, there are significant challenges to overcome before these technologies can be considered mainstream. Regardless, currently, there is intense enthusiasm on the part of clinicians who are calling for increased collaboration between computer scientists, biomedical engineers, and interventional radiologists as machine learning is posited to play a more prominent role in interventional radiology procedures, from informing the initial diagnosis to patient selection and intraprocedural guidance.

4. Conclusions

The emerging role of AI may offer the opportunity to better tailor treatment to patients according to "big data" that can be rapidly analyzed, uncovering new insights that may otherwise have required decades of prospective trials. Thus, this new approach could most likely result in a paradigm shift in the near future, definitively changing the current conventional treatment algorithms of tumour therapy, providing superior really personalized care to patients.

Conflicts of Interest

The authors declare that they have no conflicts of interest.

References

[1] S. Russell and P. Norvig, *Artificial Intelligence: A Modern Approach*, Prentice-Hall, Upper Saddle River, NJ, USA, 2nd edition, 2003.

[2] Z. Obermeyer and E. J. Emanuel, "Predicting the future—big data, machine learning and clinical medicine," *New England Journal of Medicine*, vol. 375, no. 13, pp. 1216–1219, 2016.

[3] R. A. Castellino, "Computer aided detection (CAD): an overview," *Cancer Imaging*, vol. 5, no. 1, pp. 17–19, 2005.

[4] F. Rosenblatt, "The perceptron: a probabilistic model for information storage and organization in the brain," *Psychological Review*, vol. 65, no. 6, pp. 386–408, 1958.

[5] C. Mohan, "Artificial intelligence in radiology—are we treating the image or the patient?," *Indian Journal of Radiology and Imaging*, vol. 28, no. 2, pp. 137–139, 2018.

[6] C. M. Bishop, *Pattern Recognition and Machine Learning*, Springer, New York, NY, USA, 2006.

[7] E. Alpaydin, *Introduction to Machine Learning*, MIT Press, Cambridge, MA, USA, 3rd edition, 2014.

[8] D. Shen, G. Wu, and H. I. Suk, "Deep learning in medical image analysis," *Annual Review of Biomedical Engineering*, vol. 19, pp. 221–248, 2017.

[9] L. Saba, N. Dey, A. S Ashour et al., "Automated stratification of liver disease in ultrasound: an online accurate feature classification paradigm," *Computer Methods and Programs in Biomedicine*, vol. 130, pp. 118–134, 2016.

[10] L. Saba, R. Sanfilippo, N. Tallapally et al., "Evaluation of carotid wall thickness by using computed tomography and semiautomated ultrasonographic software," *Journal for Vascular Ultrasound*, vol. 35, no. 3, pp. 136–142, 2011.

[11] D. Dey, S. Gaur, K. A. Ovrehus et al., "Integrated prediction of lesion-specific ischaemia from quantitative coronary CT angiography using machine learning: a multicentre study," *European Radiology*, vol. 28, no. 6, pp. 2655–2664, 2018.

[12] H. J. W. L. Aerts, "The potential of radiomic-based phenotyping in precision medicine: a review," *JAMA Oncology*, vol. 2, no. 12, pp. 1636–1642, 2016.

[13] V. Kumar, Y. Gu, S Basu et al., "Radiomics: the process and the challenges," *Magnetic Resonance Imaging*, vol. 30, no. 9, pp. 1234–1248, 2012.

[14] P. Lambin, E. Rios-Velazquez, R. Leijenaar et al., "Radiomics: extracting more information from medical images using

advanced feature analysis," *European Journal of Cancer*, vol. 48, no. 4, pp. 441–446, 2012.

[15] T. Kooi, G. Litjens, B. van Ginneken et al., "Large scale deep learning for computer aided detection of mammographic lesions," *Medical Image Analysis*, vol. 35, pp. 303–312, 2017.

[16] G. S. Handelman, H. K. Kok, R. V. Chandra, A. H. Razavi, M. J. Lee, and H. Asadi, "eDoctor: machine learning and the future of medicine," *Journal of Internal Medicine*, vol. 284, no. 6, pp. 603–619, 2018.

[17] K. Yasaka, H. Akai, O. Abe, and S. Kiryu, "Deep learning with convolutional neural network for differentiation of liver masses at dynamic contrast-enhanced CT: a preliminary study," *Radiology*, vol. 286, no. 3, pp. 887–896, 2018.

[18] B. Letzen, C. J. Wang, and J. Chapiro, "The role of artificial intelligence in interventional oncology: a primer," *Journal of Vascular and Interventional Radiology*, vol. 30, no. 1, pp. 38–41.e1, 2019.

[19] A. Abajian, N. Murali, L. J. Savic et al., "Predicting treatment response to intra-arterial therapies for hepatocellular carcinoma with the use of supervised machine learning—an artificial intelligence concept," *Journal of Vascular and Interventional Radiology*, vol. 29, no. 6, pp. 850–857.e1, 2018.

[20] H. Asadi, R. Dowling, B. Yan, and P. Mitchell, "Machine learning for outcome prediction of acute ischemic stroke post intra-arterial therapy," *PloS One*, vol. 9, no. 2, Article ID e88225, 2014.

[21] H. Asadi, H. K. Kok, S. Looby, P. Brennan, A. O'Hare, and J. Thornton, "Outcomes and complications following endovascular treatment of brain arteriovenous malformations: a prognostication attempt using artificial intelligence," *World Neurosurgery*, vol. 96, pp. 562–569.e1, 2016.

[22] A. Mewes, B. Hensen, F. Wacker, and C. Hansen, "Touchless interaction with software in interventional radiology and surgery: a systematic literature review," *International Journal of Computer Assisted Radiology and Surgery*, vol. 12, no. 2, pp. 291–305, 2017.

[23] J. P. Wachs, H. I. Stern, Y. Edan et al., "A gesture-based tool for sterile browsing of radiology images," *Journal of the American Medical Informatics Association*, vol. 15, no. 3, pp. 321–323, 2008.

[24] L. C. Ebert, G. Hatch, G. Ampanozi, M. J. Thali, and S. Ross, "You can't touch this touch-free navigation through radiological images," *Surgical Innovation*, vol. 19, no. 3, pp. 301–307, 2012.

[25] J. H. Tan, C. Chao, M. Zawaideh, A. C. Roberts, and T. B. Kinney, "Informatics in radiology: developing a touchless user interface for intraoperative image control during interventional radiology procedures," *Radiographics*, vol. 33, no. 2, pp. E61–E70, 2013.

[26] G. E. H. El-Shallaly, B. Mohammed, M. S. Muhtaseb, A. H. Hamouda, and A. H. M. Nassar, "Voice recognition interfaces (VRI) optimize the utilization of theatre staff and time during laparoscopic cholecystectomy," *Minimally Invasive Therapy & Allied Technologies*, vol. 14, no. 6, pp. 369–371, 2005.

[27] S. K. Herniczek, A. Lasso, T. Ungi, and G. Fichtinger, "Feasibility of a touch-free user interface for ultrasound snapshot-guided nephrostomy," in *Proceedings of SPIE 9036, Medical Imaging 2014: Image-Guided Procedures, Robotic Interventions, and Modeling, 90362F*, San Diego, CA, USA, February 2014.

[28] M. Müller, M.-C. Rassweiler, J. Klein et al., "Mobile augmented reality for computer-assisted percutaneous nephrolithotomy," *International Journal of Computer Assisted Radiology and Surgery*, vol. 8, no. 4, pp. 663–675, 2013.

[29] M. Solbiati, K. M. Passera, A. Rotilio et al., "Augmented reality for interventional oncology: proof-of-concept study of a novel high-end guidance system platform," *European Radiology Experimental*, vol. 2, no. 1, p. 18, 2018.

[30] K. Seals, R. Al-Hakim, P. Mulligan et al., "The development of a machine learning smart speaker application for device sizing in interventional radiology," in *Proceedings of the SIR Annual Scientific Meeting*, Dallas, TX, USA, March 2019.

Hindawi
Journal of Oncology
Volume 2019, Article ID 4634309, 9 pages
https://doi.org/10.1155/2019/4634309

Research Article

Portal Vein Embolization with PVA and Coils before Major Hepatectomy: Single-Center Retrospective Analysis in Sixty-Four Patients

R. Camelo,[1] **J. H. Luz**,[2,3] **F. V. Gomes**,[2,3] **E. Coimbra**,[2,4] **N. V. Costa**,[2,3] **and T. Bilhim**[2,3]

[1]*Radiology Department, Hospital de São José, CHLC, 1150-199 Lisbon, Portugal*
[2]*Interventional Radiology Department, Centro Hepato-Bilio-Pancreático e de Transplantação, Hospital Curry Cabral, CHLC, 1069-166 Lisbon, Portugal*
[3]*Nova Medical School, Faculdade de Ciências Médicas, Universidade Nova de Lisboa, Lisbon, Portugal*
[4]*Head Interventional Radiology Department—Centro Hepato-Bilio-Pancreático e de Transplantação, Hospital Curry Cabral, CHLC, Lisbon, Portugal*

Correspondence should be addressed to R. Camelo; ritameiracamelo@gmail.com

Received 9 May 2019; Accepted 23 August 2019; Published 10 October 2019

Academic Editor: Riccardo Masetti

Objectives. Portal vein embolization (PVE) stimulates hypertrophy of the future liver remnant (FLR) and improves the safety of extended hepatectomy. This study evaluated the efficacy of PVE, performed with PVA and coils, in relation to its effect on FLR volume and ratio. Secondary endpoints were the assessment of PVE complications, accomplishment of liver surgery, and patient outcome after hepatectomy. *Materials and Methods*. All patients who underwent PVE before planned major hepatectomy between 2013 and 2017 were retrospectively analyzed, comprising a total of 64 patients. Baseline patient clinical characteristics, imaging records, liver volumetric changes, complications, and outcomes were analyzed. *Results*. There were 45 men and 19 women with a mean age of 64 years. Colorectal liver metastasis was the most frequent liver tumor. The majority of patients ($n = 53$) had a right PVE. FLR increased from a mean value of 484 ml ± 242 to 654 ml ± 287 ($p < 0.001$) after PVE. Two major complications were experienced after PVE: 1 case of left hepatic artery branch laceration and 1 case of hemoperitoneum and hemothorax. A total of 44 (69%) patients underwent liver surgery. Twenty-one patients were not taken to surgery due to disease progression ($n = 18$), liver insufficiency ($n = 1$), and insufficient FLR volume ($n = 1$), and one patient declined surgery ($n = 1$). *Conclusions*. PVE with PVA and coils was accomplished safely and promoted a high FLR hypertrophy yield, enabling most of our patients to be submitted to the potentially curative treatment of liver tumor resection.

1. Introduction

Liver resection of hepatic tumors is the firstline treatment option for curative intent in hepatic malignancies, and in order to accomplish free surgical margins, an extended hepatectomy is required up until 45% of liver tumors [1]. However, the main cause for not performing the planned hepatic resection is inadequate future liver remnant (FLR) volume before surgery. Consequently, FLR size must be optimized to prevent postoperative liver failure (PLF), the principal cause of postoperative death after major hepatectomy [2]. In order to extend the indications of main hepatic resection and to prevent PLF, preoperative portal vein embolization (PVE) has been performed through the last decades, allowing atrophy of the future resected liver segments and hypertrophy of the FLR [3, 4].

It is suggested an FLR to total functional liver volume (TFLV) ratio of at least 25% in patients without hepatic dysfunction, and minimum ratios of 35 to 40% in patients with compromised hepatic function (e.g., obstructive jaundice, chronic liver disease, or intensive chemotherapy) [5–10]; however, the minimum total hepatic volume required to avoid PLF has not been precisely determined. PVE has a high technical success rate approaching 100% in most

of the series [11], and only a small number of unsuccessful techniques have been reported [12, 13]. The resection rate after PVE must be about 80 to 85%, although this rate may decrease to 70% in cirrhotic patients. The main reasons for not performing the liver resection after PVE are local tumor progression and peritoneal or other metastases discovered at the follow-up computed tomography (CT), magnetic resonance imaging (MRI), or laparotomy. Insufficient hypertrophy after PVE is rare, occurring in less than 10% of the patients in secondary liver malignancies; however, it can occur in up to 20% cirrhotic patients [11, 14].

PVE is considered safe and effective, and many hepatobiliary units worldwide adopt it as their principal strategy for FLR increase before major hepatic resection. Other approaches for preoperative hepatic augmentation have been used such as arterial embolization, hepatic vein embolization, and portal vein ligation. Once compared with arterial embolization, PVE presents lower toxicity not only because side effects are minor but also because signs and symptoms of postembolization syndrome (e.g., nausea and vomiting, fever, and pain) are uncommon. Abnormal liver function after PVE is frequently subtle and temporary, and about 50% of patients have no considerable change [2].

Since one of the most important properties of an embolic material is its capacity to induce FLR hypertrophy when used for PVE, we wanted to access this specific outcome in our own series of patients at our high-volume liver surgery and transplant center.

2. Materials and Methods

2.1. Patient Population. The Institutional Review Board of our center approved this study protocol. Between 2013 and 2017, all patients treated with PVE before planned major hepatectomy were identified. Baseline patient clinical characteristics, imaging records, liver volumetric data, and postoperative course were collected retrospectively.

2.2. Inclusion and Exclusion Criteria. All patients who underwent PVE before planned major hepatectomy between 2013 and 2017 were retrospectively analyzed. Exclusion criteria were as follows: unavailable or inadequate imaging data (CT and/or MR) before and after PVE, previous segmentectomy and/or hepatectomy, and PVE with other embolic agents beside PVA plus coils. The analyzed cohort comprised 64 patients (Figure 1).

2.3. Study Endpoints. Our main endpoint was to assess the efficacy of PVE, performed with PVA and coils, in relation to its effect on FLR volume and ratio. Secondary endpoints were the assessment of PVE complications, attainment of hepatic surgery, patient outcome after liver resection, and survival.

2.4. PVE Technical Considerations. Patients were allocated to a hospital bed, with an anticipated 24 h hospitalization, before the PVE procedure. The PVE technique adopted in our institution has been described elsewhere [13, 15]. In brief, the portal vein was accessed through a transhepatic ultrasound-guided puncture. The ipsilateral portal vein approach (the liver puncture is accomplished in the tumor bearing liver lobe and not the FLR) was adopted when possible, always avoiding tumor transgression. A branch from the anterior sectorial right portal vein was preferentially punctured instead of a branch from the posterior sector. A micropuncture kit (MAK—Merit Medical, South Jordan UT, USA) was used to access the portal vein. Portal angiography (Philips angiography suite FD-20, Netherlands) was performed, using a reversed curve catheter Simmons II 4F (Cordis, USA), to assess the anatomical pattern of the portal vein, through an automated injector with a 25 ml volume of contrast at a 7 ml per second flow protocol. Using the same 4F catheter, catheterization and embolization of non-FLR portal branches with PVA particles (Merit Medical) was performed first to achieve flow stasis. PVA particles from 150 to 700 μm in size were injected in a stepwise fashion. Smaller particles (150 to 250 μm) were infused primarily until significant decrease in forward flow was detected. This form of distal embolization is thought to constraint development of collateral circulation that may potentially limit hypertrophy [13]. Metallic pushable 0.035-inch coils (Cook Medical, Bloomington, IN, USA) were then deployed proximally to inhibit venous inflow and subsequently decrease the possibility of recanalization. Likewise, with PVA particles, smaller size coils are deployed more distally in the portal vein branches, such as 6 mm in diameter, and up to 12 mm diameter coils are deployed more proximally. A postembolization direct portography is acquired to ensure proper embolization of the aimed portal branches and to check for any immediate complication such as coil migration. Gelfoam slurry embolization of the percutaneous transhepatic tract to the portal vein branch was performed to finish the procedure. During the PVE procedure, intravenous prophylactic antibiotics were permanently administered, and hospital discharge patients were posteriorly kept on oral analgesic administration, as required.

2.5. Volumetric Assessment of Future Liver Remnant: Primary Outcome. Since FLR volume correlates with the development of PLF, a systematic assessment of liver volumetry during preoperative planning is critical, especially in the setting of baseline liver dysfunction or anticipated extended hepatectomy [16]. Hepatic contrast-enhanced CT, with a 5.0 mm or less slice thickness, with a 16-detector row multislice CT scanner (Siemens) was performed prior to and 4–7 weeks after PVE. On single slices, the both total liver, tumor, and FLR (accordingly to previously surgical planning) were delineated with a handheld cursor using a freely downloadable open-source image analysis software package: OsiriX®—a validated software for liver volumetric evaluation [17]. When the total regions of interest were selected within one series, the volumetric calculations were obtained using OsiriX® by multiplying surface and slice thickness and

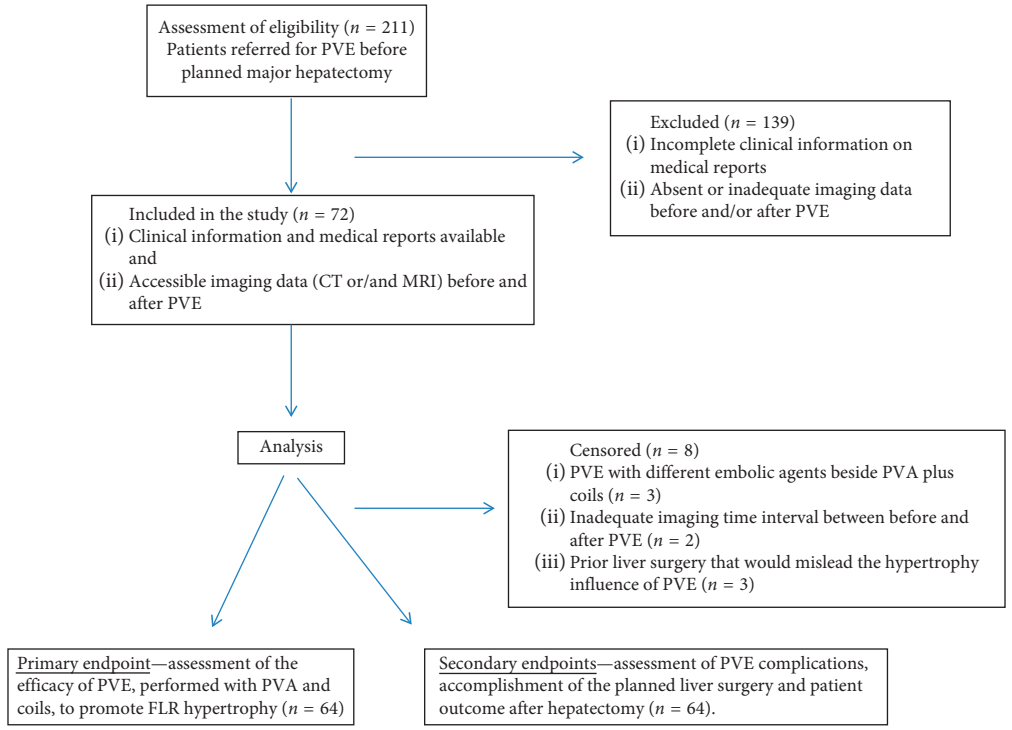

Figure 1: Patient flow chart.

then adding up individual slice volumes [17]. TFLV was defined as the total hepatic volume subtracted by the tumor volume. FLR was defined as the portion of the liver that would persist after liver resection. The ratio between the FLR and the TFLV was calculated and defined as the FLR/TFLV ratio. The increase in the FLR after PVE was also quantified and calculated by the formula (FLR after PVE−FLR before PVE) ÷ (FLR before PVE) as suggested in guidelines [14]. (Figures 2(a)–2(d))

2.6. Secondary Outcome Evaluations. For all 64 patients incorporated in our study, clinical, imaging, and laboratory data were scrutinized to the most updated available information up to July 2017. Liver function tests, including serum levels of total bilirubin (TB), aspartate aminotransferase (AST), and international normalized ratio (INR) were measured prior to PVE and surgery. Patients were analyzed for tumor type, administration of systemic chemotherapy before PVE, number of chemotherapy cycles, type of systemic chemotherapy administered, number of PVA vials and coils per patient in each PVE procedure, major and minor adverse events after PVE, submission to the planned liver surgery, reasons for not performing the previously deliberate surgery, surgical complications, period of hospitalization, and death after PVE and surgery. Adverse events were categorized as proposed in previous publications [18, 19] and considered major if they triggered (>48 h) or prolonged hospitalization and required unintentional increment in level of care or resulted in long-lasting adverse effects and death [20]. Minor complications were categorized as those which required minimal therapy or prolonged hospitalization for observation only [21]. Survival was calculated to compare patients submitted or not to the planned hepatic surgery after PVE.

2.7. Statistical Analysis. Mean, standard deviation, and range were estimated for numerical variables as descriptive statistics, while absolute numbers and percentages were calculated for categorical variables. Paired t-test or paired Wilcoxon rank-sum test, as appropriated, were used to compare TFLV and FLR volumes before and after PVE. To test associations between liver volumes before and after PVE (e.g., FLR/TFLV ratio before and after PVE), linear regression models were used. The association between variables (e.g., liver tumor histology and FLR increase) was tested using Fisher's exact test and chi-squared test. A p value below 0.05 was considered significant. All statistical analyses were performed using R software. The confidence intervals are based on a 95% confidence level. Survival rates were calculated from the date of PVE with Kaplan–Meier methods.

3. Results

The baseline clinical characteristics of the 64 patients are summarized in Table 1.

There were 45 (70%) men and 19 (30%) women with a mean age of 64 years ± 12 (range, 42–84 years). Of these 64 patients, 47 (73%) patients were diagnosed with colorectal liver metastases, 12 (19%) patients with cholangiocarcinoma, 4 (6%) patients with hepatocellular carcinoma, and one (2%) patient with hydatid cyst. Liver cirrhosis was diagnosed in two (3%) patients. Forty-one (64%) patients were submitted to systemic chemotherapy before PVE, and the most

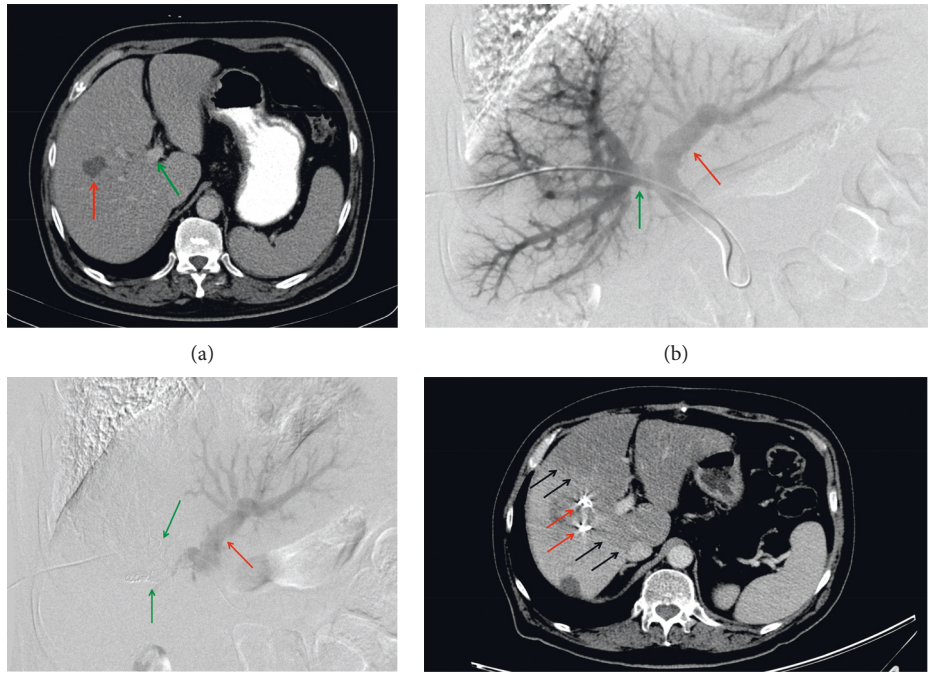

(a) (b) (c) (d)

Figure 2: (a) A 66-year-old male with colorectal cancer presenting with right liver lobe metastasis. Computed tomography shows a small left liver (the planned surgery was a right hepatectomy), insufficient for the future right hepatectomy resection. Red arrow: liver metastasis. Green arrow: left portal vein. (b) Portography acquired immediately before portal vein embolization shows a normal portal vein anatomy. Green arrow: right portal vein; red arrow: left portal vein. (c) Portography immediately after portal vein embolization shows satisfactory occlusion of the anterior and posterior sectorial portal vein branches. Red arrow: left portal vein; green arrows: right portal branches occluded. (d) Computed tomography 4 weeks after portal vein embolization shows a significant increase in left liver volume (hypertrophy rate of 51%). Red arrows: coils placed in the right portal vein branches; black arrows: definition of the liver ischemic line between the right and left hepatic lobes.

frequent type of systemic chemotherapy was FOLFIRI ($n = 9.23\%$).

PVE was performed successfully in all 64 patients. Embolization required a mean number of 7.75 ± 2.9 vials of PVA and 9.73 ± 4.2 coils. No coil migration was reported on the cohort. One patient had biliary obstruction at presentation and was percutaneously drained previously PVE. In 63 (98%) patients, the ipsilateral approach was adopted in contrast with 1 patient, in which the contralateral option was required for PVE due to large tumor volume precluding safe access through the right liver lobe. Mean hospital stay was 2.6 days $\pm$ 1.61 after PVE. Fifty-three (83%) patients had a right PVE, two (3%) patients had a right PVE plus segment IV (RPVE + IV) embolization, one (1%) patient had a right PVE plus right hepatic vein embolization, five (8%) patients had a left PVE, and three (5%) patients had a left PVE plus right anterior sectorial embolization.

3.1. Volumetric Liver Results and Laboratory Values. After PVE patients were submitted to volumetric CT to assess FLR growth with a median time interval of 36.2 ± 14.4 days. FLR increased from a mean value of 484 ml $\pm$ 242 to 654 ml $\pm$ 287 ($p < 0.001$) after PVE, corresponding to a mean FLR increase of $40\% \pm 29\%$ and a mean FLR/TFLV ratio increase of $11\% \pm 5\%$. The TFLV increased from 1399 ± 347 to 1428 ± 380 after PVE (Figure 3).

Tumor volume increased from a mean value of 114 ml $\pm$ 377 to 138 ml $\pm$ 386 after PVE. Right liver volume decreased from a mean value of 985 ml $\pm$ 393 to 853 ml $\pm$ 386 after PVE (Table 2).

Laboratory data, regarding total bilirubin, AST, and INR before PVE and before surgery, were 1.41 ± 2.37 and 2.08 ± 5.24; 40 ± 23.63 and 55.94 ± 76; 1.07 ± 0.15 and 1.22 ± 0.45, respectively. There was an inverse (negative) relation between the FLR volume before PVE and FLR volume increase induced by PVE (correlation coefficient = −0.46; $p < 0.001$) (Figure 4).

3.2. PVE Adverse Events. Two out of 64 patients submitted to PVE experienced major adverse event (3.1%): 1 case of left hepatic artery branch laceration and 1 case of hemoperitoneum and hemothorax. The first patient was a 73-year-old man with colorectal liver metastases, submitted to right PVE, through a contralateral puncture, due to extensive metastatic burden in the right liver lobe. During the procedure, unintended left hepatic artery branch laceration occurred, with immediate perihepatic hematoma formation. A femoral arterial access was established but no evidence of active bleeding was seen on dedicated angiography, suggesting interruption of the arterial bleeding. The patient remained stable and was discharged 4 days later. The latter patient was a 71-year-old female with cholangiocarcinoma.

Table 1: Patients' characteristics.

Number of patients	64
Age, mean (SD)	63.84 (11.56)
Sex, *N* (%)	
Female	19 (29.69)
Male	45 (70.31)
Tumor type, *N* (%)	
Hepatocellular carcinoma	4 (6.25)
Colangiocarcinoma	12 (18.75)
Colorectal metastases	47 (73.44)
Hydatid cyst	1 (1.56)
Cirrhosis, *N* (%)	
Absent	62 (96.88)
Present	2 (3.12)
Cirrhosis etiology, *N* (%)	
HCV	1 (1.56)
None identified	63 (98.44)
Chemo before PVE, *N* (%)	
No	23 (35.94)
Yes	41 (64.06)
Type of systemic chemotherapy, *N* (%)	
FOLFIRI	9 (23.08)
FOLFIRI + bevacizumab	2 (5.13)
FOLFIRI + cetuximab	5 (12.82)
FOLFIRI + panitumumab	1 (2.56)
FOLFIRINOX	1 (2.56)
FOLFOX	6 (15.38)
FOLFOX + bevacisumab	2 (5.13)
FOLFOX + cetuximab	2 (5.13)
FOLFOX + folfirinox	1 (2.56)
FOLFOX + folfirinox + cetuximab	1 (2.56)
XELOX + cetuximab	1 (2.56)
XELIRI	1 (2.56)
Xeloda + FOLFIRI + erbitux	1 (2.56)
XELOX	3 (7.69)
XELOX + bevacizumab	2 (5.13)
XELOX + XELIRI	1 (2.56)
Chemo cycles, mean (SD)	3.38 (4.36)
Biliary drainage before PVE, *N* (%)	
No	63 (98.44)
Yes	1 (1.56)
Arterial embolization, *N* (%)	
No	64 (100)

HCV: hepatitis C virus; PVE: portal vein embolization.

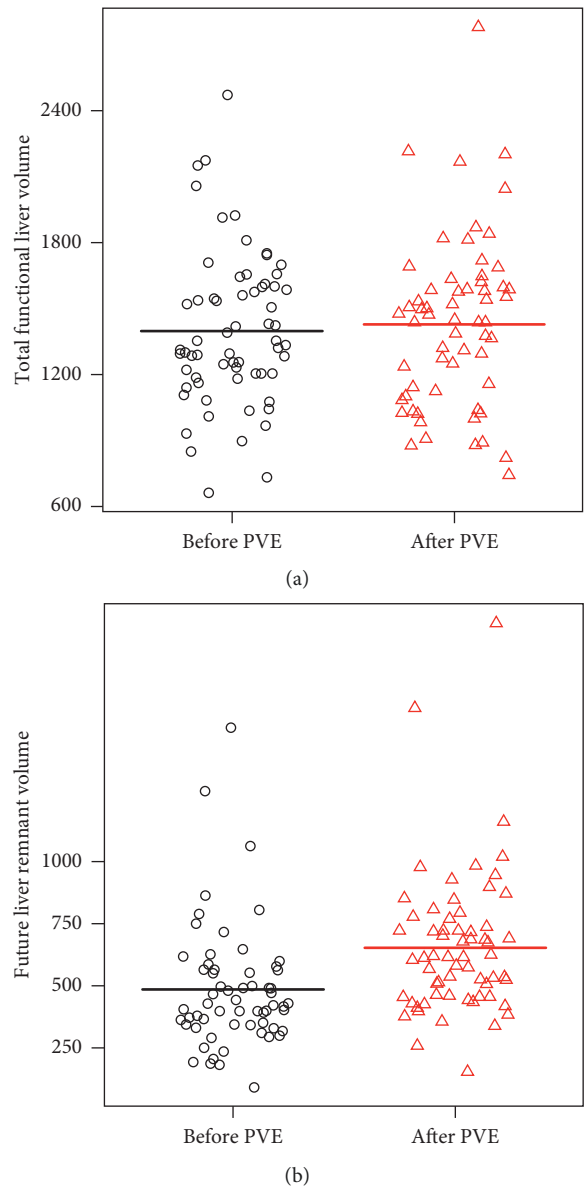

Figure 3: (a) Total functional liver volume before and after portal vein embolization (in milliliters). Differences were not statistically significant. (b) Future liver remnant volume before and after portal vein embolization (in milliliters). Differences were statistically significant ($p < 0.001$).

Two hours after PVE, the patient developed signs of hemorrhagic shock, and a hemoperitoneum and hemothorax were diagnosed. An angiography was performed, and no active bleeding was depicted. There was no need for thoracic drainage. No underlying etiology was found, and this patient also recovered well. This event prolonged her hospital stay for 6 days. Four patients had minor complications (6.2%) with 3 cases of fever and 1 case of nausea and vomiting (Table 2).

3.3. Surgical Outcomes. Twenty patients (31.2%) were not submitted to surgery as a result of disease progression ($n = 17$), liver insufficiency ($n = 1$), insufficient FLR volume, and disease progression ($n = 1$), and one patient declined surgery ($n = 1$). A total of 44 (68.8%) patients underwent liver surgery, and the performed hepatic procedures are listed in Table 3.

Complications during and immediately after hepatic resection were (Table 4) biliary fistula ($n = 1$), intraoperative hepatic bleeding ($n = 1$), abscess ($n = 2$), principal biliary duct laceration ($n = 1$), and portal vein and small bowel laceration ($n = 1$) that were successfully managed. Postoperative hepatic insufficiency was reported in one patient who died 32 days after surgery. Surgical-related mortality was thus 2.3% ($n = 1$). Mean hospital stay was 18 days ± 14.58 after liver surgery. Accomplishment of the planned liver surgery was related with better overall survival in contrast

Table 2: PVE and main outcome.

Number of patients	64
PVE segments, *N* (%)	
Right	53 (82.81)
Right + IV	2 (3.12)
Right + RHV	1 (1.56)
Left	5 (7.81)
Left + ARS	3 (4.69)
PVE ipsi or contralateral, *N* (%)	
Contra	1 (1.56)
Ipsi	63 (98.44)
PVA total vials, mean (SD)	7.75 (2.93)
Total coils, mean (SD)	9.73 (4.21)
Adverse events, *N* (%)	
Fever	3 (4.69)
Hemoperitoneum and hemothorax: angiography did not reveal active bleeding	1 (1.56)
Left arterial branch lateration	1 (1.56)
Nausea and vomiting	1 (1.56)
None	58 (90.62)
Hospital stay in days, mean (SD)	2.59 (1.61)
TFLV, mean (SD)	1399.02 (346.92)
TFLV after PVE, mean (SD)	1428.62 (379.58)
FLRV, mean (SD)	484.31 (241.64)
FLRV after PVE, mean (SD)	653.61 (286.66)
Right liver volume before PVE, mean (SD)	984.89 (393.31)
Right liver volume after PVE, mean(SD)	853.06 (386.42)
Tumor volume before PVE, mean (SD)	114.03 (377.4)
Tumor volume after PVE, mean (SD)	137.76 (385.8)
Increase in the FLR ratio, mean (SD)	11.14 (4.83)
Increase in the FLR percent degree of hypertrophy, mean (SD)	40.16 (28.75)

PVE: portal vein embolization; RHV: right hepatic vein; ARS: anterior right sector; TFLV: total functional liver volume; FLRV: future liver remnant volume; FLR: future liver remnant.

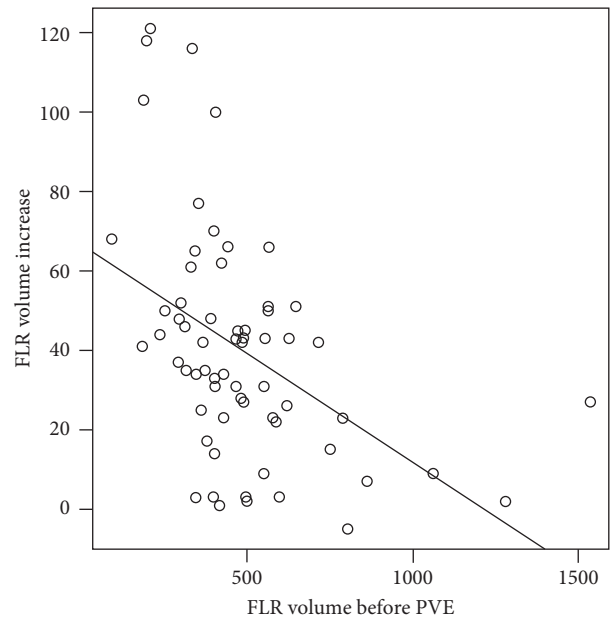

Figure 4: Future liver remnant volume increase versus future liver remnant volume before PVE. There was a negative correlation between those two variables, demonstrating that those patients with the smallest FLR volumes obtained superior volume increase after PVE.

Table 3: Patient outcome.

Total of patients	64
Type of hepatectomy, *N* (%)	
RH	21 (47.73)
RH + I	4 (9.09)
RH + I + IV	1 (2.27)
RH + IV	10 (22.73)
LH	6 (13.64)
LH + V/VII	1 (2.27)
Tx	1 (2.27)
Reason for no surgery, *N* (%)	
Liver failure	1 (5.00)
Insufficient volume + disease progression	1 (5.00)
Disease progression	17 (85.00)
Patient declined surgery	1 (5.00)
Total bilirubin before PVE, mean (SD)	1.41 (2.37)
Total bilirubin before surgery, mean (SD)	2.08 (5.24)
AST before PVE, mean (SD)	40.41 (23.63)
AST before surgery, mean (SD)	59.94 (76)
INR before pve, mean (SD)	1.07 (0.15)
INR before surgery, mean (SD)	1.22 (0.45)

RH: right hepatectomy; LH: left hepatectomy; Tx: transplant; PVE: portal vein embolization; AST: aspartate aminotransferase; INR: international normalized ratio.

with those patients in whom surgery was declined ($p < 0.001$) (Figure 5).

The preoperative data of the patients are listed in Table 3.

4. Discussion

Currently, preoperative PVE is an important technique to be considered, in the proper clinical setting, before major hepatectomy. This procedure helps diminish postoperative morbidity and mortality through the achievement of a sufficient nontumoral liver—FLR—volume precluding the occurrence of postoperative liver failure that may be present in up to 20% of patients [5]. In the present cohort liver, failure after PVE and surgery was reported in only 1 patient (2.3%) highlighting the importance of presurgical PVE.

One of the fundamental aspects of PVE is the elected embolic material. The best agent is one which originates permanent embolization without recanalization, has a significant toleration by the patient, and is effortless to administer [13]. PVA particles are secure, cause minor periportal reaction, and originate long-lasting portal vein occlusion when they are used in combination with coils [22]. Nevertheless, a recent systematic review [11] and two retrospective studies [23, 24] reported that PVE with N-butyl-cyanoacrylate (NBCA) had a more robust effect in FLR hypertrophy than PVE with PVA and coils. Moreover, a study performed by de Baere et al. [25], in an animal model, showed that PVE with NBCA induced a significantly greater increase in hepatic lobules volume when compared with other embolic materials. Although there seems to be a

Table 4: Patient outcome: surgical complications.

Surgical complications, *N* (%)	
Principal biliary duct laceration	1 (2.13)
Abscess	2 (4.26)
Biliary fistula	1 (2.13)
Hemorrhage	2 (4.26)
Hepatic failure	1 (2.13)
Portal vein and small bowel laceration	1 (2.13)
None	39 (82.98)
Length of hospital stay, mean (SD)	17.72 (14.58)

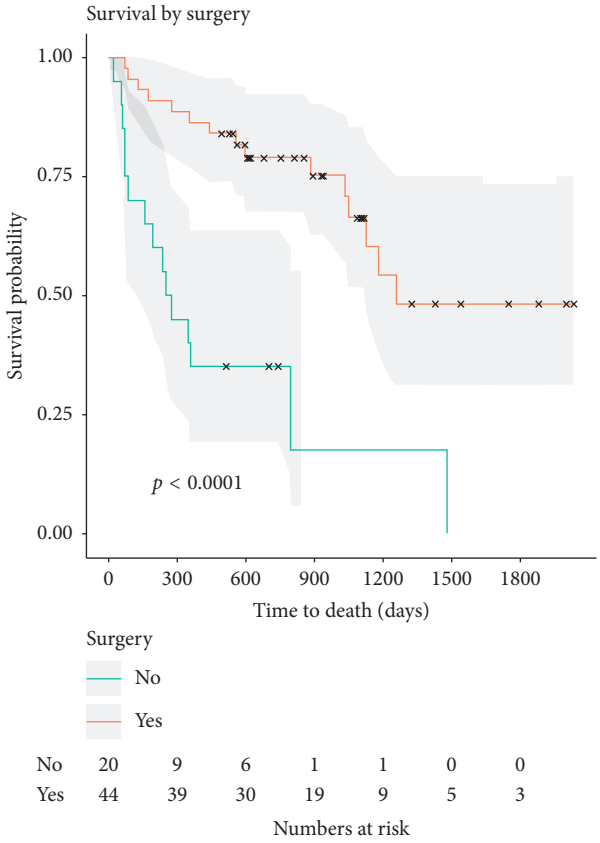

Figure 5: Overall survival according to surgery. Accomplishment of the planned liver surgery was associated with better overall survival when compared to those patients in whom surgery was declined ($p < 0.001$).

significant benefit in FLR hypertrophy with the use of NBCA, no prospective randomized trials approaching this topic are currently available. This adhesive embolic material, NBCA, that might be more efficient, does require specific and dedicated training and is associated with nontarget embolization [26]. In addition, considering the use of vascular plugs in PVE, according to one study [27], there were no significant differences between PVA plus coils, PVA plus plug, and PVA plus plug and coils regarding future liver remnant hypertrophy after PVE.

Since one of the most important properties of an embolic material is its capacity to induce liver growth when used for PVE, we wanted to evaluate this specific outcome in our own series of patients. In our retrospective cohort of 64 patients submitted to PVE with PVA plus coils, we obtained a 40% increase in the FLR after a median of 36 days. Compared with other published hypertrophy rates, our results were equal or superior to those of most previous studies [13, 27, 28]. Some series showed a higher hypertrophy response, as in the Kishi et al. study [29]. However, it is difficult to establish a direct comparison of our results to the latter and other studies due to relevant technical differences such as segment IV portal vein embolization. In their study, Kishi et al. reported a high FLR hypertrophy rate of 54% after RPVE + IV embolization. Interestingly, in the study by Madoff et al. [13], it was also demonstrated a higher hypertrophy rate after right PVE + IV embolization, even though that higher value was similar to that reported in our own study without segment IV embolization. Furthermore, the real benefit of segment IV portal vein embolization is still not clear. A study by de Baere et al. reported an increase in the FLR of 68% and 69% after right PVE and RPVE + VI embolization, respectively, showing no difference in hypertrophy rates when segment IV embolization was performed [30]. This study also demonstrated a superior FLR rate compared with our results, although differences among these studies make it difficult to establish linear comparison.

One relevant aspect of our study was the adoption of PVA as the embolic material. Madoff et al. [31] showed that tris-acryl microspheres performed favorably, in hypertrophy results, than PVA for PVE plus segment IV embolization. While these results do suggest that it might be possible to obtain better regenerative results with tris-acryl microspheres, they had a different study population (they only included patients submitted to right PVE + IV), and using numerous tris-acryl microspheres vials would drastically increase the cost of PVE at our institution since it is significantly more expensive in our local setting.

Two major complications after PVE were recorded in our series (3.1%), consisting of one case of hemoperitoneum and hemothorax and one case of left hepatic artery laceration. The latter patient was a 73-year-old man with colorectal liver metastases, underwent right PVE through a contralateral approach, and was the only patient in our study on whom the FLR puncture was performed. This major complication might be explained by the use of the contralateral approach. The contralateral approach has known advantages such as direct catheterization of the desired portal branches, use of shorter catheters, and avoidance of tumor transgression in high tumor burden patients. Nevertheless, the contralateral puncture is somewhat trickier in patients with very small FLRs and disadvantageous body habitus and has the inherent disadvantage of risking injury to the FLR [32]. However, the largest study, comprising 188 patients, concerning PVE complications suggested that the contralateral approach does not impose higher risks compared with the other performed approaches [18].

In our study, 31% of the patients were not submitted to hepatic surgery, which is slightly more than the reported in a recent systematic review [11] where 20% (358/1, 791) of the initially planned hepatectomies after PVE were cancelled. Most of these patients had tumor progression. We only found 16% of complications after liver surgery, which is

considerably below the complication rates (25%–30%) reported in most similar series [30, 33, 34]. This might reflect a more rigorous criterion for surgery selection and a higher cancelation rate of the originally planned liver resection [13, 35].

Our study has limitations, such as the retrospective design and the exclusion of part of the cohort from the analysis due to missing imaging data. The strengths of our study were the application of the same PVE technique along many years of practice and the overall homogeneous patient population comprised almost exclusively by noncirrhotic patients, which would otherwise have puzzled our hypertrophy outcomes due to the known effects of cirrhosis in liver regeneration [36].

In conclusion, we demonstrated herein that PVE with PVA and coils could be accomplished with a low incidence of major complications. It is also associated with a high FLR hypertrophy yield and enables patients to be submitted to the potentially curative treatment of liver tumor resection with minimal postoperative liver failure rates.

Abbreviations

PVE: Portal vein embolization
FLR: Future liver remnant
PLF: Postoperative liver failure
TFLV: Total functional liver volume
CT: Computed tomography
MR: Magnetic resonance
PVA: Polyvinyl alcohol
TB: Total bilirubin
AST: Aspartate aminotransferase
INR: Index normalized ratio
NBCA: N-butyl-cyanoacrylate
RPVE: Right portal vein embolization.

Data Availability

The patient data (baseline patient clinical characteristics, imaging records, liver volumetric data, and postoperative course) used to support the findings of this study are available from the corresponding author upon request.

Conflicts of Interest

The authors declare that they have no conflicts of interest.

Acknowledgments

The authors would like to thank Paula Mendes Luz, MD, PhD, not only for assistance with statistical analysis but also for comments and suggestions.

References

[1] D. C. Broering, C. Hillert, G. Krupski et al., "Portal vein embolization vs. portal vein ligation for induction of hypertrophy of the future liver remnant," *Journal of Gastrointestinal Surgery*, vol. 6, no. 6, pp. 905–913, 2002.

[2] R. Loffroy, S. Favelier, O. Chevallier et al., "Preoperative portal vein embolization in liver cancer: indications, techniques and outcomes," *Quantitative Imaging in Medicine and Surgery*, vol. 5, no. 5, pp. 730–739, 2015.

[3] T. Aoki and K. Kubota, "Preoperative portal vein embolization for hepatocellular carcinoma: consensus and controversy," *World Journal of Hepatology*, vol. 8, no. 9, pp. 439–445, 2016.

[4] M. Makuuchi, K. Takayasu, T. Takuma et al., "Preoperative transcatheter embolization of the portal venous branch for patients receiving extended lobectomy due to the bile duct carcinoma," *The Journal of the Japanese Practical Surgeon Society*, vol. 45, no. 12, pp. 1558–1564, 1984.

[5] J.-N. Vauthey, A. Chaoui, K.-A. Do et al., "Standardized measurement of the future liver remnant prior to extended liver resection: methodology and clinical associations," *Surgery*, vol. 127, no. 5, pp. 512–519, 2000.

[6] E. K. Abdalla, M. E. Hicks, and J. N. Vauthey, "Portal vein embolization: rationale, technique and future prospects," *British Journal of Surgery*, vol. 88, no. 2, pp. 165–175, 2001.

[7] T. Shimamura, Y. Nakajima, Y. Une et al., "Efficacy and safety of preoperative percutaneous transhepatic portal embolization with absolute ethanol: a clinical study," *Surgery*, vol. 121, no. 2, pp. 135–141, 1997.

[8] K. C. Lee, H. Kinoshita, K. Hirohashi, S. Kubo, and R. Iwasa, "Extension of surgical indications for hepatocellular carcinoma by portal vein embolization," *World Journal of Surgery*, vol. 17, no. 1, pp. 109–115, 1993.

[9] K. Kubota, M. Makuuchi, K. Kusaka et al., "Measurement of liver volume and hepatic functional reserve as a guide to decision-making in resectional surgery for hepatic tumors," *Hepatology*, vol. 26, no. 5, pp. 1176–1181, 1997.

[10] D. Azoulay, D. Castaing, A. Smail et al., "Resection of nonresectable liver metastases from colorectal cancer after percutaneous portal vein embolization," *Annals of Surgery*, vol. 231, no. 4, pp. 480–486, 2000.

[11] K. P. van Lienden, J. W. van den Esschert, W. de Graaf et al., "Portal vein embolization before liver resection: a systematic review," *CardioVascular and Interventional Radiology*, vol. 36, no. 1, pp. 25–34, 2013.

[12] D. C. Madoff, M. E. Hicks, J.-N. Vauthey et al., "Transhepatic portal vein embolization: anatomy, indications, and technical considerations," *RadioGraphics*, vol. 22, no. 5, pp. 1063–1076, 2002.

[13] D. C. Madoff, M. E. Hicks, E. K. Abdalla, J. S. Morris, and J.-N. Vauthey, "Portal vein embolization with polyvinyl alcohol particles and coils in preparation for major liver resection for hepatobiliary malignancy: safety and effectiveness-study in 26 patients," *Radiology*, vol. 227, no. 1, pp. 251–260, 2003.

[14] A. Denys, P. Bize, N. Demartines, F. Deschamps, and T. De Baere, "Quality improvement for portal vein embolization," *CardioVascular and Interventional Radiology*, vol. 33, no. 3, pp. 452–456, 2010.

[15] R. Avritscher, T. de Baere, R. Murthy, F. Deschamps, and D. Madoff, "Percutaneous transhepatic portal vein embolization: rationale, technique, and outcomes," *Seminars in Interventional Radiology*, vol. 25, no. 2, pp. 132–145, 2008.

[16] A. A. Rahnemai-Azar, J. M. Cloyd, S. M. Weber et al., "Update on liver failure following hepatic resection: strategies for prediction and avoidance of post-operative liver insufficiency," *Journal of Clinical and Translational Hepatology*, vol. 6, no. 1, pp. 97–104, 2018.

[17] J. R. van der Vorst, R. M. van Dam, R. S. A. van Stiphout et al., "Virtual liver resection and volumetric analysis of the future liver remnant using open source image processing software," *World Journal of Surgery*, vol. 34, no. 10, pp. 2426–2433, 2010.

[18] D. R. Di Stefano, T. de Baere, A. Denys et al., "Preoperative percutaneous portal vein embolization: evaluation of adverse events in 188 patients," *Radiology*, vol. 234, no. 2, pp. 625–630, 2005.

[19] S. N. Goldberg, C. J. Grassi, J. F. Cardella et al., "Image-guided tumor ablation: standardization of terminology and reporting criteria," *Radiology*, vol. 235, no. 3, pp. 728–739, 2005.

[20] C. J. Leoni, J. E. Potter, M. P. Rosen, D. P. Brophy, and E. V. Lang, "Classifying complications of interventional procedures: a survey of practicing radiologists," *Journal of Vascular and Interventional Radiology*, vol. 12, no. 1, pp. 55–59, 2001.

[21] D. K. Filippiadis, C. Binkert, O. Pellerin, R. T. Hoffmann, A. Krajina, and P. L. Pereira, "Cirse quality assurance document and standards for classification of complications: the cirse classification system," *CardioVascular and Interventional Radiology*, vol. 40, no. 8, pp. 1141–1146, 2017.

[22] J. R. Duncan, M. E. Hicks, S.-R. Cai, E. M. Brunt, and K. P. Ponder, "Embolization of portal vein branches induces hepatocyte replication in swine: a potential step in hepatic gene therapy," *Radiology*, vol. 210, no. 2, pp. 467–477, 1999.

[23] B. Guiu, P. Bize, D. Gunthern, N. Demartines, N. Halkic, and A. Denys, "Portal vein embolization before right hepatectomy: improved results using *n*-butyl-cyanoacrylate compared to microparticles plus coils," *CardioVascular and Interventional Radiology*, vol. 36, no. 5, pp. 1306–1312, 2013.

[24] A. Jaberi, S. S. Toor, D. K. Rajan et al., "Comparison of clinical outcomes following glue versus polyvinyl alcohol portal vein embolization for hypertrophy of the future liver remnant prior to right hepatectomy," *Journal of Vascular and Interventional Radiology*, vol. 27, no. 12, pp. 1897–1905.e1, 2016.

[25] T. de Baere, A. Denys, and V. Paradis, "Comparison of four embolic materials for portal vein embolization: experimental study in pigs," *European Radiology*, vol. 19, no. 6, pp. 1435–1442, 2009.

[26] J. H. M. Luz, P. M. Luz, T. Bilhim et al., "Portal vein embolization with *n*-butyl-cyanoacrylate through an ipsilateral approach before major hepatectomy: single center analysis of 50 consecutive patients," *Cancer Imaging*, vol. 17, no. 1, p. 25, 2017.

[27] M. Malinowski, D. Geisel, V. Stary et al., "Portal vein embolization with plug/coils improves hepatectomy outcome," *Journal of Surgical Research*, vol. 194, no. 1, pp. 202–211, 2015.

[28] A. Deipolyi, Y. Zhang, A. Khademhosseini et al., "Portal vein embolization: impact of chemotherapy and genetic mutations," *Journal of Clinical Medicine*, vol. 6, no. 3, p. 26, 2017.

[29] Y. Kishi, D. C. Madoff, E. K. Abdalla et al., "Is embolization of segment 4 portal veins before extended right hepatectomy justified?," *Surgery*, vol. 144, no. 5, pp. 744–751, 2008.

[30] T. de Baere, C. Teriitehau, F. Deschamps et al., "Predictive factors for hypertrophy of the future remnant liver after selective portal vein embolization," *Annals of Surgical Oncology*, vol. 17, no. 8, pp. 2081–2089, 2010.

[31] D. C. Madoff, E. K. Abdalla, S. Gupta et al., "Transhepatic ipsilateral right portal vein embolization extended to segment IV: improving hypertrophy and resection outcomes with spherical particles and coils," *Journal of Vascular and Interventional Radiology*, vol. 16, no. 2, pp. 215–225, 2005.

[32] R. Avritscher, E. Duke, and D. C. Madoff, "Portal vein embolization: rationale, outcomes, controversies and future directions," *Expert Review of Gastroenterology & Hepatology*, vol. 4, no. 4, pp. 489–501, 2010.

[33] O. Farges, J. Belghiti, R. Kianmanesh et al., "Portal vein embolization before right hepatectomy: prospective clinical trial," *Annals of Surgery*, vol. 237, no. 2, pp. 208–217, 2003.

[34] G. Giraudo, M. Greget, E. Oussoultzoglou, E. Rosso, P. Bachellier, and D. Jaeck, "Preoperative contralateral portal vein embolization before major hepatic resection is a safe and efficient procedure: a large single institution experience," *Surgery*, vol. 143, no. 4, pp. 476–482, 2008.

[35] D. Ribero, E. K. Abdalla, D. C. Madoff, M. Donadon, E. M. Loyer, and J.-N. Vauthey, "Portal vein embolization before major hepatectomy and its effects on regeneration, resectability and outcome," *British Journal of Surgery*, vol. 94, no. 11, pp. 1386–1394, 2007.

[36] N. Vauthey, E. Okamoto, E. Kawamura et al., "Dynamics of normal and injured human liver regeneration after hepatectomy as assessed on the basis of computed tomography and liver function," *Hepatology*, vol. 18, no. 1, pp. 79–85, 1993.

Hindawi
Journal of Oncology
Volume 2019, Article ID 1369274, 8 pages
https://doi.org/10.1155/2019/1369274

Research Article

Intraoperative Ultrasound Staging for Colorectal Liver Metastases in the Era of Liver-Specific Magnetic Resonance Imaging: Is It Still Worthwhile?

Serena Langella,[1] **Francesco Ardito**,[2] **Nadia Russolillo**,[1] **Elena Panettieri**,[2] **Serena Perotti**,[1] **Caterina Mele**,[2] **Felice Giuliante**,[2] **and Alessandro Ferrero**[1]

[1]*Department of General and Oncological Surgery, Ospedale Mauriziano "Umberto I", Torino, Italy*
[2]*Unit of Hepatobiliary Surgery, Fondazione Policlinico Universitario A. Gemelli IRCCS, Università Cattolica Del Sacro Cuore, Rome, Italy*

Correspondence should be addressed to Felice Giuliante; felice.giuliante@unicatt.it

Received 23 April 2019; Revised 24 July 2019; Accepted 11 August 2019; Published 22 September 2019

Guest Editor: György Kovacs

Background. To assess the efficacy of intraoperative ultrasound (IOUS) compared with liver-specific magnetic resonance imaging (MRI) in patients with colorectal liver metastases (CRLMs). *Methods*. From January 2010 to December 2017, 721 patients underwent MRI as a part of preoperative workup within 1 month before hepatectomy and were considered for the study. Early intrahepatic recurrence (relapse at cut surface excluded) was assessed 6 months after the resection and was considered as residual disease undetected by IOUS and/or MRI. IOUS and MRI performance was compared on a patient-by-patient basis. Long-term results were also studied. *Results*. A total of 2845 CRLMs were detected by MRI, and the median number of CRLMs per patient was 2 (1–31). Preoperative chemotherapy was administered in 489 patients (67.8%). In 177 patients, 379 new nodules were intraoperatively found and resected. Among 379 newly identified nodules, 317 were histologically proven CRLMs (11.1% of entire series). The median size of new CRLMs was 6 ± 2.5 mm. Relationships between intrahepatic vessels and tumors differed between IOUS and MRI in 128 patients (17.7%). The preoperative surgical plan was intraoperatively changed for 171 patients (23.7%). Overall, early intrahepatic recurrence occurred in 8.7% of cases. To assess the diagnostic performance, 24 (3.3%) recurrences at the cut surface were excluded; thus, 5.4% of early relapses were considered for analysis. The sensitivity of IOUS was superior to MRI (94.5% vs 75.1%), while the specificity was similar (95.7% vs 95.9%). Multivariate analysis at the hepatic dome or subglissonian and mucinous histology revealed predictive factors of metastases missing at MRI. The 5-year OS (52.1% vs 37.8%, $p = 0.006$) and DF survival (45.1% vs 33%, $p = 0.002$) were significantly worse among patients with new CRLMs than without. *Conclusions*. IOUS improves staging in patients undergoing resection for CRLMs even in the era of liver-specific MRI. Intraoperative detection of new CRLMs negatively affects oncologic outcomes.

1. Introduction

Various imaging modalities have been developed in the field of liver surgery for accurate detection of colorectal metastases (CRLMs) [1]. Nevertheless, additional CRLMs can be found at the time of surgery in up to 25% of patients [2–9]. We previously reported [9] that intraoperative ultrasonography (IOUS) enabled detection of 17.6% of new nodules in patients undergoing resection for CRLMs. In this series, we also demonstrated that IOUS provides significant information about vascular relationships between tumors and hepatic vessels. Therefore, surgical plan was modified according to IOUS findings in 24.6% of cases. The published data on the impact of intraoperative staging are extremely heterogeneous because of differences among centers in preoperative diagnostic workup and surgical policies. Moreover, magnetic resonance imaging (MRI) with liver-specific contrast agent has dramatically improved the

sensitivity of detection of liver tumors [10, 11]. Although the efficacy of this new imaging modality to stage hepatic disease in patients with CRLMs has been reported in several studies [12, 13], whether IOUS can improve liver staging when MRI is performed as a part of preoperative workup remains unclear. The aim of this study is to assess the efficacy of IOUS compared with liver-specific MRI in patients undergoing hepatectomy for CRLMs.

2. Materials and Methods

Between January 2010 and December 2017, 721 consecutive patients who underwent liver resection for CRLMs at two institutions (Ospedale Mauriziano, Torino, and Policlinico Gemelli, Roma, Italy) were considered for the study. Eligibility criteria were one- or two-stage resection for CRLMs (with or without preoperative chemotherapy), age ≥18 years, written informed consent, preoperative MRI with liver-specific contrast agent performed within 1 month before hepatectomy, IOUS accomplished by surgeon during the procedure, postoperative follow-up at least 6 months.

Data from prospectively collected databases were retrospectively reviewed. The collection and registration of the original database were performed according to regulations and with the approval of the institutional review boards of the two hospitals.

Primary endpoint was to compare diagnostic performance of MRI and IOUS to stage intrahepatic disease. The performances of IOUS and MRI were also compared in patients who did not receive preoperative chemotherapy. Secondly, we evaluated the impact of new CRLMs intraoperatively found on long-term outcomes.

2.1. Preoperative Workup. At diagnosis, all patients were evaluated with computed tomography (CT) scans and MRI. CT scans were performed with a multislice helical CT using a 3 mm collimation and reconstruction at 1 and 2.5 mm. Images were acquired using a triphasic hepatic protocol following a noncontrast evaluation of the liver. Images were obtained 11, 80, and 180 seconds after the start of intravenous injection of iopromide (Ultravist® 370, Bayer HealthCare Pharmaceuticals Inc., Wayne, NJ) at a rate of 3.5 mL/s. MRI was conducted on a 1.5 T superconducting system using a liver-specific contrast agent (EOB-gadoxetic acid disodium, Primovist, Bayer Schering Pharma AG, Berlin, Germany). All MR images were preoperatively evaluated by radiologists skilled in liver pathology and diffusion-weighted imaging (DWI). Fluorodeoxyglucose positron emission tomography was also performed in selected cases. After chemotherapy, restaging was accomplished by MRI and thoracic CT scans or thoracoabdominal CT scans in the presence of extrahepatic disease. Chemotherapy response was assessed by using the Response Evaluation Criteria in Solid Tumors (RECIST) [14].

2.2. Intraoperative Staging. Abdominal exploration and intraoperative liver ultrasonography (Aloka Prosound Alpha 7 with 7.5 MHz intraoperative miniconvex probe, Aloka Co., Tokyo, Japan; Philips HDI® 5000 SonoCT with 8 MHz to 4 MHz intraoperative convex probe ATL Entos CT8-4, Koninklijke Philips Electronics, Eindhoven, Netherlands) were always performed as the first step to assess the site, extent of the disease, and the tumor's relationships with major intrahepatic vessels and to define the extension of the required resection. The surgeon conducted IOUS for all patients according to a standardized protocol. A similar technique was used for laparoscopic liver ultrasound. This was performed with a multifrequency (5–10 MHz) flexible linear-array laparoscopic transducer (UST-5536-7.5; Hitachi Aloka Medical) and a Pro Focus 2202 Ultrasound System with Laparoscopic Transducer Type 8666-RF (Bk Medical, Herlev, Denmark).

Contrast-enhanced intraoperative ultrasound (CEIOUS) was additionally performed in selected cases. CEIOUS was achieved with a convex 2–6 MHz harmonic frequency transducer. In all patients, 2.4 mL sulfur hexafluoride microbubbles (SonoVue®, Bracco Imaging, Milan, Italy) was injected intravenously through a peripheral vein by the anesthesiologist.

All nodules consistent with CRLMs found intraoperatively by IOUS and/or CEIOUS that were not detected at preoperative MRI were classified as new lesions. During surgery, MR images were always available on a computer screen, which allowed a real-time comparison with intraoperative findings. In patients who underwent chemotherapy, disappeared liver metastases (DLMs) on preoperative MRI that were detected intraoperatively were not considered new lesions.

2.3. Histopathologic Examination. The pathologist was informed about the site of preoperatively detected CRLMs and new nodules. Specimens were fixed, embedded in paraffin, and stained with hematoxylin-eosin. Then, 0.5 cm slices were taken for microscopic examination. Steatosis was estimated as the percentage of involved hepatocytes and categorized as defined by Kleiner et al. [15]: no fatty change (<5%), mild (5% to <33%), moderate (33% to <66%), or severe (≥66%).

2.4. Diagnostic Performance Analysis. We conducted patient-by-patient analysis to evaluate MRI and intraoperative staging performance (IOUS and CEIOUS). Early intrahepatic recurrences were registered at 6 months after the resection and were considered residual disease undetected by intraoperative staging and/or MRI (false negative: FN). Recurrences were assessed using radiological imaging during the follow-up. Patients were evaluated every 3 months with physical examination, measurement of CEA levels, and abdominal ultrasonography or thoracoabdominal CT. Local recurrence on the cut liver surface was not considered an FN. In patient-by-patient analysis, sensitivity was defined as the number of patients without FN lesions divided by the total number of patients. Conversely, specificity was defined as the number of patients without false-positive (FP) lesions divided by the total number of patients. By definition, we considered the positive and negative predictive values (PPV and NPV, respectively) as the proportions of positive and negative results in true-positive and true-negative results. The likelihood ratio was

calculated for both positive (LR+, likelihood ratio positive: sensibility/1−specificity) and negative (LR−, likelihood ratio negative: 1−sensibility/specificity) results.

2.5. Definitions

Indirect signs to identify liver metastases by IOUS were presence of bile duct dilatation, distortion, or interruption of the venous wall.

Types of hepatectomies were classified according to the Brisbane 2000 terminology [16].

Were considered mucinous CRLMs, those histologically proven liver metastases comprising more than 50% mucinous carcinoma.

Local recurrence was defined as intrahepatic relapse at cut surface of the previous hepatectomy.

Subglissonian metastasis was defined as lesions within 1 cm of the liver surface.

2.6. Statistical Analysis. All statistical analyses were performed using IBM SPSS software (v20.1). The distribution of variables was analyzed using the Kolmogorov–Smirnov test. Categorical variables were compared using the chi-square test, Fisher's exact test, or Pearson's test as appropriate. Continuous variables were compared between groups using the unpaired t-test or Mann–Whitney U test, as appropriate. Continuous variables were presented as median ± standard deviation (SD) or range. Categorical variables were represented as number and percentage in brackets. Diagnostic performance was evaluated assessing sensitivity, specificity, PPV, NPV, and likelihood ratio. Cohen's kappa coefficient was used to assess the interrater reliability of preoperative and intraoperative imaging. The results have been interpreted as follows: values ≤0 as indicating no agreement and 0.01–0.20 as none to slight, 0.21–0.40 as fair, 0.41–0.60 as moderate, 0.61–0.80 as substantial, and 0.81–1.00 as almost perfect agreement. Uni- and multivariate binary logistic regression analyses were performed to assess the predictive factors for missing CRLMs at MRI. After univariate analysis, a p value ≤0.05 was considered to include variables in the multivariate analysis. Receiver operating characteristic curves were plotted to identify the value of preoperative number of metastases and median number of neoadjuvant chemotherapy cycle in predicting missing CRLMs at MRI with a high sensitivity and specificity. Disease-free survival was measured from the date of hepatic resection until the date of radiographic detection of recurrence, death, or last follow-up. Overall survival was measured from the date of hepatic resection until the date of death or last follow-up. The Kaplan–Meier method was used to estimate survival probabilities, which were compared using the log-rank test. All p values were two sided, and $p \leq 0.05$ was considered statistically significant.

3. Results

Patients were investigated with a median of 3 (range 2–4) preoperative imaging modalities (US, CT scan, and MRI and PET). All patients were staged with MRI, and fluorodeoxyglucose positron emission tomography was undertaken in 317 (43.9%) patients. A total of 2845 CRLMs were detected preoperatively using MRI. The median number of CRLMs per patients was 2 (1–31). Multiple (more than 3) CRLMs were observed in 358 (49.6) patients. The median diameter was 24 ± 22.05 mm. In 56 (7.7%) patients, CRLMs were from mucinous cancer.

Preoperative chemotherapy was administered in 489 patients (67.8%). In this subgroup, DLMs were present in 52 of 489 (10.6%) patients. Hepatic resections were minor in 592 (82.1%) patients. Among these, multiple liver resections were required in 517 (87.3%) cases. Minor resections were distributed as follows: 459 (77.5%) nonanatomical, 60 (10.1%) anatomical, and 73 (12.3%) both anatomical and nonanatomical. Two stage procedures were accomplished in 30 (4.2%) patients. Redo-resection for recurred CRLMs was performed in 50 of 721 patients (6.9%). A laparoscopic approach was used in 103 (14.3%) patients to perform 11 (10.7%) major and 92 (89.3%) minor hepatectomies.

Preoperative and operative data are detailed in Table 1.

3.1. Intraoperative Findings and Management. In 177 patients, 379 (13.3%) new nodules were intraoperatively found and resected. Among 379 newly identified nodules, 317 (83.6%) were histologically proven CRLMs (11.1% of entire series). The 62 FP cases (16.4%) were classified by pathologists as hemangiomas (19), focal steatosis (14), biliary hamartoma (12), granulomatous inflammation (9), fibrosis (6), and focal nodular hyperplasia (2). Furthermore, 38 (73%) of 52 DLMs were found intraoperatively (not considered new CRLMs).

The liver was hyperechoic in half of the patients (363, 50.3%). The median new CRLM size was 6 ± 2.5 mm, and most were hypoechoic (77.3%). The new CRLMs were only rarely detected by indirect signs (3.8%) or CE-IOUS (5.9%). Features of new CRLMs were summarized in Table 2.

Seventy out of 317 (22%) new lesions were located at the hepatic dome (Segments (Sgs) 8 and 4a). The remaining new nodules were distributed as follows: nine in Sg 1 (2.8%), 31 in Sg 2 (9.7%), 38 in Sg 3 (11.9%), 41 in Sg 4b (12.9%), 43 in Sg 5 (13.5%), 45 in Sg 6 (14.2%), and 40 in Sg 7 (12.7%). Twenty-eight new CRLMs were sited within 1 cm from the liver surface.

Vascular relationships between intrahepatic vessels and tumors differed between IOUS and MRI in 128 patients (17.7%). In 31 (4.3%) patients, 46 (1.6%) lesions suspected for metastases at preoperative imaging were not identified or assessed intraoperatively as metastases. Among the 46 lesions left in situ because of IOUS findings, only two were subsequently diagnosed as metastases during the follow-up (rate of FN lesion 4.3%). Overall, in 171 (23.7%) patients, the preoperative surgical plan changed according to intraoperative findings. Commonly, in case of new CRLMs, limited additional resections were required (83%).

Overall, 232 (32.2%) patients were scheduled for upfront surgery (without preoperative chemotherapy). Among these, MRI preoperatively identified 504 CRLMs, and the median

Table 1: Preoperative and operative characteristics of 721 patients with 2845 CRLMs preoperatively assessed by MRI (whole population) and 232 patients who did not receive preoperative chemotherapy.

Characteristics	Whole population $n = 721$	Patients without chemotherapy $n = 232$
Age (years), median ± SD	64 ± 10.8	66 ± 10.0
Male, *n* (%)	453 (62.2)	149 (64.2)
BMI (kg/m^2), median ± SD	25 ± 3.34	27 ± 4.0
Preoperative chemotherapy	489 (67.8)	—
Number of cycles, median ± SD	5 ± 6.5	—
Oxaliplatin based, *n* (%)	358 (49.7)	—
Irinotecan based, *n* (%)	208 (28.8)	—
Biologics, *n* (%)	309 (42.9)	—
Response to chemotherapy*		
PR	306 (62.6)	—
SD	154 (31.5)	—
PD	29 (5.9)	—
Preoperative radiologic workup		
PET total body, *n* (%)	317 (44)	107 (46.1)
Number of LMs, median (range)	2 (1–31)	1 (1–4)
Maximum diameter (mm), median ± SD	24 ± 22.05	19.4 ± 23.0
Types of resection		
(1) Minor hepatectomy, *n*(%)	592 (82.1)	194 (83.6)
(2) Laparoscopic resection, *n*(%)	103 (14.3)	62 (26.7)
(3) Redo-resection, *n*(%)	50 (6.9)	28 (18)

BMI, body mass index; PR, partial response; SD, stable disease; PD, progression disease. *Rates calculated on 489 patients who received preoperative chemotherapy.

Table 2: Details of new CRLMs intraoperatively found in the whole population and in patients who did not receive preoperative chemotherapy.

New CRLM Features	Whole population ($n = 317$)	Patients without chemotherapy ($n = 31$)
Diameter (mm), median ± SD	6 ± 2.5	5 ± 2.3
Number per patients, median (range)	1 (1–9)	1 (1–6)
US aspect		
Hypoechoic, *n* (%)	245 (77.3)	27 (87)
Hyperechoic, *n* (%)	46 (14.5)	1 (9.6)
Isoechoic, *n* (%)	11 (3.4)	1 (3.2)
Location subglissonian, *n* (%)	75 (23.6)	6 (19.3)
New CRLMs identified by CE-IOUS, *n* (%)	19 (5.9)	2 (6.4)
New CRLMs identified by indirect signs, *n* (%)	12 (3.8)	1 (3.2)

number of CRLMs per patient was 1 (1–4). In this subset of patients, IOUS detected 68 (13.5%) histologically proven CRLMs in 31 patients (13.3%). IOUS also revealed 5 (0.9%) new nodules in 4 (1.7%) patients that—after resection—were classified by the pathologist as benign lesions (FP). On the other hand, all but one CRLM identified at MRI were confirmed intraoperatively. The median size of new CRLMs was 5 mm (1–7). CRLMs newly identified were mainly hypoechoic (27/31, 87%). Features of new CRLMs are summarized in Table 2.

3.2. Diagnostic Performance Analysis. Performance of MRI and intraoperative staging was compared on a patient-by-patient basis.

Overall early intrahepatic recurrences were 8.7%. To assess the diagnostic performance, 24 (3.3%) recurrences at the cut surface were excluded; thus, 5.4% of early relapses were considered for analysis. According to the rates of FP and FN patients, IOUS was more sensitive than MRI (94.5% vs 75.1%), while the specificity was similar (95.7% vs 95.9%). PPV of MRI was 79.7% vs 93.5% of IOUS while NPV was 95.7% (MRI) vs 96.5% (IOUS). The LR− was 0.26 (MRI) vs 0.07 (IOUS), and the LR+ was 17.5 (MRI) vs 21.9 (IOUS). Finally, Cohen's kappa coefficient was 0.73, indicating a substantial agreement between MRI and IOUS.

Diagnostic performance was also assessed among patients who did not receive preoperative chemotherapy. In this subset of patients, IOUS revealed a higher sensitivity (MRI 84%, IOUS 97.4%). Both sensitivity and sensibility (MRI 99.5%, IOUS 98.3%) were improved compared to those of the whole population with a substantial agreement between MRI and IOUS (Cohen's kappa coefficient = 0.80). All parameters considered for diagnostic performance analysis are detailed in Table 3.

3.3. Predictor of Missing CRLMs at MRI. We assessed predictors of missing CRLMs at MRI. Receiver operating characteristic curve analysis revealed a significant predictive value of the median number of preoperative chemotherapy

Table 3: Performance of intraoperative staging and MRI.

	Whole Population		No preop. chemotherapy	
	MRI	IOUS[1]	MRI	IOUS
Number of patients without FN lesions	541	682	195	226
Total number of patients	721	721	232	232
Sensitivity (%)	75.1	94.5	84.1	97.4
PPV (%)	79.7	93.5	83.7	97.8
LR−	0.26	0.07	0.16	0.03
	MRI	IOUS[1]	MRI	IOUS
Number of patients without FP lesions	692	690	231	228
Total of patients	721	721	232	232
Specificity (%)	95.9	95.7	99.5	98.3
NPV (%)	95.7	96.5	97.4	97.7
LR+	17.5	21.9	84	48.5

MRI, magnetic resonance imaging; FP, false positive; FN, false negative; PPV, positive predictive value; NPV, negative predictive value. [1]IOUS with or without contrast enhancement.

cycles (area under the curve 0.605; $p < 0.001$, $n = 5$ cycles, sensitivity 61.3%, and specificity 53.7%) and median number of metastases at preoperative imaging (area under curve 0.624; $p < 0.001$, $n = 3$ cycles, sensitivity 58.5%, and specificity 60%) for missing colorectal metastases at MRI.

Univariate analysis showed an increased risk to miss CRLMs at MRI among male patients ($p = 0.011$) and those who received preoperative chemotherapy ($p = 0.002$), particularly related to an irinotecan-based regimen ($p = 0.001$) or association with biologic agents ($p < 0.001$) and to the number of cycles administered ($p < 0.001$). MRI also more frequently missed CRLMs in cases of multiple (>3) lesions, metastases from mucinous tumors ($p < 0.001$), and nodules located at the hepatic dome or subglissonian ($p < 0.001$). In multivariate analysis, only location at the hepatic dome or subglissonian and mucinous histology resulted in predictive factors of missing metastases at MRI ($p < 0.001$). Results of uni- and multivariate analyses are reported in Table 4.

3.4. Intraoperative Staging and Long-Term Outcomes. Overall, 487 patients experienced recurrence after resection, whereas the liver was the site of relapse in 199 cases. Intrahepatic recurrences were significantly more frequent in patients with new CRLMs than without (36.2 vs 26.8%, $p = 0.027$). The R1 resection rate was 26.0% in patients with new CRLMs and 27.0% in patients without new CRLMs ($p = 0.834$). Adjuvant chemotherapy was administered similarly among patients with or without new CRLMs (66.4% vs 67.1%, $p = 0.768$). Among 721 patients, 3 postoperative deaths were excluded from survival analysis. Two-stage hepatectomy ($n = 8$) was considered part of one procedure. Finally, 710 patients were considered for analysis.

The 5-year OS (52.1% vs 37.8%, $p = 0.006$) and DF survival (45.1% vs 33%, $p = 0.002$) were significantly worse among patients with new CRLMs than without (Figures 1(a) and 1(b)).

4. Discussion

Nowadays, MRI with liver-specific agents is the most accurate radiologic imaging modality to stage hepatic disease in patients with CRLMs [10, 14]. As suggested by several studies, the evaluating hepatocyte-specific uptake enables accurate detection and characterization of CRLMs [11]. Furthermore, DWI allows an evaluation of changes in the diffusion properties of water molecules in tissues, which adds useful information to conventional imaging sequences [17]. These advantages of MRI are maintained even after chemotherapy. Macera et al. [18] demonstrated that combining DWI with gadoxetic agent-enhanced MRI (EOB-MRI) significantly increased the diagnostic accuracy (89.2%, 95%CI 83.4–93.4) and sensitivity (91%, 95%CI 85.1–95.1) in patients with CRLMs with preoperative chemotherapy; this was particularly effective in the detection of small lesions (<1 cm). In a randomized trial [13], comparison of the total number of CRLM detected at initial imaging *versus* the number found intraoperatively and at pathological examination of resected specimens showed the greatest number of patients with equal assessments (88%) in the EOB-MRI group (compared with 74% and 62% in conventional MRI and CT scan groups, respectively). Diagnostic confidence was high or very high for 98.3% of patients with EOB-MRI; consequently, surgical plans were less frequently changed during surgery (28%) compared with patients staged by conventional MRI (32%) or CT scan (47%).

Considering the improved performance of MRI over time, it can be assumed that intraoperative staging has a limited value at present. In the present study, the diagnostic performance of IOUS was superior to MRI. New histologically proven CRLMs were found in 11.1% of patients. The high rate of FN explains the low sensitivity of MRI. However, in patient-by-patient analysis, specificity remains high for both MRI and IOUS. This reflects the low FP rate for both techniques, which enable adequate characterization of liver nodules in most cases. In 2013, we demonstrated [9] that IOUS showed the best diagnostic performance compared with CT scan, PET, and MRI. We assessed the performance of staging techniques comparing the pre- and intraoperative findings with the results of pathological examination and early intrahepatic recurrence at 6 months after surgery as an indicator of residual disease. This parameter is a good marker for FN for both preoperative staging and intraoperative staging, and it allows precise evaluation of the drawbacks of IOUS. Therefore, this methodological approach was also applied in the present series.

Table 4: Univariate and multivariate analyses of factors predicting missing metastases at MRI.

	Univariate analysis			Multivariate analysis	
	Missing CRLMs ($n = 146$)	No missing CRLMs ($n = 575$)	p	OR (CI 95%)	p
Age (years)	63 ± 10.6	64 ± 10.8	0.742	—	
Sex male	105 (71.9)	348 (60.5)	0.011	n.s.	
BMI ≥30 kg/m^2	24 (16.4)	85 (14.8)	0.618		
Chemotherapy regimen data					
Preoperative chemotherapy	115 (78.8)	374 (65.0)	0.002	n.s	
Oxaliplatin based	82 (56.2)	276 (48.0)	0.078	—	
Irinotecan based	58 (39.7)	150 (26.1)	0.001	n.s	
Oxaliplatin or irinoteca plus biologics*	87 (59.6)	222 (38.6)	<0.001	n.s	
Number of cycles	6 ± 7.50	4 ± 5.66	<0.001	—	
Number of cycles >5	94 (64.4)	284 (49.4)	0.001	n.s	
Preoperative imaging data					
Number of CRLMs	4 ± 3.9	2 ± 4.2	<0.001	—	
Number of CRLMs >3	97 (66.4)	261 (45.4)	<0.001	n.s	
Diameter (mm)	20 ± 17.2	24 ± 23.0	0.103	—	
Location					
Subglissonian	25 (17.1)	3 (0.5)	<0.001	44.494 (11.785–167.977)	<0.001
Hepatic dome	60 (41)	10 (1.7)	<0.001	46.097 (20.911–101.617)	<0.001
Mucinous histology	42 (28.8)	14 (2.4)	<0.001	23.805 (11.173–50.719)	<0.001
Redo-resection	8 (5.5)	42 (7.3)	0.438	—	
Hepatic steatosis	111 (76.0)	396 (68.9)	0.091	—	
Mild	59 (40.4)	232 (40.3)	0.988	—	
Moderate	42 (28.7)	117 (20.3)	0.037	n.s.	
Severe	10 (6.8)	47 (8.1)	0.720	—	
No fatty	35 (23.9)	179 (31.1)	0.112	—	

Data are expressed as number (%) or median ± SD. BMI, body mass index; LM, liver metastasis; MRI, magnetic resonance imaging; IOUS, intraoperative ultrasonography. *Bevacizumab or cetuximab or panitumumab.

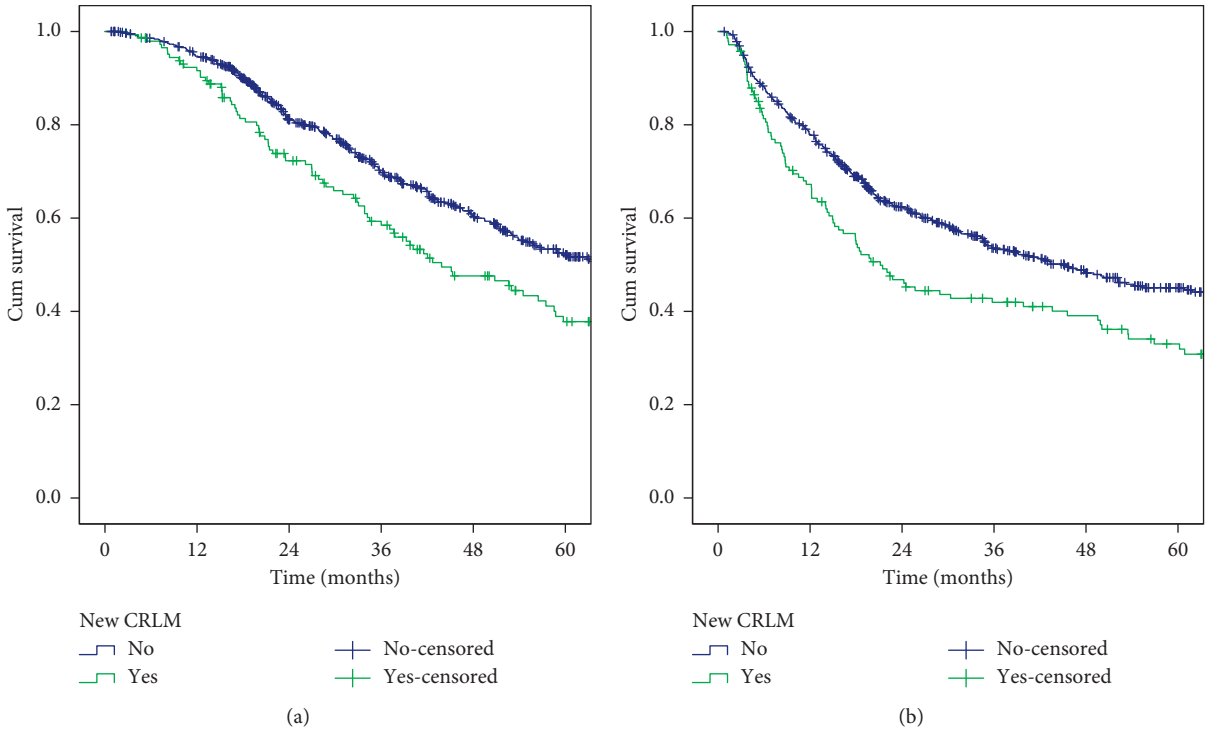

Figure 1: Overall (a) and disease-free (b) survival rates after hepatectomy. Comparison between patients with new CRLMs (green line) and without (blue line).

It is well known that preoperative chemotherapy may negatively affect the accuracy of preoperative staging and intraoperative staging [19]. This is mainly due to the chemotherapy-related changes in liver parenchyma and modification of CRLM features. After chemotherapy, MRI with liver-specific contrast agents guarantees the most accurate preoperative staging of hepatic disease compared to other imaging modalities [20]. However, some small CRLMs may disappear at preoperative MRI after chemotherapy [21]. In this series, vanishing metastases at preoperative MRI were excluded from the analysis to avoid a possible overestimation of new CRLMs intraoperatively found. Moreover, to overcome the potential bias related to the chemotherapy administration, we also evaluated the diagnostic performance of MRI and IOUS in patients who underwent liver resection without preoperative chemotherapy. In this subset of patients, sensibility and sensitivity of both MRI and IOUS were improved. Nevertheless, IOUS assured the higher sensitivity rate.

To depict the pitfalls in the MRI staging, we assessed the predictors of "missing" metastases at MRI. Multivariate analysis demonstrated an increased risk of missing CRLMs at MRI in the case of subglissonian nodules or located at hepatic dome, such as for metastases from mucinous tumors. The liver surface can be better assessed intraoperatively [5, 18, 22, 23]; moreover, the evaluation of the hepatic dome during MRI may be limited by artefacts related to respiratory movement. Furthermore, mucinous tumors could mimic benign lesions, worsening the diagnostic accuracy, particularly in the case of small nodules [24, 25]. In agreement with previous studies [4, 9], we confirmed that newly identified CRLMs are more likely to be hypoechoic. Because of steatosis or postchemotherapy changes in the hepatic parenchyma, patients who underwent hepatectomy for CRLMs often present a "bright" liver. This condition enables detection of hypoechoic nodules and reduces the value of CE-IOUS staging because the liver is naturally enhanced [2]. These findings could explain the high accuracy of IOUS reported in the present series, even if CE-IOUS was not performed systematically.

Several surgical series [2–9] have reported the superiority of IOUS to stage hepatic disease in CRLMs compared with various imaging modalities. The improvements of imaging modalities over the years represent a challenge for the current role of IOUS. As expected, the rate of new CRLMs found by IOUS decreased in the most recent series but remains noteworthy (ranging from 8% to 21%). Unfortunately, results from published studies cannot be generalized because of extreme variability related to the different preoperative workup and technological progress over time. Notably, the present study considered many patients resected in recent years at two tertiary centers. This population is homogeneous, and the process of MRI with liver-specific contrast agents was similar for all patients. Previous published data also showed that the impact on management is extremely heterogeneous and it is strongly affected by surgical policies. Our centers shared a parenchymal sparing philosophy to face CRLMs; this explains the significant impact of intraoperative findings on changing surgical plans.

In patients with HCC, the intraoperative detection of new tumors negatively affects oncologic outcomes [26]. However, the impact of new CRLMs on long-term outcomes has been poorly evaluated. In the present study, we showed that hepatic recurrences are significantly more frequent among patients with newly identified CRLMs and they present worse OS and DF survival. We previously demonstrated that additional CRLMs are more likely to be found in patients with more aggressive disease. We therefore suggest considering the new CRLMs during postoperative decision making along with other known prognostic factors. For example, this subset of patients may benefit from adjuvant chemotherapy to reduce the risk of relapse. Moreover, because the possibility of reresection for recurred CRLMs can significantly improve survival [27], we also suggest a strict postoperative surveillance to detect and manage hepatic recurrences as early as possible.

This study presents some limitations, mainly related to its retrospective nature. Even if both IOUS and RM were performed by surgeons and radiologists skilled in the field of liver malignancies, different physicians were involved in the study. Nevertheless, this is the largest series to date focusing on this topic and comparing the performance of MRI with liver-specific contrast agents to IOUS.

In conclusion, IOUS improves staging in patients undergoing resection for CRLMs even in the era of liver-specific MRI. Intraoperative detection of new CRLMs negatively affects oncologic outcomes.

Data Availability

The prospective data used to support the findings of this study are restricted by the ethics committee of Mauriziano Hospital in order to protect patient privacy. Data are available from corresponding author for researchers who meet the criteria for access to confidential data.

Disclosure

This paper is based on a previous communication of preliminary results during the 12th Biennial E-AHPBA Congress, 23–26 May 2017, Mainz, Germany.

Conflicts of Interest

The authors declare that they have no conflicts of interest.

Acknowledgments

The authors thank Dr. Elena Ostuni and Dr. Fabio Forchino for their contribution to data collection.

References

[1] M. C. Niekel, S. Bipat, and J. Stoker, "Diagnostic imaging of colorectal liver metastases with CT, MR imaging, FDG PET, and/or FDG PET/CT: a meta-analysis of prospective studies including patients who have not previously undergone treatment," *Radiology*, vol. 257, no. 3, pp. 674–684, 2010.

[2] G. Torzilli, F. Botea, F. Procopio et al., "Use of contrast-enhanced intraoperative ultrasonography during liver surgery for colorectal cancer liver metastases—its impact on operative outcome. Analysis of a prospective cohort study," *European Journal of Cancer Supplements*, vol. 6, no. 11, pp. 16–23, 2008.

[3] C. Sietses, M. R. Meijerink, S. Meijer, and M. P. van den Tol, "The impact of intraoperative ultrasonography on the surgical treatment of patients with colorectal liver metastases," *Surgical Endoscopy*, vol. 24, no. 8, pp. 1917–1922, 2010.

[4] M. G. van Vledder, T. M. Pawlik, S. Munireddy, U. Hamper, M. C. de Jong, and M. A. Choti, "Factors determining the sensitivity of intraoperative ultrasonography in detecting colorectal liver metastases in the modern era," *Annals of Surgical Oncology*, vol. 17, no. 10, pp. 2756–2763, 2010.

[5] S. Hata, H. Imamura, T. Aoki et al., "Value of visual inspection, bimanual palpation, and intraoperative ultrasonography during hepatic resection for liver metastases of colorectal carcinoma," *World Journal of Surgery*, vol. 35, no. 12, pp. 2779–2787, 2011.

[6] M. D'Hondt, F. Vandenbroucke-Menu, S. Préville-Ratelle et al., "Is intra-operative ultrasound still useful for the detection of a hepatic tumour in the era of modern pre-operative imaging?," *HPB (Oxford)*, vol. 13, no. 9, pp. 665–669, 2011.

[7] A. M. Lucchese, A. N. Kalil, A. Schwengber, E. Suwa, and G. G. Rolim de Moura, "Usefulness of intraoperative ultrasonography in liver resections due to colon cancer metastasis," *International Journal of Surgery*, vol. 20, pp. 140–144, 2015.

[8] J. Hoareau, A. Venara, J. Lebigot et al., "Intraoperative contrast-enhanced ultrasound in colorectal liver metastasis surgery improves the identification and characterization of nodules," *World Journal of Surgery*, vol. 40, no. 1, pp. 190–197, 2016.

[9] A. Ferrero, S. Langella, F. Giuliante et al., "Intraoperative liver ultrasound still affects surgical strategy for patients with colorectal metastases in the modern era," *World Journal of Surgery*, vol. 37, no. 11, pp. 2655–2663, 2013.

[10] S. Patel, S. Cheek, H. Osman, and D. R. Jeyarajah, "MRI with gadoxetate disodium for colorectal liver metastasis: is it the new "imaging modality of choice"?," *Journal of Gastrointestinal Surgery*, vol. 18, no. 12, pp. 2130–2135, 2014.

[11] N. Seo, M.-S. Park, K. Han et al., "Magnetic resonance imaging for colorectal cancer metastasis to the liver: comparative effectiveness research for the choice of contrast agents," *Cancer Research and Treatment*, vol. 50, no. 1, pp. 60–70, 2018.

[12] T. D. Vreugdenburg, N. Ma, J. K. Duncan, D. Riitano, A. L. Cameron, and G. J. Maddern, "Comparative diagnostic accuracy of hepatocyte-specific gadoxetic acid (Gd-EOB-DTPA) enhanced MR imaging and contrast enhanced CT for the detection of liver metastases: a systematic review and meta-analysis," *International Journal of Colorectal Disease*, vol. 31, no. 11, pp. 1739–1749, 2016.

[13] C. J. Zech, P. Korpraphong, A. Huppertz et al., "Randomized multicentre trial of gadoxetic acid-enhanced MRI versus conventional MRI or CT in the staging of colorectal cancer liver metastases," *British Journal of Surgery*, vol. 101, no. 6, pp. 613–621, 2014.

[14] P. Therasse, S. G. Arbuck, E. A. Eisenhauer et al., "New guidelines to evaluate the response to treatment in solid tumors. European organization for research and treatment of cancer, national cancer institute of the United States, national cancer institute of Canada," *Journal of the National Cancer Institute*, vol. 92, no. 3, pp. 205–216, 2000.

[15] D. E. Kleiner, E. M. Brunt, M. Van Natta et al., "Design and validation of a histological scoring system for nonalcoholic fatty liver disease," *Hepatology*, vol. 41, no. 6, pp. 1313–1321, 2005.

[16] S. M. Strasberg, J. Belghiti, P.-A. Clavien et al., "The Brisbane 2000 terminology of liver anatomy and resection," *HPB*, vol. 2, no. 3, pp. 333–339, 2000.

[17] B. Taouli and D. M. Koh, "Diffusion-weighted MR imaging of the liver: a critical look," *Radiology*, vol. 254, pp. 47–66, 2010.

[18] A. Macera, C. Lario, M. Petracchini et al., "Staging of colorectal liver metastases after preoperative chemotherapy. Diffusion-weighted imaging in combination with Gd-EOB-DTPA MRI sequences increases sensitivity and diagnostic accuracy," *European Radiology*, vol. 23, no. 3, pp. 739–747, 2013.

[19] P. J. A. Robinson, "The effects of cancer chemotherapy on liver imaging," *European Radiology*, vol. 19, no. 7, pp. 1752–1762, 2009.

[20] C. S. van Kessel, C. F. M. Buckens, M. A. A. J. van den Bosch, M. S. van Leeuwen, R. van Hillegersberg, and H. M. Verkooijen, "Preoperative imaging of colorectal liver metastases after neoadjuvant chemotherapy: a meta-analysis," *Annals of Surgical Oncology*, vol. 19, no. 9, pp. 2805–2813, 2012.

[21] A. Ferrero, S. Langella, N. Russolillo, L. Vigano', R. Lo Tesoriere, and L. Capussotti, "Intraoperative detection of disappearing colorectal liver metastases as a predictor of residual disease," *Journal of Gastrointestinal Surgery*, vol. 16, no. 4, pp. 806–814, 2012.

[22] A. Foroutani, A. M. Garland, E. Berber et al., "Laparoscopic ultrasound vs triphasic computed tomography for detecting liver tumors," *Archives of Surgery*, vol. 135, no. 8, pp. 933–938, 2000.

[23] L. Viganò, A. Ferrero, M. Amisano, N. Russolillo, and L. Capussotti, "Comparison of laparoscopic and open intraoperative ultrasonography for staging liver tumours," *British Journal of Surgery*, vol. 100, no. 4, pp. 535–542, 2013.

[24] A. Lacout, M. El Hajjam, C. Julie, P. Lacombe, and J. P. Pelage, "Liver metastasis of a mucinous colonic carcinoma mimicking a haemangioma in T2-weighted sequences," *Journal of Medical Imaging and Radiation Oncology*, vol. 52, no. 6, pp. 580–582, 2008.

[25] L. J. Qian, J. Zhu, Z. G. Zhuang, Q. Xia, Q. Liu, and J. R. Xu, "Spectrum of multilocular cystic hepatic lesions: CT and MR imaging findings with pathologic correlation," *Radiographics*, vol. 33, no. 5, pp. 1419–1433, 2013.

[26] K. Zhang, N. Kokudo, K. Hasegawa et al., "Detection of new tumors by intraoperative ultrasonography during repeated hepatic resections for hepatocellular carcinoma," *Archives of Surgery*, vol. 142, no. 12, pp. 1170–1175, 2007.

[27] L. Viganò, N. Russolillo, A. Ferrero, S. Langella, E. Sperti, and L. Capussotti, "Evolution of long-term outcome of liver resection for colorectal metastases: analysis of actual 5-year survival rates over two decades," *Annals of Surgical Oncology*, vol. 19, no. 6, pp. 2035–2044, 2012.

Hindawi
Journal of Oncology
Volume 2019, Article ID 4049287, 8 pages
https://doi.org/10.1155/2019/4049287

Research Article

Quantitative Volumetric Assessment of Ablative Margins in Hepatocellular Carcinoma: Predicting Local Tumor Progression Using Nonrigid Registration Software

P. Hendriks,[1,2] **W. A. Noortman**,[1,2] **T. R. Baetens**,[1] **A. R. van Erkel**,[1] **C. S. P. van Rijswijk**,[1] **R. W. van der Meer**,[1] **M. J. Coenraad**,[3] **L. F. de Geus-Oei**,[1,4] **C. H. Slump**,[5] **and M. C. Burgmans**[1]

[1]*Department of Radiology, Leiden University Medical Center, Leiden, Netherlands*
[2]*Technical Medicine, University of Twente, Enschede, Netherlands*
[3]*Department of Gastroenterology and Hepatology, Leiden University Medical Center, Leiden, Netherlands*
[4]*Biomedical Photonic Imaging Group, TechMed Centre, University of Twente, Enschede, Netherlands*
[5]*Department of Robotics and Mechatronics, University of Twente, Enschede, Netherlands*

Correspondence should be addressed to P. Hendriks; p.hendriks@lumc.nl

Received 25 April 2019; Revised 13 July 2019; Accepted 28 August 2019; Published 19 September 2019

Academic Editor: Roberto Iezzi

Purpose. After radiofrequency ablation (RFA) of hepatocellular carcinoma (HCC), pre- and postinterventional contrast-enhanced CT (CECT) images are usually qualitatively interpreted to determine technical success, by eyeballing. The objective of this study was to evaluate the feasibility of quantitative assessment, using a nonrigid CT-CT coregistration algorithm. *Materials and Methods*. 25 patients treated with RFA for HCC between 2009 and 2014 were retrospectively included. Semiautomated coregistration of pre- and posttreatment CECT was performed independently by two radiologists. In scans with a reliable registration, the tumor and ablation area were delineated to identify the side and size of narrowest RFA margin. In addition, qualitative assessment was performed independently by two other radiologists to determine technical success and the anatomical side and size of narrowest margin. Interobserver agreement rates were determined for both methods, and the outcomes were compared with occurrence of local tumor progression (LTP). *Results*. CT-CT coregistration was technically feasible in 18/25 patients with almost perfect interobserver agreement for quantitative analysis ($\kappa = 0.88$). The interobserver agreement for qualitative RFA margin analysis was $\kappa = 0.64$. Using quantitative assessment, negative ablative margins were found in 12/18 patients, with LTP occurring in 8 of these patients. In the remaining 6 patients, quantitative analysis demonstrated complete tumor ablation and no LTP occurred. *Conclusion*. Feasibility of quantitative RFA margin assessment using nonrigid coregistration of pre- and postablation CT is limited, but appears to be a valuable tool in predicting LTP in HCC patients ($p = 0.013$).

1. Introduction

Radiofrequency ablation (RFA) has been recognized as first line treatment for very early-stage hepatocellular carcinoma (HCC) (lesion diameter <2 cm) and is used as treatment for unresectable early-stage HCC (solitary lesion, or a maximum of 3 lesions with a diameter ≤3 cm each), according to the Barcelona Clinic for Liver Cancer (BCLC) staging system [1, 2]. As a result of the implementation of surveillance in high-risk populations, diagnosis of BCLC very early- or early-stage HCC is now feasible in up to 60% of all new HCC cases in developed countries [3]. This makes RFA an increasingly used treatment modality. Recurrence rates for RFA in very early-stage HCC patients are comparable to those after surgical treatment [1]. However, higher recurrence rates are found in patients treated for larger HCC lesions [4–6].

After RFA treatment, two types of intrahepatic recurrences may occur. Local tumor progression (LTP) is found in up to 50% of ablations [7] and is known to be associated with insufficient ablative margin, large tumor size,

blood vessels in the direct proximity of the tumor, and adhesion of viable tumor cells to the RFA electrodes [8]. Distant intrahepatic recurrence is related more to systemic parameters, such as the presence of vascular invasion, multifocal disease, elevated alpha-fetoprotein blood levels, and hepatitis C viral infection [9].

The preferred treatment for early-stage HCC is surgical resection. However, many patients are not eligible for this treatment, due to cirrhosis with portal hypertension, unfavorable tumor location, and/or comorbidities [1, 10]. Thermal ablation is considered as the treatment of choice for unresectable early-stage HCC up to 5 cm. Distant intrahepatic recurrence rates after resection and ablation are similar, but LTP rates are higher after ablation and negatively affect overall survival [4–6, 11]. To improve the results of RFA in unresectable early-stage HCC, a reduction of LTP rates appears to be crucial.

Histological confirmation of total tumor necrosis after RFA is not possible. In many centers, the current workflow involves qualitative assessment of RFA margins by scrolling through pre- and postinterventional images, separately. Technical success is considered when a predefined amount of energy is successfully delivered to the tumor, and complete tumor coverage with sufficient ablative margins is confirmed on contrast-enhanced computed tomography (CECT) [8]. In general, an ablative margin of >5 mm, or ideally 10 mm, is recommended [8]. These values are rather arbitrarily derived from surgical standards and supported by some studies [10–12]. However, the evidence is limited, and no standardized way of ablative margin assessment is currently available.

Supportive ablation verification software has gained interest. However, at this moment, software dedicated to quantitative ablation margin assessment is lacking and available software has not been validated in large patient cohorts. Merging of pre- and postablation scans can be performed using either nonrigid or rigid coregistration software. Nonrigid coregistration algorithms allow more degrees of freedom in the transformation to fit a scan better onto another. Besides global linear transformations, like translation and rotation, the algorithm may, e.g., use radial basis functions or other free form deformation models that allow for local warping of the image to find a better registration. Mirada RTx (Mirada Medical Ltd., Oxford, UK) is a software application developed for radiation therapy treatment planning that uses nonrigid registration of medical image datasets including computed tomography (CT) and magnetic resonance imaging (MRI). This software was used in this study.

The primary objective of this study was to assess the feasibility of quantitative three-dimensional (3D) margin assessment after nonrigid CT-CT coregistration of pre- and postinterventional imaging, using Mirada RTx. Secondary objectives were to compare quantitative ablative margin assessment with the current workflow of qualitative assessment and to assess whether quantitative assessment allows prediction of local tumor progression.

2. Methodology

2.1. Patients. All patients that were consecutively treated with RFA for de novo HCC between January 2009 and March 2014 ($n = 79$) in our institution were identified retrospectively. The diagnosis of HCC was based on either histology or radiological findings according to European Association for the Study of the Liver (EASL) criteria (arterial enhancing lesion >1 cm with washout on the late phase on CT or MRI). Exclusion criteria were multifocal disease ($n = 27$), surgical approach ($n = 4$), adjuvant trans-arterial chemoembolization (TACE) ($n = 7$), lateral patient positioning on the postablation scan ($n = 11$), and extensive metal artifacts caused by in-vivo RFA probes ($n = 5$). Finally, 25 patients were included in this study. Baseline characteristics of this cohort are shown in Table 1. Pre- and postablation multiphase CECT scans with an arterial and portal venous phase were available for all patients.

2.2. RFA Procedure. Percutaneous RFA procedures were performed under general anesthesia and with image guidance of ultrasound and/or CT. Based on tumor size and availability, one of the single electrode RFA systems (3 cm exposed tip Cooltip (Covidien Ltd., Gosport, Hampshire, United Kingdom)) or StarBurst XL (AngioDynamics, Amsterdam, Netherlands)) or multiple electrode RFA systems (3 or 4 cm exposed tip Cooltip with switch control system (Covidien Ltd.)) was used. The ablation time was set 12 minutes for single Cooltip electrode and 16 minutes for the multiple Cooltip electrodes. Temperature-based ablation was performed with the StarBurst XL electrode.

Immediately after ablation, a CECT scan of the liver was performed on a 16-slice spiral CT (Aquilion-16, Toshiba, Tokyo, Japan) with the following settings: 120 kV, rotation 0.5 s, and 16×1 mm scanning. Dose weight-dependent Ultravist 370 contrast agent or Xenetix 350 contrast agent was used with a 15-second and 75-second delay after bolus triggering for arterial phase and portal venous phase, respectively. Consequently, the CECT scans were qualitatively evaluated for technical success. The ablation was considered technically successful if the coagulation area fully encompassed the tumor in the absence of residual tumor enhancement. This assessment was done by visual comparison of the tumor location on preprocedural CT and area of necrosis on the postprocedural CT ("eyeballing") and 2D measurements.

2.3. Follow-Up. All patients underwent blood tests (including alpha-fetoprotein) and CECT every three months after treatment. Upon discretion of the referring physician or interventional radiologist, multiphase MRI was used instead of CECT. Liver explants of patients that underwent an orthotopic liver transplantation (OLTx) were pathologically examined for local tumor progression. The median follow-up time was 9.5 months.

2.4. Scoring. CT-CT registration and delineation of the tumor volume and RFA ablation volume were performed in Mirada RTx software. Two radiologists independently performed the CT-CT coregistration and delineation of the tumor and RFA ablation volume, while being blinded for

Table 1: Characteristics of analyzed patients.

	n	
Total	25	
Age		
Mean (SD)	62, 1	11.8
Sex		
Male	20	80.0%
Female	5	20.0%
Cirrhosis presence		
Yes	25	100.0%
No	0	0.0%
Ascites presence		
Yes	7	28.0%
No	18	72.0%
Etiology		
Hepatitis B	2	8.0%
Hepatitis C	8	32.0%
Alcohol abuse	15	60.0%
NASH	2	8.0%
Cryptogenic	1	4.0%
ECOG		
0	24	96.0%
1	1	4.0%
Child–Pugh score		
A	12	48.0%
B	13	52.0%
C	0	0.0%
BCLC		
Very early	10	40.0%
Early	15	60.0%
Lesion size (mm)		
Median (range)	20	12–45
Year of RFA		
2009–2011	10	31.3%
2012–2014	15	46.9%

NASH = nonalcoholic steatohepatitis; ECOG = Eastern Cooperative Oncology Group; BCLC = Barcelona Clinic for Liver Cancer; RFA = radiofrequency ablation. More etiological factors could be present in one patient.

follow-up information. CT-CT coregistration was performed using a semiautomated nonrigid registration. Manual alterations were possible by rotation and translation of a scan or with use of a rigid landmark algorithm. The registration performance was graded on a 5-point scale (1 = completely unreliable coregistration; 2 = suboptimal coregistration; 3 = sufficient quality of coregistration, but not accurate enough for measurements in mm; 4 = good coregistration; 5 = perfect coregistration). Patients with coregistration performances of 1–3 were excluded from further analysis.

A greyscale-based semiautomatic delineation tool was used with manual adjustments for segmentation of the tumor and ablation volume. RFA margins were quantitatively assessed in a fused image window. The narrowest margin (in mm) as well as the anatomical location of the narrowest margin or largest tumor residue was determined. Interobserver agreement was determined for the categorical assessment of margin size (1: negative, 2: 0 to 5 mm, or 3: ≥5 mm). A "negative" margin was defined as tumor extending beyond the boundaries of the ablation zone on the overlay of pre- and postablation CT. This would not necessarily mean that the tumor was incompletely ablated. The ablation may have caused tissue shrinkage, and as a result, the ablation area may be smaller than the tumor even when the tumor was completely ablated. The side of LTP occurrence was correlated with the side of the minimal ablative margin or largest tumor residual. A comparison of patient characteristics between those with and without LTP was performed.

Two other radiologists independently repeated the qualitative assessment of the pre- and postablation scans for technical success and determined categorical ablative margins (1: negative, 2: 0 to 5 mm, or 3: ≥5 mm), while being blinded for follow-up information. Also, the anatomical side of narrowest margin was recorded. Interobserver agreement rates were determined for technical success and margin size. In both the quantitative and the qualitative assessment, a consensus reevaluation took place by the two radiologists for determining technical success for cases they initially disagreed on.

2.5. Statistics. Interobserver agreement was determined with use of unweighted Cohen's kappa statistics. A κ of 0 meant that the agreement was similar to chance, whereas a κ of 1 meant perfect agreement [13].

Continuous data were analyzed with the independent *t*-test and categorical data with the chi-square test. SPSS version 23.0 was used to perform the data analysis, and a significance interval of 5% was used. Boxplots were created using GraphPad Prism 5 (GraphPad Software, San Diego, California, USA).

3. Results

3.1. Patients. The coregistration quality of pre- and postablation scans was rated ≤3 in 7/25 (28.0%) patients, who were therefore excluded for further analysis. Table 2 shows all patient and tumor characteristics of the 18 remaining cases that were technically feasible for quantitative analysis.

3.2. Scoring. The interobserver agreement for *quantitative* assessment with use of CT-CT coregistration and delineation was almost perfect, with a κ of 0.88 (SE: 0.12 and $p < 0.01$). Categorical agreement on the minimal margin size (negative, 0 to 5 mm, or ≥5 mm) was similar with a κ of 0.88 (SE: 0.12 and $p < 0.01$). A consensus reevaluation of one case led to agreement on technical success that the radiologists initially disagreed on.

The interobserver agreement of two radiologists who *qualitatively* assessed the ablative margins was moderate: 0.64 (SE: 0.33 and $p < 0.01$). Agreement on categorical margin assessment was very poor (negative, 0 to 5 mm, or ≥5 mm) with a κ of 0.24 (SE of 0.28 and $p = 0.16$). Consensus was reached between the observers on technical success for two cases that they initially disagreed on, for further analysis.

3.3. Local Tumor Progression Rate. In 8 out of 18 patients (44.4%), LTP was found, either radiologically (5/8), or

Table 2: Characteristics of patients technically feasible for quantitative analysis.

	Total		No LTP		LTP		
	n		*n*		*n*		*p* value
Total	**18**		10		8		
Age							
Mean (SD)		**64.9 (9.0)**		66.1 (10.7)		63.4 (6.5)	*0.538*
Sex							
Male	**14**	**77.8%**	7	70.0%	7	87.5%	*0.375*
Female	**4**	**22.2%**	3	30.0%	1	12.5%	
Cirrhosis presence							
Yes	**18**	**100.0%**	10	100.0%	8	100.0%	
No	**0**	**0.0%**	0	No	0	0.0%	
Ascites presence							
Yes	**5**	**27.8%**	3	30.0%	2	25.0%	*0.814*
No	**13**	**72.2%**	7	70.0%	6	75.0%	
Etiology							
Hepatitis B	**0**		0		0		*0.800*
Hepatitis C	**4**		2		2		*0.410*
Alcohol abuse	**5**		2		3		*0.180*
NASH	**2**		2		0		*0.250*
ECOG							
0	**17**	**94.4%**	10	100.0%	7	87.5%	*0.250*
1	**1**	**5.6%**	0	No	1	12.5%	
Child–Pugh score							
A	**9**	**50.0%**	5	50.0%	4	50.0%	*1.000*
B	**9**	**50.0%**	5	50.0%	4	50.0%	
BCLC							
Very early	**6**	**33.3%**	3	30.0%	3	37.5%	*0.737*
Early	**12**	**66.7%**	7	70.0%	5	62.5%	
Lesion size							
Median in mm (range)		**22 (12–27)**		22 (12–27)		22 (16–25)	
OLTx <18 months							
Yes	**6**	**33.3%**	3	30.0%	3	37.5%	*0.737*
No	**12**	**66.7%**	7	70.0%	5	62.5%	
Distant intrahepatic recurrence							
Yes	**1**	**5.6%**	1	10.0%	0	0.0%	*0.357*
No	**17**	**94.4%**	9	90.0%	8	100.0%	
RFA on target quantitative assessment							
Yes	**6**	**33.3%**	6	60.0%	0	0.0%	*0.013*
No	**12**	**66.7%**	4	40.0%	8	100.0%	
RFA on target qualitative assessment							
Yes	**16**	**88.9%**	10	100.0%	6	75.0%	*0.094*
No	**2**	**11.1%**	0		2	25.0%	
Year of RFA							
2009–2011	**7**	**38.9%**	2	20.0%	5	62.5%	*0.066*
2012–2014	**11**	**61.1%**	8	80.0%	3	37.5%	

NASH = nonalcoholic steatohepatitis; ECOG = Eastern Cooperative Oncology Group; BCLC = Barcelona Clinic for Liver Cancer; RFA = radiofrequency ablation. More etiological factors could be present in one patient.

histologically after OLTx (3/8). In 1 (5.6%) patient, distant intrahepatic recurrence was found. Out of the 10 (55.6%) patients who did not develop recurrence, 3 underwent OLTx within 1 year after RFA (average 9.3 months).

Differences in patient and tumor characteristics were analyzed between patients who developed LTP ($n = 8$) and patients who did not ($n = 10$). No significant differences were found in patient and tumor characteristics between the groups.

Based on the *quantitative* analysis, RFA necrosis fully encompassed the tumor in 6/18 (33.3%) of all patients, with a mean margin of 0.91 mm (SD: 1.11; range: 0–3 mm). In none of these patients, LTP was found. Out of the other 12 patients, 8 (66.7%) developed LTP (5 cases of LTP were identified radiologically, and 3 cases of LTP were pathologically proven after OLTx). LTP was associated with insufficient ablative margins, with a p value of 0.013. All patients who developed local tumor progression, did so at (one of) the anatomical side(s) with a negative ablative margin. An example of the entire workup and occurrence of local recurrence at a negative ablative margin is shown in Figure 1.

The average minimal ablative margin in all cases was −6.38 mm (SD: 4.64). The ablative margin size significantly

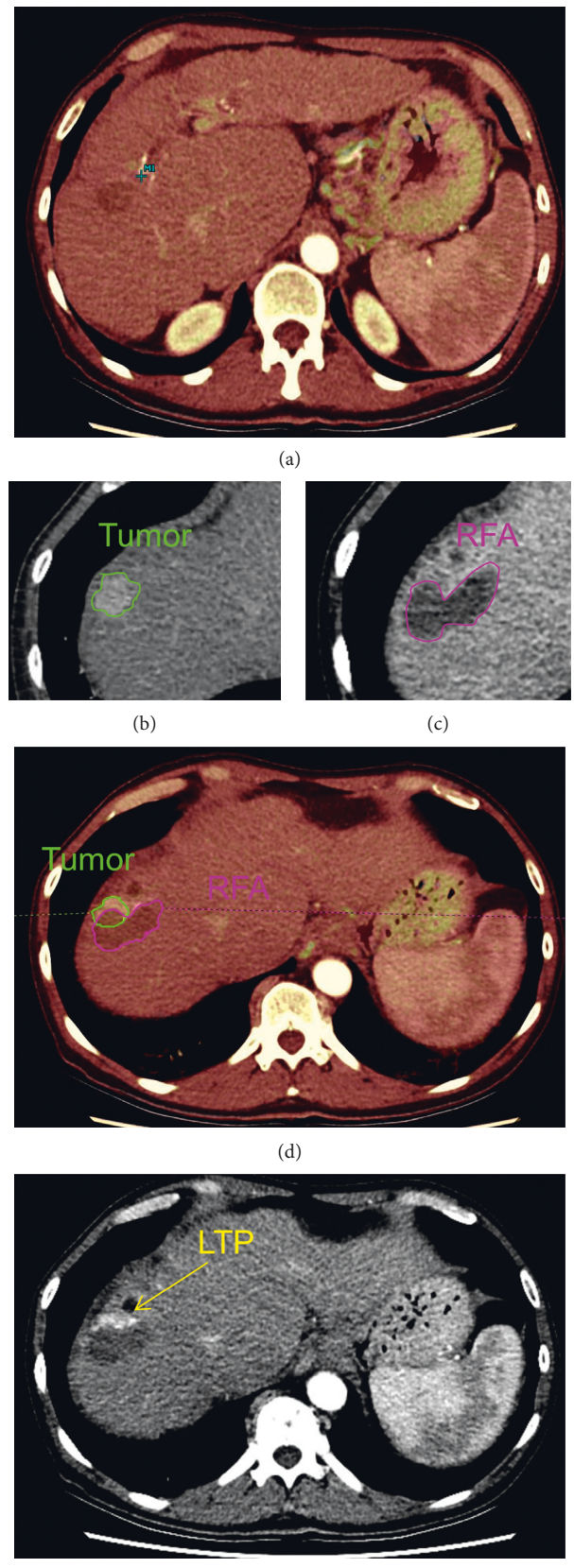

(a)

(b)

(c)

(d)

(e)

Figure 1: Image analysis protocol. (a) Registration (overlay) of preinterventional and postinterventional CT scans. (b) Semiautomatic delineation of tumor volume. (c) Semiautomatic delineation of RFA volume. (d) Image fusion plane: margin analysis by overlaying pre- and postinterventional imaging. (e) Follow-up scan with local tumor progression.

correlated to the occurrence of LTP with a p value of 0.001. The mean ablative margin of patients who developed LTP was −8.44 mm (SD: 4.27) and −0.30 mm (SD: 2.00) for patients who did not, as can be seen in Figure 2.

Based on the qualitative analysis, 16/18 (88.9%) ablation areas fully encompassed the tumor. Yet, 6 of these patients (42.9%) developed LTP during FU. In 2 (11.1%) patients, the observers concluded that the ablation zone did not completely cover the tumor; these two patients did develop LTP.

One patient developed intrahepatic distant metastatic disease within 18 months after treatment. This was a patient with a fully ablated initial tumor with no LTP.

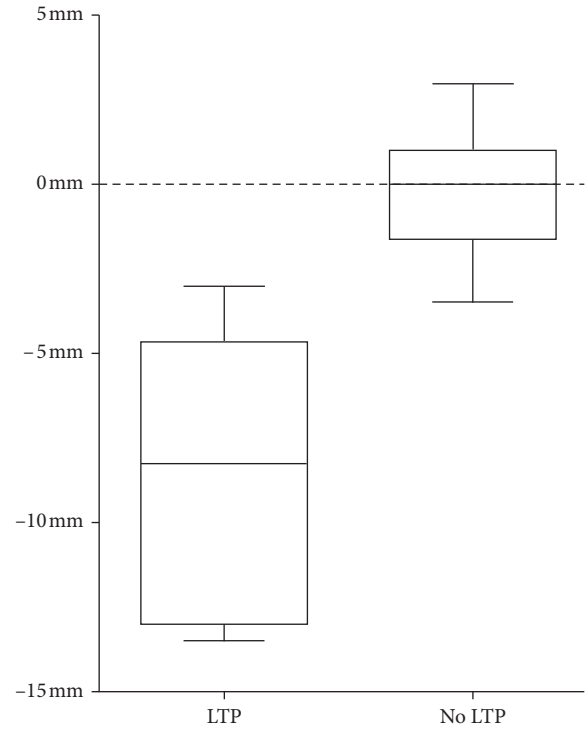

Figure 2: Boxplot of quantitative ablative margin size for patients with and without local tumor progression (LTP).

4. Discussion

In this retrospective pilot study, quantitative ablative margin assessment using Mirada RTx software was feasible only in selected patients as in 7 out of 25 patients, the performance of coregistration was insufficient. However, high interobserver agreement rates were found for quantitative assessment in the remaining 18 patients. LTP occurrence correlated with negative margin sizes with $p = 0.013$, indicating a predictive value of quantitative margin assessment.

A disadvantage of minimally invasive HCC treatments is that no pathological confirmation of treatment success can be obtained. The chance on treatment success is generally thought to increase when aiming at safety margins of 5 or 10 mm, to overcome potential heat-transduction variations caused by factors such as heat sink, tumor heterogeneity, and liver parenchyma fibrosis or cirrhosis. It is challenging to accurately assess the actual ablative margins. The results of this study indicate that conventional qualitative assessment is prone to overestimation of the obtained ablative margins. Only 2 out of 8 patients who developed LTP were identified qualitatively, whereas all 8 patients were identified using quantitative assessment.

Other studies have addressed the potential of quantitative assessment of ablation margins. A rigid registration algorithm was used in the largest study, by Kim et al. [12]. They analyzed 110 HCC tumors and found a cutoff value of >3 mm as a minimal ablation safety margin. Remarkably, in only 3/110 (2.7%) ablations, the target of 5 mm safety margin was actually met. Smaller studies used a nonrigid registration algorithm similar to ours. In a retrospective study in 31 patients with HCC, nonrigid registration of pre- and postablation CT scans using Hepacare software (Siemens, Germany) was feasible with an interobserver agreement comparable to our findings [14]. In another small cohort study, correlation between margin size and LTP was evaluated in a heterogeneous cohort with different tumor types [15]. In this study, no interobserver agreement analysis was performed. To our knowledge, the current study has been the first study in which both the feasibility of using a nonrigid registration algorithm and the correlation between margin size and LTP were reviewed, in a homogeneous HCC population.

As the liver is a deformable organ, a nonrigid registration seems to be a better fit for reliable registration. The Mirada RTx software used in this pilot study is not dedicated for the quantification of ablation margins but has the tools necessary for delineation and nonrigid registration. For future research, the software should be adopted with the purpose to optimize registration of pre- and postablation scans. Adding a step for selecting the liver as volume of interest in which optimal registration should be strived for may increase the registration success for the purpose of ablation margin measurements.

In the quantitative assessment, none of the patients with a fully ablated tumor developed LTP, even in those cases where no safety margin was found. However, tissue shrinks during ablation, which influences the quantification of safety margins [16–18]. A 0 mm ablative margin on post-RFA imaging may therefore denote a fully ablated tumor with a few millimeter of margin, as a result of tissue shrinkage. To be fully able to interpret treatment success without pathological confirmation, a better understanding of heat conduction and tissue shrinkage would be necessary, as the latter seems to occur in an inhomogeneous and unpredictable way [16]. Quantification of ablative margins therefore remains arbitrary, as it may not reflect the actual distance between the boundary of the initial tumor and the boundary of the ablation area. To use the software as a decision support tool during ablation procedures, prospective studies in larger patient cohorts are needed to determine the risk of recurrence for different ablation margins and to set a standard for the optimal ablation margin.

The LTP rate of 44.4% in this study is comparable to studies with a similar patient population. In a large randomized study that included 701 patients treated with RFA, the HEAT III study, tumor progression rates of 53.3% were found after treatment with RFA in a population with slightly more unfavorable patient and tumor characteristics [19].

The main limitations of this study are its retrospective design and low sample size. Although the initial cohort consisted of 79 patients, only 25 patients were included, of which 18 patients were assessable for the final analysis. The majority of patients were excluded for this pilot study to prevent potential bias in follow-up data. Secondary exclusion (7/25 included patients) due to unfeasible registration could potentially be reduced by performing a CT scan immediately before and after the ablation. To optimize coregistration of the CT scans, the scan should be acquired with the patient in an identical position and during a similar inhalation mode or with use of high-jet ventilation.

Clinically, LTP is not the most valuable outcome measure. This study was designed as a pilot study to evaluate software that assesses the completeness of a local treatment. Therefore, LTP was chosen as the most relevant parameter for this study rather than survival.

5. Conclusion

Feasibility of coregistration of pre- and postablation CT images using Mirada RTx software was found for selected patients (18/25), as difference in position and shape of the liver may hamper reliable image coregistration. For patients in whom coregistration is feasible, the interobserver agreement is high, confirming the robustness of this method. Compared to qualitative assessment, quantitative assessment of ablative margins allows better prediction of LTP and may thus be a better method to determine technical success. To increase the feasibility of CT-CT coregistration as a method to determine the endpoint of ablation, there is a need for optimized scanning protocols and dedicated software prospective studies in larger patient cohorts are needed to better determine the risk of recurrence for different ablation margins and to define a cutoff value for the optimal margin.

Data Availability

The data used to support the findings of this study are included within the article.

Disclosure

This research was presented as an oral presentation at Amsterdam Interventional Oncology Symposium (AMIOS 2018).

Conflicts of Interest

The authors declare that there are no conflicts of interest regarding the publication of this paper.

Acknowledgments

Mirada RTx software was provided as in-kind contribution by Mirada Medical Ltd., Oxford, UK.

References

[1] A. Forner, J. M. Llovet, and J. Bruix, "Hepatocellular carcinoma," *The Lancet*, vol. 379, no. 9822, pp. 1245–1255, 2012.

[2] T. Livraghi, F. Meloni, M. Di Stasi et al., "Sustained complete response and complications rates after radiofrequency ablation of very early hepatocellular carcinoma in cirrhosis: is resection still the treatment of choice?," *Hepatology*, vol. 47, no. 1, pp. 82–89, 2008.

[3] European Association for the Study of the Liver, European Organisation for Research and Treatment of Cancer, "EASL–EORTC clinical practice guidelines: management of hepatocellular carcinoma," *Journal of Hepatology*, vol. 48, no. 4, pp. 599–641, 2012.

[4] S.-M. Lin, C. J. Lin, C. C. Lin, C. W. Hsu, and Y. C. Chen, "Randomised controlled trial comparing percutaneous radiofrequency thermal ablation, percutaneous ethanol injection, and percutaneous acetic acid injection to treat hepatocellular carcinoma of 3 cm or less," *Gut*, vol. 54, no. 8, pp. 1151–1156, 2005.

[5] M. Morimoto, K. Numata, M. Kondou, A. Nozaki, S. Morita, and K. Tanaka, "Midterm outcomes in patients with intermediate-sized hepatocellular carcinoma," *Cancer*, vol. 116, no. 23, pp. 5452–5460, 2010.

[6] J. Hänsler, M. Frieser, V. Tietz et al., "Percutaneous radiofrequency ablation of liver tumors using multiple saline-perfused electrodes," *Journal of Vascular and Interventional Radiology*, vol. 18, no. 3, pp. 405–410, 2007.

[7] T. Hori, K. Nagata, S. Hasuike et al., "Risk factors for the local recurrence of hepatocellular carcinoma after a single session of percutaneous radiofrequency ablation," *Journal of Gastroenterology*, vol. 38, no. 10, pp. 977–981, 2003.

[8] L. Crocetti, T. de Baere, and R. Lencioni, "Quality improvement guidelines for radiofrequency ablation of liver tumours," *CardioVascular and Interventional Radiology*, vol. 33, no. 1, pp. 11–17, 2010.

[9] A. Colecchia, R. Schiumerini, A. Cucchetti et al., "Prognostic factors for hepatocellular carcinoma recurrence," *World Journal of Gastroenterology*, vol. 20, no. 20, pp. 5935–5950, 2014.

[10] T. Nakazawa, S. Kokubu, A. Shibuya et al., "Radiofrequency ablation of hepatocellular carcinoma: correlation between local tumor progression after ablation and ablative margin," *American Journal of Roentgenology*, vol. 188, no. 2, pp. 480–488, 2007.

[11] M. Liao, X. Zhong, J. Zhang et al., "Radiofrequency ablation using a 10-mm target margin for small hepatocellular carcinoma in patients with liver cirrhosis: a prospective randomized trial," *Journal of Surgical Oncology*, vol. 115, no. 8, pp. 971–979, 2017.

[12] Y.-S. Kim, W. J. Lee, H. Rhim, H. K. Lim, D. Choi, and J. Y. Lee, "The minimal ablative margin of radiofrequency ablation of hepatocellular carcinoma (>2 and <5 cm) needed to prevent local tumor progression: 3D quantitative assessment using CT image fusion," *American Journal of Roentgenology*, vol. 195, no. 3, pp. 758–765, 2010.

[13] A. J. Viera and J. M. Garrett, "Understanding interobserver agreement: the kappa statistic," *Family Medicine*, vol. 37, no. 5, pp. 360–363, 2005.

[14] K. W. Kim, J. M. Lee, E. Klotz et al., "Safety margin assessment after radiofrequency ablation of the liver using registration of preprocedure and postprocedure CT images," *American Journal of Roentgenology*, vol. 196, no. 5, pp. W565–W572, 2011.

[15] S. Tani, S. Tatli, N. Hata et al., "Three-dimensional quantitative assessment of ablation margins based on registration of pre- and post-procedural MRI and distance map," *International Journal of Computer Assisted Radiology and Surgery*, vol. 11, no. 6, pp. 1133–1142, 2016.

[16] L. Farina, N. Weiss, Y. Nissenbaum et al., "Characterisation of tissue shrinkage during microwave thermal ablation," *International Journal of Hyperthermia*, vol. 30, no. 7, pp. 419–428, 2014.

[17] C. Rossmann, E. Garrett-Mayer, F. Rattay, and D. Haemmerich, "Dynamics of tissue shrinkage during ablative temperature exposures," *Physiological Measurement*, vol. 35, no. 1, pp. 55–67, 2014.

[18] C. L. Brace, T. A. Diaz, J. L. Hinshaw, and F. T. Lee Jr., "Tissue contraction caused by radiofrequency and microwave ablation: a laboratory study in liver and lung," *Journal of Vascular and Interventional Radiology*, vol. 21, no. 8, pp. 1280–1286, 2010.

[19] W. Y. Tak, S.-M. Lin, Y. Wang et al., "Phase III HEAT study adding lyso-thermosensitive liposomal doxorubicin to radiofrequency ablation in patients with unresectable hepatocellular carcinoma lesions," *Clinical Cancer Research*, vol. 24, no. 1, pp. 73–83, 2018.

Hindawi
Journal of Oncology
Volume 2019, Article ID 4564707, 7 pages
https://doi.org/10.1155/2019/4564707

Research Article

Yttrium-90-Labeled Anti-Glypican 3 Radioimmunotherapy Halts Tumor Growth in an Orthotopic Xenograft Model of Hepatocellular Carcinoma

Andrew D. Ludwig,[1] **Kevin P. Labadie**,[1] **Y. David Seo**,[1] **Donald K. Hamlin**,[2] **Holly M. Nguyen**,[3] **Vimukta M. Mahadev**,[1] **Raymond S. Yeung**,[1] **D. S. Wilbur**,[2] **and James O. Park**[1]

[1]*Department of Surgery, University of Washington, Seattle, WA, USA*
[2]*Department of Radiation Oncology, University of Washington, Seattle, WA, USA*
[3]*Department of Urology, University of Washington, Seattle, WA, USA*

Correspondence should be addressed to Andrew D. Ludwig; ludwiga@uw.edu

Received 26 April 2019; Accepted 21 August 2019; Published 15 September 2019

Guest Editor: Tiago Bilhim

Hepatocellular carcinoma (HCC) is the second most lethal malignancy globally and is increasing in incidence in the United States. Unfortunately, there are few effective systemic treatment options, particularly for disseminated disease. Glypican-3 (GPC3) is a proteoglycan cell surface receptor overexpressed in most HCCs and provides a unique target for molecular therapies. We have previously demonstrated that PET imaging using a ^{89}Zr-conjugated monoclonal anti-GPC3 antibody (αGPC3) can bind to minute tumors and allow imaging with high sensitivity and specificity in an orthotopic xenograft mouse model of HCC and that serum alpha-fetoprotein (AFP) levels are highly correlated with tumor size in this model. In the present study, we conjugated ^{90}Y, a high-energy beta-particle-emitting radionuclide, to our αGPC3 antibody to develop a novel antibody-directed radiotherapeutic approach for HCC. Luciferase-expressing HepG2 human hepatoblastoma cells were orthotopically implanted in the livers of athymic nude mice, and tumor establishment was verified at 6 weeks after implantation by bioluminescent imaging and serum AFP concentration. Tumor burden by bioluminescence and serum AFP concentration was highly correlated in our model. Yttrium-90 was conjugated to αGPC3 using the chelating agent 1,4,7,10-tetraazacyclododecane-1,4,7,10-tetraacetic acid (DOTA) and injected via the tail vein into the experimental mice at a dose of 200 μCi/mouse or 300 μCi/mouse. Control mice received DOTA-αGPC3 without radionuclide. At 30 days after a single dose of the radioimmunotherapy agent, mean serum AFP levels in control animals increased dramatically, while animals treated with 200 μCi only experienced a minor increase, indicating cessation of tumor growth, and animals treated with 300 μCi experienced a reduction in serum AFP concentration, indicating tumor shrinkage. Mean tumor-bearing liver weight in control animals was also significantly greater than that in animals that received either dose of ^{90}Y-αGPC3. These results were achieved without significant toxicity as measured by body condition scoring and body weight. The results of this preclinical pilot demonstrate that GPC3 can be used as a target for radioimmunotherapy in an orthotopic mouse model of HCC and may be a target of clinical significance, particularly for disseminated HCC.

1. Introduction

Hepatocellular carcinoma (HCC) is recognized as the fifth most common cancer and second leading cause of cancer-related deaths worldwide, resulting in over 750,000 deaths annually [1]. Though there has been progress in surgical and nonsurgical treatment for HCC, the prognosis remains poor, particularly for late-stage disease. Sorafenib, a multikinase inhibitor and the best form of chemotherapy for advanced disease, has been shown to prolong median survival and time

to progression by only 3 months [2]. Because of this dismal prognosis, novel targets and therapies are desperately needed.

Glypican-3 (GPC3) is a heparan sulfate proteoglycan found on the cell surface of human embryonic stem cells. It is anchored by glycosylphosphatidylinositol and regulates growth and morphogenesis through insulin-like growth factor and hedgehog signaling pathways [3, 4]. Its importance in regulating cell growth is underscored by a loss-of-function mutation in GPC3 that causes Simpson–Golabi–Behmel syndrome, a condition of skeletal and organ overgrowth [5]. Expression of GPC3 in the fetal liver is observed from 18 to 30 weeks of gestation, but no GPC3 expression is seen in normal adult liver cells [3, 6, 7]. Conversely, high expression of GPC3 is seen in HCC, is correlated with AFP expression, and can be used to differentiate HCCs from benign liver lesions [8–10]. In addition, the level of expression of GPC3 in HCC patients is correlated with poorer prognosis and risk of recurrence after primary resection or liver transplant [11–15].

Because of this differential expression and cell surface location, GPC3 is a promising tumor marker for diagnostic and therapeutic purposes in HCC. We have previously demonstrated the utility of antibody-directed ^{89}Zr radioisotopes as PET contrast agents to identify GPC3-expressing orthotopic liver tumors *in vivo* [16, 17]. In the current report, we describe the development of a novel antibody-directed therapeutic radioisotope in the form of a ^{90}Y-*α*GPC3 conjugate and study its effect on *in vivo* HCC tumor growth in our orthotopic mouse model.

2. Materials and Methods

2.1. Cell Lines and Tissue Culture. Luciferase-expressing GPC3-positive HepG2-Red-FLuc HCC cells were purchased from PerkinElmer (Bioware, cat. no. BW134280). Cell lines were maintained in a monolayer at 37°C in Dulbecco's modified Eagle's medium (DMEM; Gibco) supplemented with 10% fetal bovine serum (FBS; Gibco) in a humidified atmosphere of 95%/5% air/CO_2.

2.2. Anti-GPC3 IgG1 Generation (as Previously Described [16]). RBF/DnJ mice were immunized with recombinant carrier-free human GPC3 protein in Freund's adjuvant solution. After several boost injections, antiserum ELISAs confirmed the presence of the *α*GPC3 IgG. Additional boost injections were delivered to ensure IgM/IgG switch, which was verified on ELISA with IgG titrated to 1 : 10,000. After final prefusion boost injections, mice were euthanized, their spleens were harvested, 1×10^8 splenocytes were fused on a ratio of 1 : 1 with FOX-NY myeloma cells, and the resultant hybridomas were resuspended in adenine/aminopterin/thymidine FBS solution. Clones producing high titers of GPC3 IgG1 were selected using capture ELISA with goat antimouse IgG1 for isotyping.

2.3. Production of ^{90}Y-αGPC3 Antibody. To demetallate the *α*GPC3 antibody, it was dialyzed against metal-free HEPES (50 mM HEPES (*N*-(2-hydroxyethyl)piperazine-*N*′-ethanesulfonic acid), 150 mM NaCl, and 1 mM EDTA adjusted to 8.5 pH and passed over a Chelex 100 (Biorad) column to remove metals) with a minimum of 6 buffer changes over 3 days at 4°C using Chelex 100 resin at each buffer change to scavenge metals. The metal-free *α*GPC3 was added to a DOTA-Bn-NCS (Macrocyclics) solution (10 mg/mL in DMSO), and the reaction was allowed to run overnight at room temperature with gentle mixing. The reaction mixture was then dialyzed against a metal-free citrate buffer (50 mM sodium citrate and 150 mM NaCl with pH 5.5) over 3 days at 4°C followed by dialysis against 150 mM saline for another 3 days. Each buffer change contained Chelex resin to scavenge metals. Demetallated ammonium acetate (500 mM, pH 5.3) and ^{90}Y were combined followed by *α*GPC3-DOTA, prepared as above, and incubated at 45°C for 1 hr before cooling to room temperature. The reaction was quenched with diethylenetriamine pentaacetic acid (DTPA). The labeled antibody was then separated from unreacted ^{90}Y via a PD-10 column (GE Healthcare) and eluted in PBS prior to analysis by thin layer chromatography (TLC) to verify radiochemical purity. Acid-washed vials and pipette tips were used for all steps.

2.4. Flow Cytometry. In vitro binding of the DOTA-*α*GPC3 conjugate was evaluated by flow cytometry. HepG2-Red-FLuc cells were grown as above until 70% confluent and then detached with 0.25% trypsin, counted, washed, and resuspended in cold phosphate-buffered saline (PBS) at a concentration of 1×10^6 cells/mL. One microgram of unconjugated or DOTA-*α*GPC3 primary antibody was added to the cell suspension and incubated for 45 minutes on ice. Primary antibody control samples received 1 μg of isotype-matched IgG1 control antibody (BD Biosciences, cat. no. 555746). Unstained samples did not receive primary antibody. The cells were then washed in cold PBS, and 1 μg of FITC-labeled goat-*α*-mouse IgG1 secondary antibody (Southern Biotech, cat. no. 1070-02) was added to the cell suspension and incubated on ice for 30 minutes in the dark. Unstained samples did not receive secondary antibody. The cells were washed in cold PBS, fixed with 1% paraformaldehyde for 15 minutes, and then washed and resuspended in cold PBS. Fixed cells were analyzed with a BD FACSCanto flow cytometer (Becton Dickinson Biosciences, Franklin Lakes, NJ) using the FACSDiva software. A minimum of 10,000 cells were analyzed for each sample in triplicate. Data analysis was performed on the FlowJo software, version 8.8.6 (Tree Star, Ashland, OR).

2.5. Animal Models. All animal studies were performed in accordance with the University of Washington Office of Animal Welfare guidelines for the humane use of animals, and all procedures were reviewed and approved by the Institutional Animal Care and Use Committee. To generate the orthotopic xenograft model, 8-week-old female athymic Nu/J mice (The Jackson Laboratory) were anesthetized using 1.5% inhaled isoflurane, and the left lobe of the liver was

exposed through an upper midline laparotomy. HepG2-Red-FLuc cells (2×10^6) in 50 μL of Dulbecco's modified Eagle's medium containing 50% Matrigel (BD Biosciences) were injected into the subcapsular space of the left lobe.

2.6. Bioluminescent Imaging. Six weeks after orthotopic HepG2 cell injection, a 75 mg/kg intraperitoneal injection of VivoGlo luciferin (Promega) was administered and imaging was performed using an IVIS Lumina II system (PerkinElmer) to verify tumor establishment and monitor the growth of intrahepatic tumors. Tumor size was calculated based on the average photon emission (photons/sec) in a 2D region of interest (ROI) covering the entire animal. The ROI was corrected for background bioluminescence, and the size of the ROI (32 cm^2) was identical for every animal imaged. Calculations were performed using the Living Image software (version 4.2; Caliper Life Sciences).

2.7. Measurement of Mouse Serum AFP. At the specified times, whole blood was obtained from animals using submandibular bleeding [18] and collected in EDTA-coated Eppendorf tubes. Serum was extracted from the fresh whole blood and then frozen and allowed to decay 10 half-lives (~27 days) in accordance with the University of Washington Environmental Health and Safety policy. The serum concentration of AFP was determined on the UniCel Dxl 800 Access Immunoassay System (Beckman Coulter) using an Access AFP alpha-fetoprotein pack (Quest Diagnostics).

2.8. In Vivo Radioimmunotherapy. Animals bearing established tumors as determined by IVIS imaging and serum AFP concentration using the above methods were randomly assigned to three experimental groups. All animals received the antibody conjugate via tail vein injections. Control animals were injected with 70 μg DOTA-conjugated αGPC3 antibody without radioisotope. Treated animals received 70 μg ^{90}Y-αGPC3 at the specified dosages of radionuclide. At 14 days after antibody injection, serum AFP was measured based on the above protocol. At 30 days after antibody injection, the animals were euthanized, blood was extracted via cardiac puncture, and livers were harvested, wet-weighed, and then placed in 10% (w/v) neutral-buffered formalin.

2.9. Statistical Analysis. All numeric data are expressed as mean ± SEM unless otherwise indicated. Excel (version 12.0.6; Microsoft) was used for statistical analysis. For continuous variables, an unpaired, 2-tailed Student's t-test was used. For multigroup comparisons, a one-way analysis of variance (ANOVA) was used. In all cases, a p value ≤0.05 was considered statistically significant.

3. Results

3.1. Flow Cytometry. Flow cytometry confirmed binding of both unconjugated and DOTA-conjugated αGPC3 to the luciferase-expressing HepG2-Red-FLuc cell line (Figure 1). The normalized geometric mean fluorescence of both unconjugated (1619.7 ± 23.2 a.u.) and DOTA-conjugated αGPC3 (1076 ± 30.0 a.u.) is significantly greater than that of unstained (95.2 ± 1.4 a.u.) and IgG1 isotype-matched primary antibody control (125.7 ± 10.5 a.u.) samples ($p < 0.001$ vs. isotype control). Though DOTA conjugation did appear to marginally affect αGPC3 antibody binding *in vitro*, mean fluorescence of conjugated samples remained >8-fold higher than that of control samples.

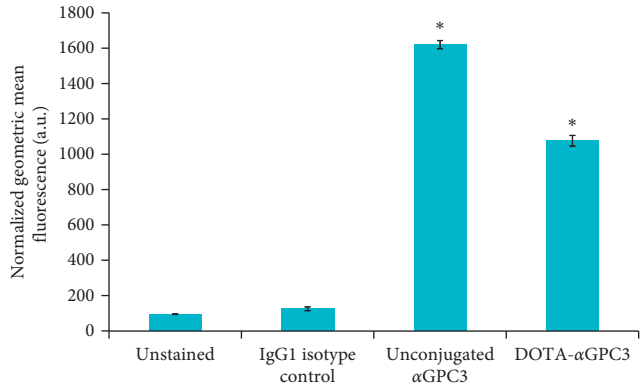

FIGURE 1: DOTA conjugation maintains αGPC3 binding *in vitro*. Flow cytometry on fixed HepG2 cells demonstrates a significant increase in mean fluorescence of both unconjugated and DOTA-conjugated αGPC3 compared to unstained cells and isotype-matched primary antibody control samples (* $p < 0.001$). Error bars represent standard deviation of triplicate measurements for >10,000 cell counts per sample.

3.2. Orthotopic Tumor Establishment. Serum AFP concentration was measured in tumor-bearing mice at six weeks after HepG2-Red-FLuc orthotopic implantation. Tumor establishment was verified by IVIS imaging at the time of serum sampling. Serum AFP levels in study animals ranged from 474.3 ng/mL to 421,600 ng/mL. Tumor bioluminescence ranged from 48.6 photons/sec to 50,340 photons/sec. Tumor bioluminescence as demonstrated by IVIS imaging correlates with serum AFP concentration with a correlation coefficient R^2 of 0.92 (Figure 2). This finding indicates that serum AFP concentration can be used to monitor tumor growth and response to treatment.

3.3. Radioimmunotherapy. To track tumor growth and response to radioimmunotherapy treatment, serum AFP concentration was monitored at 0, 14, and 30 days after administration of either low-dose (200 μCi, $n = 9$) or high-dose (300 μCi, $n = 9$) ^{90}Y conjugated to 70 μg of DOTA-αGPC3 via tail vein injection. Control animals ($n = 7$) received DOTA-αGPC3 without radionuclide. At the time of antibody injection, mean serum AFP concentration for control (75,258 ± 38,683 ng/mL), low-dose (66,434 ± 35,895 ng/ml), and high-dose (75,568 ± 45,467 ng/mL) groups was not statistically significantly different ($p = 0.98$), indicating equivalent overall tumor burden between groups at the initiation of the therapy (Figure 3).

At 14 days after antibody injection, mean serum AFP concentration of control animals increased by 578% (to

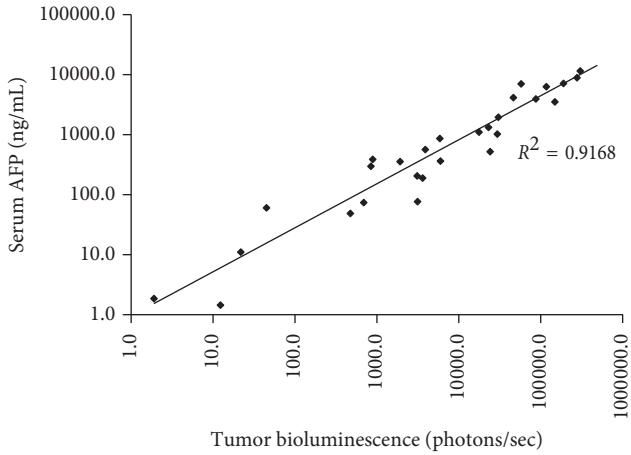

Figure 2: Plot of serum AFP concentration compared to tumor bioluminescence by IVIS imaging in tumor-bearing mice. Serum AFP concentration in mice 6 weeks after orthotopic HepG2-Red-FLuc xenograft implantation is highly correlated with tumor bioluminescence by IVIS imaging, indicating that AFP excretion by HepG2 orthotopic xenografts is dependent on tumor size.

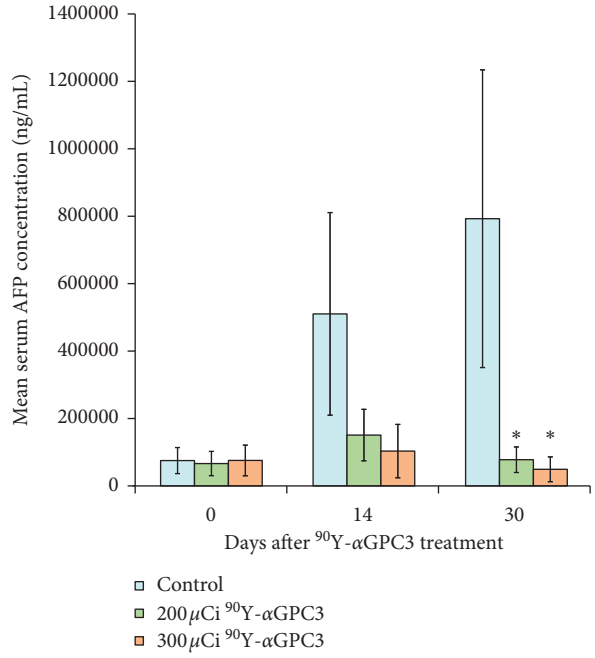

Figure 3: Mean serum AFP concentration of tumor-bearing mice at specified time points after administration of radioimmunotherapy. Serum AFP steadily increases over time in control animals ($n = 7$), while AFP concentration in animals treated with 200 μCi ($n = 9$) or 300 μCi ($n = 9$) of the ^{90}Y-αGPC3 conjugate remained at pretreatment levels and was significantly lower than that in control animals by 30 days ($^{*}p < 0.05$). Error bars represent standard error of the mean concentration.

510,284 ± 300,473 ng/ml), whereas animals that received low-dose radioimmunotherapy treatment experienced a 127% increase (to 150,800 ± 76,392 ng/mL) and animals that received high-dose treatment only experienced a 37% increase (to 103,344 ± 79,120 ng/mL). Though this trend was strong, the mean change in serum AFP concentration at 14 days between control and low-dose or high-dose treatment groups did not reach statistical significance ($p = 0.16$ and $p = 0.10$, respectively). The mean serum AFP concentration of animals treated with low-dose and high-dose ^{90}Y-αGPC3 was not statistically different from each other at 14 days ($p = 0.67$) and was not statistically different from pretreatment levels ($p = 0.33$ and $p = 0.76$, respectively).

By 30 days after radioimmunotherapy administration, mean serum AFP concentration of control animals had increased by 953% (to 792,566 ± 441,503 ng/mL) from pretreatment levels, while animals that received low-dose radioimmunotherapy treatment experienced a modest 17% increase over 30 days (to 77,820 ± 37,895 ng/mL) and animals that received high-dose treatment saw a decrease in mean serum AFP concentration by 35% (to 49,342 ± 36,800 ng/mL).

Notably, both low-dose and high-dose treatment groups experienced a decrease in mean serum AFP concentration from 14 days to 30 days by 48% and 52%, respectively. The mean change in AFP concentration over the 30-day study period was significantly different between control and low-dose groups, between control and high-dose groups, and between low- and high-dose groups ($p \leq 0.05$). However, the mean serum AFP concentrations of low-dose and high-dose treatment groups did not differ statistically from each other at 30 days after antibody injection ($p = 0.60$).

At 30 days after radioimmunotherapy treatment, study animals were euthanized and livers were removed en bloc to gauge tumor growth. The mean weight of control animal livers (2.36 ± 0.55 g) was significantly greater than that of animals that received either low-dose (1.33 ± 0.07 g) or high-dose (1.28 ± 0.08 g) ^{90}Y-αGPC3 treatment ($p \leq 0.05$; Figure 4). The mean weight of livers from animals receiving low-dose or high-dose ^{90}Y-αGPC3 treatment did not differ statistically ($p = 0.60$). During the course of the study, no animals were noted to have a significant change in body weight or body condition scoring, nor were any animal euthanized prior to the end date of the study.

4. Discussion

HCC is a common and deadly form of cancer for which few treatment options exist for late-stage or disseminated disease. In this preclinical study, we report the ability of a novel radioimmunotherapy agent, combining the radionuclide ^{90}Y with an HCC-specific antibody targeting the cell surface proteoglycan GPC3, to halt tumor growth in an orthotopic xenograft model.

To create a radioimmunotherapy agent, we conjugated a high-energy beta-emitting radionuclide, ^{90}Y, to a tumor-specific antibody using the chelating agent 1,4,7,10-tetraazacyclododecane-1,4,7,10-tetraacetic acid (DOTA). We demonstrated that conjugating this agent to αGPC3 maintained binding of the antibody *in vitro* by flow cytometry. We have previously shown that conjugating ^{89}Zr to αGPC3 with deferoxamine preserves antibody binding and specificity *in vitro* and *in vivo* [16]. Conjugation of ^{90}Y to monoclonal antibodies with DOTA is clinically relevant and

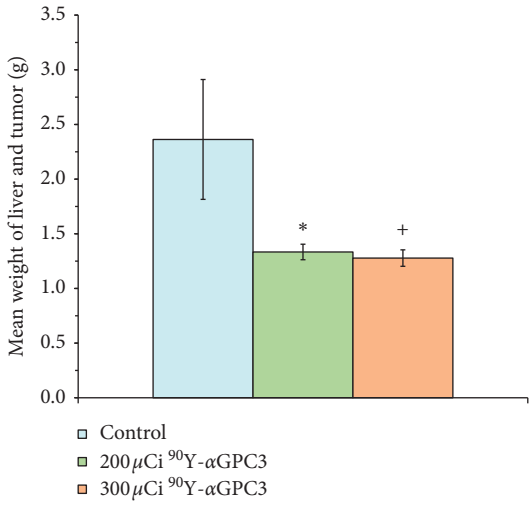

FIGURE 4: Mean weight of tumor-bearing livers at the conclusion of the 30-day radioimmunotherapy trial. The weight of tumor-bearing livers resected en bloc is increased in control animals compared to those treated with either 200 μCi or 300 μCi ^{90}Y-αGPC3 conjugate ($^{*}p = 0.05$; $^{+}p < 0.05$). Error bars represent standard error of the mean organ weight.

has been used in clinical trials for the treatment of pancreatic cancer [19], B-cell lymphoma [20], and leukemia [21]. Similarly, ^{90}Y itself is used clinically in the treatment of HCC. Radioembolization with ^{90}Y has been used in the treatment of HCC since the 1960s [22], and ^{90}Y microspheres have been shown to significantly prolong time to progression in HCC when compared to chemoembolization [23]. These efforts have demonstrated that ^{90}Y treatment is well tolerated in advanced-stage HCC [24].

In our orthotopic mouse model, we used serum AFP concentration as a corollary of tumor size, allowing a simple blood draw to track the response to treatment while animals were under radionuclide treatment. Serum AFP concentration prior to treatment was highly correlated with tumor size as established by bioluminescent imaging of the luciferase-expressing orthotopic tumors. Because of the intra-abdominal location of these tumors, external measurement of tumor volume is not possible. Others have demonstrated that serum AFP concentration is correlated with tumor size by bioluminescent and magnetic resonance imaging in a HepG2 orthotopic xenograft model [25]. Similarly, this method of correlating bioluminescence with tumor serum markers to track treatment response in orthotopic xenografts undergoing immunotherapy has been utilized successfully in several other tumor models [26]. In the clinical setting, high serum AFP concentration (>400 ng/mL) is considered diagnostic for HCC in the appropriate patient (e.g., cirrhotic or high-risk for HCC) and can be used to monitor the treatment effect and recurrence in patients whose tumors expressed AFP at diagnosis [27]. Serum AFP concentration decreasing in response to therapy in HCC was first described in the late 1970s [28] and continues to be clinically relevant as a predictor of outcome across the spectrum of HCC therapies. A similar phenomenon is present in our orthotopic model of HCC undergoing radioimmunotherapy.

We have previously demonstrated that ^{89}Zr-αGPC3 can be used as a novel imaging agent in this orthotopic xenograft HCC model. Using the same antibody and similar conjugation techniques, we extend the utility of this antibody to a therapeutic platform using ^{90}Y. Naturally, this presents the opportunity to combine tumor-specific diagnostic and therapeutic modalities using the same antibody and introduces the possibility of targeting small tumors and disseminated disease. Studies of this theranostics platform in our orthotopic xenograft model are in process. It is possible that the presence of ^{90}Y alone could account for some of the treatment effects seen in our model. However, our study utilized a single dose of radioimmunotherapy, and it is unlikely that such a dose administered systemically without tumor-specific activity could result in the sustained arrest of tumor growth over 30 days seen here. Nevertheless, we anticipate using nontargeting antibody controls in future preclinical experiments.

In addition, the direct cytotoxic effect of αGPC3 monoclonal antibodies is widely recognized. Since its characterization as a diagnostic and prognostic marker in HCC, GPC3 has been studied as a therapeutic target. A cytotoxic humanized αGPC3 monoclonal antibody, GC33, is capable of inhibiting orthotopic xenograft tumor growth [29], and clinical trials have been underway in HCC patients since 2013 [30]. Though our antibody was not designed with the intention of inducing a cytotoxic effect, control animals received DOTA-conjugated αGPC3 to account for the possible direct effect of the antibody itself. Progression of tumor growth in control animals during our study suggests that such an effect, if present, is not significant with our αGPC3 antibody.

The tumor-targeting effect of the αGPC3 antibody localizes the treatment effect of ^{90}Y to the tumor, prolonging the exposure of tumor cells to β-particle emission and limiting systemic effects. In the present study, all animals were noted to tolerate radioimmunotherapy without significant morbidity or mortality. Efforts to better quantify potential off-target effects of this novel radioimmunotherapy agent deserve further study and are currently underway.

5. Conclusions

In this study, we report the ability of a novel ^{90}Y-αGPC3 conjugate radioimmunotherapy to successfully halt the growth of luciferase-expressing HepG2 tumors in an orthoptic xenograft model of hepatocellular carcinoma. We used serum AFP as a marker of tumor size, validated by bioluminescent imaging. In our model, serum AFP levels in animals treated with a single dose of 200 μCi remained at pretreatment levels while in control animals serum AFP increased by over 900% by 30 days after treatment. In animals treated with 300 μCi of our conjugate, serum AFP levels decreased below pretreatment levels, indicating a reduction in tumor size.

Data Availability

The data used to support the findings of this study, including values behind means and standard deviations and images of

in vivo bioluminescence, are available from the corresponding author upon request.

Disclosure

This work was presented at the 58th Annual Meeting of the Society for Surgery of the Alimentary Tract (SSAT 2017).

Conflicts of Interest

The authors declare that there are no conflicts of interest regarding the publication of this paper.

Acknowledgments

The authors would like to acknowledge the University of Washington Shared IVIS Core, which was supported by the NIH Shared Instrumentation Grant (1S10OD010652-01). This work was funded through United States Department of Energy Grant (DE-SC0012445 MOD03), Chugai Pharmaceuticals Grant (UW OSP #A103633 AM02), and University of Washington ITHS Pilot Grant.

References

[1] L. A. Torre, F. Bray, R. L. Siegel, J. Ferlay, J. Lortet-tieulent, and A. Jemal, "Global cancer statistics, 2012," *CA: A Cancer Journal for Clinicians*, vol. 65, no. 2, pp. 87–108, 2015.

[2] J. Bruix and J. M. Llovet, "Major achievements in hepatocellular carcinoma," *Lancet*, vol. 373, no. 9664, pp. 614–616, 2009.

[3] B. V. Iglesias, G. Centeno, H. Pascuccelli et al., "Expression pattern of glypican-3 (GPC3) during human embryonic and fetal development," *Histology and Histopathology*, vol. 23, pp. 1333–1340, 2008.

[4] M. I. Capurro, P. Xu, W. Shi, F. Li, A. Jia, and J. Filmus, "Glypican-3 inhibits hedgehog signaling during development by competing with patched for hedgehog binding," *Developmental Cell*, vol. 14, no. 5, pp. 700–711, 2008.

[5] G. Pilia, R. M. Hughes-Benzie, A. MacKenzie et al., "Mutations in GPC3, a glypican gene, cause the Simpson-Golabi-Behmel overgrowth syndrome," *Nature Genetics*, vol. 12, no. 3, pp. 241–247, 1996.

[6] M. I. Capurro, Y.-Y. Xiang, C. Lobe, and J. Filmus, "Glypican-3 promotes the growth of hepatocellular carcinoma by stimulating canonical Wnt signaling," *Cancer Research*, vol. 65, no. 14, pp. 6245–6254, 2005.

[7] N. Yamauchi, A. Watanabe, M. Hishinuma et al., "The glypican 3 oncofetal protein is a promising diagnostic marker for hepatocellular carcinoma," *Modern Pathology*, vol. 18, no. 12, pp. 1591–1598, 2005.

[8] H. C. Hsu, W. Cheng, and P. L. Lai, "Cloning and expression of a developmentally regulated transcript MXR7 in hepatocellular carcinoma: biological significance and temporospatial distribution," *Cancer Research*, vol. 57, pp. 5179–5184, 1997.

[9] H. Jia, Q. Ye, L. Qin et al., "Human cancer biology gene expression profiling reveals potential biomarkers of human hepatocellular," *Carcinoma*, vol. 13, no. 4, pp. 1133–1140, 2007.

[10] X. Jia, J. Liu, Y. Gao, Y. Huang, and Z. Du, "Diagnosis accuracy of serum glypican-3 in patients with hepatocellular carcinoma: a systematic review with meta-analysis," *Archives of Medical Research*, vol. 45, no. 7, pp. 580–588, 2014.

[11] Y. Haruyama and H. Kataoka, "Glypican-3 is a prognostic factor and an immunotherapeutic target in hepatocellular carcinoma," *World Journal of Gastroenterology*, vol. 22, no. 1, pp. 275–283, 2016.

[12] K. Ofuji, K. Saito, T. Yoshikawa, and T. Nakatsura, "Critical analysis of the potential of targeting GPC3 in hepatocellular carcinoma," *Journal of Hepatocellular Carcinoma*, vol. 1, pp. 35–42, 2014.

[13] Y. Wu, H. Liu, and H. Ding, "GPC-3 in hepatocellular carcinoma: current perspectives," *Journal of Hepatocellular Carcinoma*, vol. 3, pp. 63–67, 2016.

[14] L. Wang, L. Pan, M. Yao, Y. Cai, Z. Dong, and D. Yao, "Expression of oncofetal antigen glypican-3 associates significantly with poor prognosis in HBV-related hepatocellular carcinoma," *Oncotarget*, vol. 7, no. 27, pp. 42150–42158, 2016.

[15] A. O. Kaseb, M. Hassan, S. Lacin et al., "Evaluating clinical and prognostic implications of glypican-3 in hepatocellular carcinoma," *Oncotarget*, vol. 7, no. 43, pp. 69916–69926, 2016.

[16] J. G. Sham, F. M. Kievit, J. R. Grierson et al., "Glypican-3-Targeted 89Zr PET imaging of hepatocellular carcinoma," *Journal of Nuclear Medicine*, vol. 55, no. 5, pp. 799–804, 2014.

[17] J. G. Sham, F. M. Kievit, J. R. Grierson et al., "Glypican-3-Targeting F(ab′)2 for 89Zr PET of hepatocellular carcinoma," *Journal of Nuclear Medicine*, vol. 55, no. 12, pp. 2032–2037, 2014.

[18] W. T. Golde, P. Gollobin, and L. L. Rodriguez, "A rapid, simple, and humane method for submandibular bleeding of mice using a lancet," *Lab Animal*, vol. 34, no. 9, pp. 39–43, 2005.

[19] A. J. Ocean, K. L. Pennington, M. J. Guarino et al., "Fractionated radioimmunotherapy with ^{90}Y-clivatuzumab tetraxetan and low-dose gemcitabine is active in advanced pancreatic cancer: a phase 1 trial," *Cancer*, vol. 118, no. 22, pp. 5497–5506, 2012.

[20] F. Kraeber-Bodere, A. Pallardy, H. Maisonneuve et al., "Consolidation anti-CD22 fractionated radioimmunotherapy with ^{90}Y-epratuzumab tetraxetan following R-CHOP in elderly patients with diffuse large B-cell lymphoma: a prospective, single group, phase 2 trial," *The Lancet Haematology*, vol. 4, no. 1, pp. e35–e45, 2017.

[21] P. Chevallier, T. Eugene, N. Robillard et al., "^{90}Y-labelled anti-CD22 epratuzumab tetraxetan in adults with refractory or relapsed CD22-positive B-cell acute lymphoblastic leukaemia: a phase 1 dose-escalation study," *The Lancet Haematology*, vol. 2, no. 3, pp. e108–e117, 2015.

[22] I. M. Ariel, "Treatment of inoperable primary pancreatic and liver cancer by the intra-arterial administration of radioactive isotopes (Y^{90} radiating microspheres)," *Annals of Surgery*, vol. 162, no. 2, pp. 267–278, 1965.

[23] R. Salem, A. C. Gordon, S. Mouli et al., "Y^{90} radioembolization significantly prolongs time to progression compared with chemoembolization in patients with hepatocellular carcinoma," *Gastroenterology*, vol. 151, no. 6, pp. 1155–1163.e2, 2016.

[24] A. Saini, A. Wallace, S. Alzubaidi et al., "History and evolution of Yttrium-90 radioembolization for hepatocellular carcinoma," *Journal of Clinical Medicine*, vol. 8, no. 1, p. 55, 2019.

[25] S. E. Woodfield, Y. Shi, R. H. Patel et al., "A novel cell line based orthotopic xenograft mouse model that recapitulates human hepatoblastoma," *Scientific Reports*, vol. 7, no. 1, article 17751, 2017.

[26] T. Poeschinger, A. Renner, T. Weber, and W. Scheuer, "Bioluminescence imaging correlates with tumor serum marker, organ weights, histology, and human DNA levels

during treatment of orthotopic tumor xenografts with antibodies," *Molecular Imaging and Biology*, vol. 15, no. 1, pp. 28–39, 2013.

[27] E. S. Bialecki and A. M. Di Bisceglie, "Diagnosis of hepatocellular carcinoma," *HPB*, vol. 7, no. 1, pp. 26–34, 2005.

[28] P. J. Johnson, R. Williams, H. Thomas, S. Sherlock, and I. M. Murray-Lyon, "Induction of remission in hepatocellular carcinoma with doxorubicin," *The Lancet*, vol. 311, no. 8072, pp. 1006–1009, 1978.

[29] T. Ishiguro, M. Sugimoto, Y. Kinoshita et al., "Anti-glypican 3 antibody as a potential antitumor agent for human liver cancer," *Cancer Research*, vol. 68, pp. 9832–9838, 2008.

[30] A. X. Zhu, P. J. Gold, A. B. El-Khoueiry et al., "First-in-man phase I study of GC33, a novel recombinant humanized antibody against glypican-3, in patients with advanced hepatocellular carcinoma," *Clinical Cancer Research*, vol. 19, no. 4, pp. 920–928, 2013.

Hindawi
Journal of Oncology
Volume 2019, Article ID 6089340, 7 pages
https://doi.org/10.1155/2019/6089340

Research Article

Evaluation of Contrast-Enhanced Intraoperative Ultrasound in the Detection and Management of Liver Lesions in Patients with Hepatocellular Carcinoma

Cristina Pace,[1] Vittorio Nardone,[1] Silvia Roma,[1] Fabrizio Chegai,[1] Luca Toti,[2] Tommaso Maria Manzia,[2] Giuseppe Tisone,[2] and Antonio Orlacchio[1]

[1]*Department of Diagnostic and Interventional Radiology, University Hospital Tor Vergata, Viale Oxford 81, 00133 Rome, Italy*
[2]*Department of Surgery, Liver Unit-University Hospital Tor Vergata, Viale Oxford 81, 00133 Rome, Italy*

Correspondence should be addressed to Antonio Orlacchio; aorlacchio@uniroma2.it

Received 18 April 2019; Revised 4 July 2019; Accepted 11 July 2019; Published 5 August 2019

Guest Editor: Abdul-Naser Elzouki

Aim. To evaluate the role of contrast-enhanced intraoperative ultrasound (CE-IOUS) during liver surgery in the detection and management of liver lesions in patients with hepatocellular carcinoma (HCC). *Materials and Methods*. From December 2016 to December 2017, 50 patients with HCC, who were candidates for liver resection, were evaluated with intraoperative ultrasound (IOUS). For all patients, MRI and/or CT were performed before surgery. During surgery, IOUS was performed after liver mobilization, and when nodules that had not been detected in the preoperative MRI and/or CT were observed, CE-IOUS scans were carried out with the dual purpose of better characterizing the unknown lesion and discovering new lesions. *Results*. In 12 patients, IOUS showed 14 nodules not detected by preoperative MRI and/or CT, before surgery. Out of the 12 lesions, five presented vascular features compatible with those of malignant HCC to the evaluation with CE-IOUS and four of these were simultaneously treated with intraoperative radiofrequency ablation (RFA). The fifth lesion was resected by the surgeon. The remaining nine lesions recognized by IOUS were evaluated as benign at CE-IOUS and considered regenerative nodules. The last diagnosis was confirmed during follow-up obtained by means of CT and/or MRI after 1, 3, 6, or 12 months. *Conclusion*. In our experience, CE-IOUS is a useful diagnostic tool in both benign pathologies, such as regenerative nodules, and malignant liver lesions. The advantage of this approach is the possibility of intraoperatively characterizing, based on vascularization patterns, lesions that could not be diagnosed by preoperative imaging, resulting in modification of the surgical therapy decision and expansion of the resection or intraoperative ablation.

1. Introduction

Hepatocellular carcinoma (HCC) is the fifth most common malignancy and is one of the main causes of cancer-related death worldwide. This condition is expected to increase further in upcoming years [1, 2]. Modern cross-sectional imaging plays a crucial role in detection and characterization of focal liver lesions, being essential before starting any type of therapy. Moreover, imaging has a significant role during local ablative treatments and on the assessment of the efficacy of percutaneous procedures [3]. The management of HCC involves multiple disciplines including hepatology, surgery, diagnostic and interventional radiology, oncology, and pathology [4, 5].

Nowadays, both contrast-enhanced computed tomography (CE-CT) and magnetic resonance imaging (MRI) with or without liver-specific contrast agent [6] have greatly improved the detection and characterization of liver tumors.

Recent innovations such as contrast-enhanced ultrasound imaging (CEUS) [7, 8] have raised the standards for HCC diagnosis as demonstrated by numerous studies [9, 10].

Hepatic resection is part of the conventional treatment for patients with primary liver cancers; however, the majority of

HCCs are not suitable for curative resection at the time of diagnosis [11].

Intraoperative ultrasound (IOUS) is an important tool used during surgical treatment of liver cancers, and particularly in patients with HCC [12, 13], especially when palpable tumors are found intraoperatively and it is mandatory to decide whether resection of malignant lesions is necessary or a lesion appears benign [14].

Proper collaboration between surgeons and interventional radiologists during liver resection in HCC patients is necessary, in order to increase chances of radical treatment in patients with multinodular HCC. Although liver resection represents the first choice of treatment for primary liver cancer, giving the patient the best chance of long-term survival [15], extensive resections of hepatic parenchyma expose patients to the risk of posthepatectomy liver failure (PHLF) associated with a high frequency of postoperative complications, mortality, and an increased length of hospital stay [16].

Thus, radiofrequency ablation (RFA), a widely accepted minimally invasive technique able to destroy tumor effectively and safely [17, 18], should be available during surgical liver resection, in order to save resection of unnecessary healthy hepatic parenchyma.

However, incorrect targeting on imaging could cause inadequate placement of the RFA needle which, in turn, could lead to the need of more treatment sessions or more frequent local recurrence after RFA [19]. It has been demonstrated that CE-IOUS is an accurate diagnostic technique in detecting and characterizing focal liver lesion, and its use in surgical navigation has already been reported in many studies [20–24].

The aim of this study is to evaluate the role of CE-IOUS during liver surgery in the detection and management of liver lesions, as it is known that the technique helps to better characterize the already known lesions. Noteworthy to mention is the fact that not all lesions detected by CE-IOUS in cirrhotic patients with HCC are malignant [21]; therefore, the possibility of intraoperatively characterizing lesions not evident in preoperative imaging is fundamental to guarantee these patients the best therapeutic strategy, performing intraoperative RFA or expanding resection, and more accurate follow-up.

2. Materials and Methods

2.1. Patients Selection. This is a retrospective study conducted with the approval of the ethics committee, and informed consents were obtained from all patients. From December 2016 to December 2017, 58 patients with chronic liver disease affected by HCC and who were candidates for liver resection were included. Based on the exclusion criteria, 8 patients, lost in follow-up, were excluded from the study. CE-IOUS was performed in 12 cirrhotic patients who presented lesions not evident in preoperative imaging with IOUS evaluation. Cirrhosis was documented by the histological evaluation performed during liver follow-up. The etiology of cirrhosis was hepatitis C in 5 patients, hepatitis B and NASH in 1 patient, alcoholic hepatitis in 2 patients, and cryptogenic hepatitis in 4 patients.

2.2. Preoperative Imaging. All patients underwent CT or MRI or both with contrast medium administration before surgery. Contrast-enhanced MRI examinations were performed with a 1.5 T imaging system (Philips Achieva) using T1-weighted (W) turbo spin-echo (TSE), T2-W TSE sequences integrated with fat suppression, dual sequences, and diffusion-weighted imaging (DWI), following an intravenous bolus of 0.1 mmol gadoteridol (ProHance, Bracco SpA, Milan, Italy) per kg of body weight administered at a rate of 2 mL/s and 20 mL of sodium chloride solution. CE-CT scans were performed with a GE Revolution EVO (GE Healthcare, Milan, Italy) pre- and postintravenous injection of 110–130 mL iopamidol (Iopamiro (300 mgI/ml), Bracco SpA, Milan, Italy) with helical scan, 0.6 sec rotation time, pitch 0.9, 120 kV, 250 mA, and image thickness of 2.50 mm. MRI and CT data were acquired in three phases: the hepatic arterial, the portal venous, and the equilibrium. Intraoperative ultrasound patients were treated with open surgery. During surgery, IOUS was performed after liver mobilization and, when nodules that had not been detected in the preoperative MRI and/or CT were observed, CE-IOUS scans were carried out with the dual purpose of better characterizing the unknown lesion and discovering new lesions. CE-IOUS was performed with MyLab Twice (Esaote SpA, Genoa, Italy), equipped with a IOT 342 linear transducer (Top-View) that covering a wider frequency range (3–11 MHz). All lesions were counted and mapped. CE-IOUS was performed with intravenous injection through a peripheral vein of 5 mL ultrasound contrast agent composed of sulphur hexafluoride microbubbles stabilized by a phospholipid shell (SonoVue, Bracco SpA, Milan, Italy). Immediately after the injection, 20 mL saline was injected in the same way. The arterial, portal, and late phases of contrast enhancement were recorded and analyzed. The late phase ended with disappearance of the microbubbles from the circle occurring after 240–360 seconds from the start of the examination [7]. Following the first US contrast medium injection, a full examination of the liver was carried out, segment by segment, to search for new lesions. Only in the case of the patient with two lesions in the two different lobes, two administrations of ultrasound contrast agent, each 2.5 mL, were performed, taking care to wait 6 minutes between one administration and another in order to avoid artifacts. After any RFA, a further CE-IOUS was performed. There were no artifacts or need for flash because a sufficient amount of time elapsed between the CE-IOUS pre- and posttreatment with radiofrequency. The maximum total dose allowed was 3 doses of 5.0 mL.

2.3. Histological Analysis and Intraoperative Radiofrequency Thermoablation. For all lesions considered malignant at IOUS and CE-IOUS, biopsy and histological examination were performed. They were treated with surgical resection or with intraoperative RFA. RFA was performed using the RF generator 3000 (Boston Scientific) by positioning the active tip of the needle (LeVeen 14 G) into the lesion with 4 cm of displayed hooks. The RFA procedures were made according to setting of manufacturer up to a final output with roll-off

obtained two times. The outcomes of the treatment with RFA were monitored intraoperatively with further ultrasound contrast medium administration and subsequently with follow-up obtained by means of CT and/or MRI after 1, 3, 6, or 12 months.

3. Results

Fifty patients were evaluated with IOUS during surgical resection for HCC. In 12 cirrhotic patients, IOUS showed focal lesions not detected by preoperative MRI and/or CT, before surgery. The average age of the patients (six women and six men) was 69.4 years (range 52–78 years).

IOUS during hepatic resection of HCC demonstrated 14 nodules. One patient had two lesions in two different lobes, and another patient had two suspected lesions close to each other in the same lobe. These newly detected lesions were evaluated during liver surgery using CE-IOUS, in an attempt to discriminate benign from malignant lesions and decide on treatment in real time. CE-IOUS data were analyzed based on the lesions' wash-in and washout during the arterial, portal venous, and late venous phases. Depending on the vascularization patterns, lesions were characterized as malignant or benign and, if possible, a differential diagnosis was given. Signs of malignancy were considered: arterial phase hyperenhancement followed by late (>60 s) washout [25]. The CE-IOUS allowed us to characterize 14 nodules, with an average size of 10.2 mm (range 7.2 mm–24 mm), five of which present CE-IOUS vascular features compatible with those of malignant HCC (Figures 1 and 2) and were confirmed by biopsy and histological examination. Four of the five malignant lesions detected by CE-IOUS were simultaneously treated with intraoperative RFA, and their complete ablation was intraoperatively evaluated with further ultrasound contrast medium administration. The fifth lesion was resected by the surgeon. The remaining nine lesions recognized by IOUS were evaluated as benign at CE-IOUS and considered regenerative nodules (Figure 3). Since they were small (≤1 cm), it was decided to follow up them. All patients underwent follow-up with CT and/or MRI at 1, 3, 6, and 12 months. The regenerative nodules were confirmed as such, presenting no variation in size and vascularization during follow-up. Also, the complete excision and the absence of disease residues after RFA were confirmed in the follow-up.

4. Discussion

Preoperative hepatic imaging diagnosis, such as CT, MRI, and positron emission tomography (PET), has improved considerably in recent years. In 2004, Sahani et al. [26] claimed that MRI is as sensitive as IOUS in depicting hepatic lesions before hepatic resection (86.7% and 94.3%, respectively). Moreover, Huf et al. [27] reported no statistical significance of CEUS and MRI regarding the general differential diagnosis for hepatic tumors. In this study, we highlighted the importance of the presence of interventional radiologist with CE-IOUS and RFA experience during liver resection procedures, in order to perform intraoperative ultrasound, able to ensure optimized liver surgery and able to provide an alternative treatment for unexpected new liver lesions unsuitable for resection. During the long process of the carcinogenesis of HCC, the neovascularization in small lesions may be invisible with the current imaging approaches [28]. Echogenicity of the lesions often changes especially after therapy, embolization, or RFA, which makes it difficult to identify the typical signs of malignancy, e.g., hypoechoic, irregular, and sometimes hypoechoic rim in the periphery of the lesion [29]. Early hypervascularization of HCC lesions in the arterial phase and typical washout of contrast starting in the portal venous phase and continuing in the late phase could be shown only by CEUS. In the CE-IOUS study, HCC lesions are characterized by hyperenhancement during the arterial phase and microbubbles' washout during the portal and late phases [30]. Compared to normal vessels, tumor vessels are tortuous, excessively branched, and short-circuited; thus, overall tumor vasculature appears highly disorganized [31].

The imaging characteristics typical for HCC are difficult to find in small lesions. With the limit of preoperative diagnostic imaging criteria, the Transplantation Network (OPTN)/United Network for Organ Sharing (UNOS) [32] and the Liver Imaging Reporting and Data System (US LI-RADS) [33] suggested not to diagnose, as HCC, lesions <1 cm in diameter.

CE-IOUS can have difficulty in visualizing some regions of the liver even in a mobilized liver (subdiaphragmatic segment VIII). Moreover, special ultrasound devices and a highly experienced examiner are needed to acquire high-quality contrast-enhanced ultrasound scans. In addition, ultrasound is a depth-dependent imaging modality that can reach its limits particularly in overweight patients. CE-IOUS can ensure good visualization of the liver even in overweight patients but is subject to time constraints due to the surgical situation.

This study shows that the use of high definition technique of CE-IOUS with multifrequency probes led to relevant changes in the surgical strategy for malignant liver tumors.

SonoVue® does not impair kidney function as contrast agents used for CE-CT or CE-MRI; therefore, it can be used also in case of reduced creatinine clearance or even kidney failure. The main contraindication for the use of SonoVue® is intolerance for contrast agent component that is very rare, so it is important to specifically exclude this intolerance when obtaining informed consent from the patient.

Results published by Loss et al. [34] showed that in a population of 50 patients, in 28 patients, additional lesions were found using CE-IOUS (mean tumor size of 8 mm, range 4–12 mm). Authors described a change in surgical strategy or the intraoperative application of RFA in 27 patients (54%), resulting in modification of therapy due to additional liver lesions. The largest and most comprehensive analysis of CEUS in the diagnosis of liver tumors is the multicenter prospective DEGUM study [35, 36]. It was able to be shown that CEUS has high diagnostic value for all benign and malignant liver tumor entities. The early detection of small HCC allows new chances for a successful surgery [37].

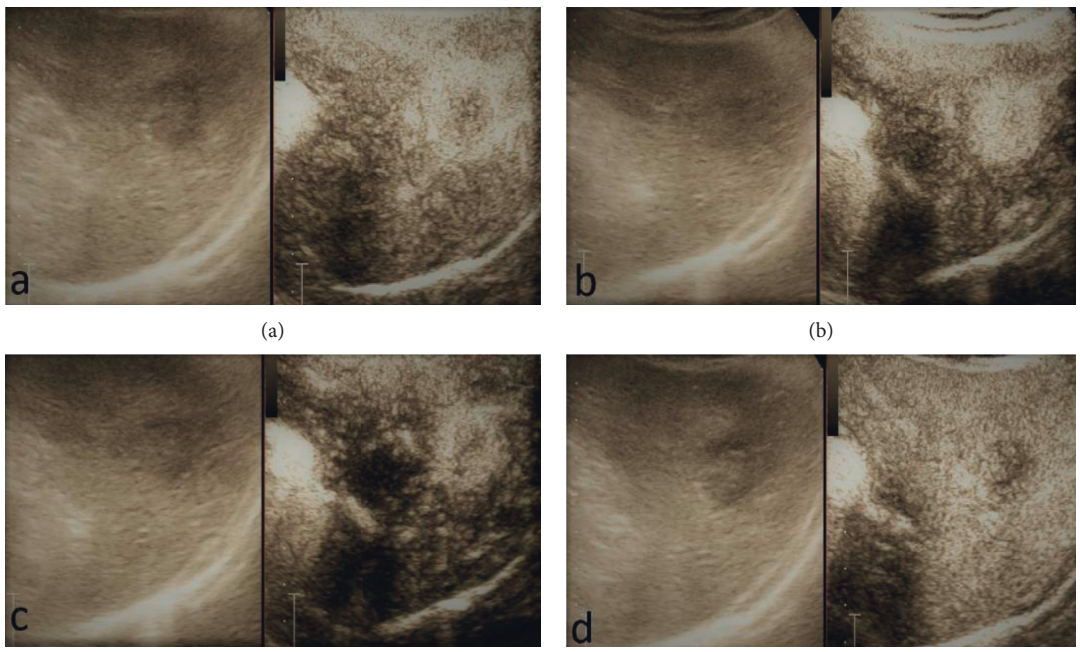

(a) (b)

(c) (d)

Figure 1: Example of typical vasculature features of CE-IOUS compatible with a malignant nodule of HCC that showed early contrast enhancement and fast washout: (a) early arterial phase; (b) arterial phase; (c) portal phase; (d) late phase.

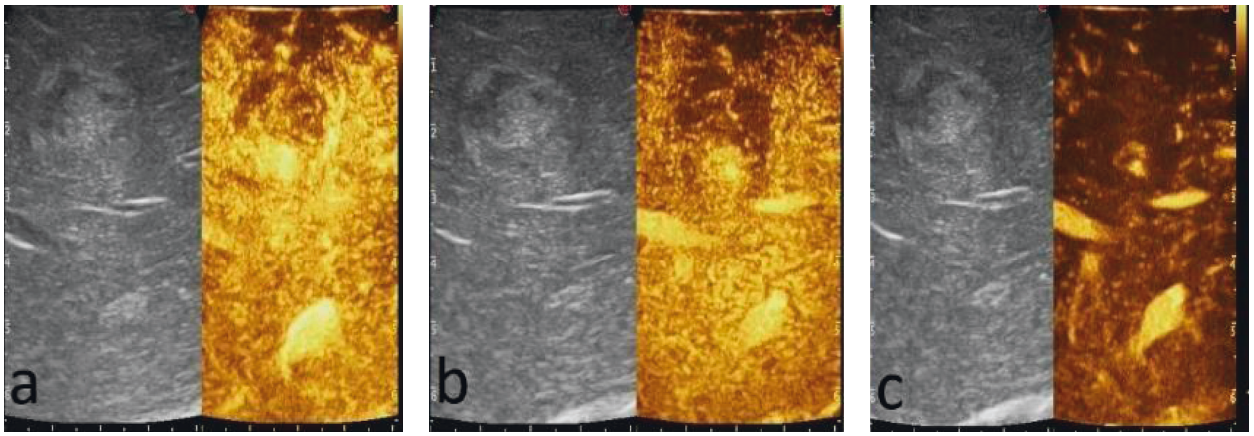

(a) (b) (c)

Figure 2: A particular CE-IOUS case showed a peripheral arterial hyperenhancing and hypoechogenic enhancing in the portal and late phases without contrast enhancement in the central area in all phases for hematic and colliquative necrosis component: (a) arterial phase; (b) portal phase; (c) late phase.

We observed that CE-IOUS provided an advantage to characterize lesions not detected by presurgical imaging, resulting in changes of the surgical therapy decision and enlargement of the resection or the application of intraoperative ablation. Particularly, we detected 14 new lesions, 5 of them classified as malignant based on CE-IOUS findings and confirmed by biopsy and histological examination. In our experience, the evidence of an additional malignant lesion modified the planned surgical strategy in a patient. In other cases of malignant lesions, in which it was not possible to extend liver resections, radiofrequency ablation (RFA) was done.

RFA has a very important role as an alternative to surgery. Some physicians prefer RFA to surgical resection for the treatment of small HCC even when the patient is eligible for surgery because of the relatively low morbidity and high quality of life [38, 39]. RFA is recommended for the treatment of HCC with a maximum diameter of 3 cm in patients with no more than three tumor masses, in whom surgery is contraindicated [11]. The technical effectiveness of RFA depends on the correct targeting of the nodule on US and adequate placement of the RFA needle [19]. CEUS has been increasingly used for detection, characterization,

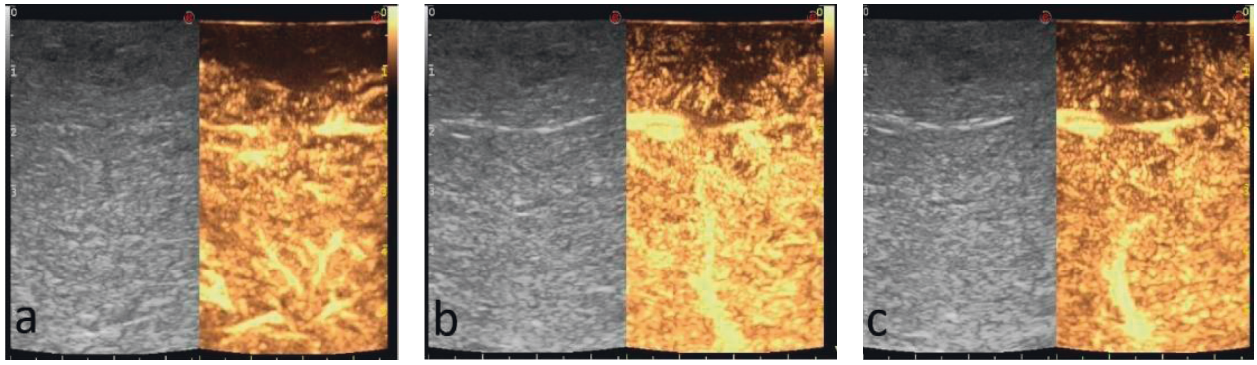

(a) (b) (c)

Figure 3: A typical hypoenhancement in all phases of regenerative nodules: (a) arterial phase; (b) portal phase; (c) late phase.

and planning of therapeutic interventions of liver tumors [9, 10].

As reported, RF ablation guided by a second-generation microbubble-enhanced US may be easier to perform and may be an efficient approach to liver malignancies that are not clearly depicted on B-mode US [11]. CE-IOUS has been reported to be useful also for RFA monitoring [40–42]. In our case, the complete ablation assessed intraoperatively with CE-IOUS was confirmed during follow-up with CT and/or MRI at 1, 3, 6, or 12 months. Also, follow-up confirms that the regenerative nodules maintained benign criteria in imaging over time, and this allows to understand how the IO-CEUS compared to the IO-US allows to effectively distinguish benign from malignant nodules and thus subjecting to the RF treatment a smaller number of lesions than all those evidenced with the IOUS, reducing complications and additional costs in terms of quality of life and economic health.

This study illustrates that intraoperating CE-IOUS allows to accurately detect and characterize liver lesions not evident in preoperative CT and MRI and that it is a useful instrument able to provide additional information during surgery and help in the RFA procedure. The results obtained with CE-IOUS reduce the diagnostic uncertainties and help in guiding the therapeutic choice, increasing the chances of obtaining the nodule's radical resection. Other than the improved characterization of already known and new lesions, CE-IOUS allowed to characterize also benign lesions as nodules of regeneration. This aspect is crucial regarding the clinical-instrumental follow-up of these nodules because, by knowing the regenerative nature of these nodules, it is possible to perform a more targeted follow-up, which is significant in dealing with cirrhotic patients that already need a thorough instrumental monitoring, especially when considering their history of HCC. There were some limitations in this study including its retrospective approach and the single-center design; moreover, the sample was too small to obtain significant statistical data. For these reasons, more studies are needed to further assess this technique.

5. Conclusion

This study demonstrated that CE-IOUS is a useful diagnostic tool in both benign and malignant liver lesions. It provides more information than the simple IOUS on the characteristics of the lesion with a dynamic study. In this way, the advantage of this approach is the possibility of intraoperatively characterizing, based on the vascularization patterns, lesions that could not be diagnosed by preoperative imaging, resulting in modification of the surgical therapy decision and expansion of the resection or intraoperative ablation.

Data Availability

The data used to support the findings of this study are available from the corresponding author upon request.

Conflicts of Interest

The authors declare that they have no conflicts of interest.

References

[1] A. P. Venook, C. Papandreou, J. Furuse, and L. Ladron de Guevara, "The incidence and epidemiology of hepatocellular carcinoma: a global and regional perspective," *The Oncologist*, vol. 15, no. 4, pp. 5–13, 2010.

[2] D. M. Parkin, F. Bray, J. Ferlay, and P. Pisani, "Estimating the world cancer burden: globocan 2000," *International Journal of Cancer*, vol. 94, no. 2, pp. 153–156, 2001.

[3] V. Vilgrain, "Advancement in HCC imaging: diagnosis, staging and treatment efficacy assessments," *Journal of Hepato-Biliary-Pancreatic Sciences*, vol. 17, no. 4, pp. 374–379, 2010.

[4] M. Omata, L. A. Lesmana, R. Tateishi et al., "Asian pacific association for the study of the liver consensus recommendations on hepatocellular carcinoma," *Hepatology International*, vol. 4, no. 2, pp. 439–474, 2010.

[5] A. Forner and J. Bruix, "Ablation for hepatocellular carcinoma: is there need to have a winning technique?," *Journal of Hepatology*, vol. 52, no. 3, pp. 310–312, 2010.

[6] A. Orlacchio, F. Chegai, S. Fabiano et al., "Role of MRI with hepatospecific contrast agent in the identification and characterization of focal liver lesions: pathological correlation in explanted livers," *La Radiologia Medica*, vol. 121, no. 7, pp. 588–596, 2016.

[7] M. Claudon, C. F. Dietrich, D. O. Cosgrove et al., "Guidelines and good practise recommendations for contrast enhanced

ultrasound (CEUS) in the liver—update 2012," *Ultraschall in Med*, vol. 34, no. 1, pp. 11–29, 2013.

[8] C. P. Nolsoe and T. Lorentzen, "International guidelines for contrast-enhanced ultrasonography: ultrasound imaging in the new millennium," *Ultrasonography*, vol. 35, no. 2, pp. 89–103, 2016.

[9] V. Salvatore and L. Bolondi, "Clinical impact of ultrasound-related techniques on the diagnosis of focal liver lesions," *Liver Cancer*, vol. 1, no. 3-4, pp. 238–246, 2012.

[10] I. Joo and B. I. Choi, "New paradigm for management of hepatocellular carcinoma by imaging," *Liver Cancer*, vol. 1, no. 2, pp. 94–109, 2012.

[11] Y. Minami and M. Kudo, "Review of dynamic contrast-enhanced ultrasound guidance in ablation therapy for hepatocellular carcinoma," *World Journal of Gastroenterology*, vol. 17, no. 45, pp. 4952–4959, 2011.

[12] Q. Lu, Y. Luo, C.-X. Yuan et al., "Value of contrast-enhanced intraoperative ultrasound for cirrhotic patients with hepatocellular carcinoma: a report of 20 cases," *World Journal of Gastroenterology*, vol. 14, no. 25, pp. 4005–4010, 2008.

[13] M. Donadon and G. Torzilli, "Intraoperative ultrasound in patients with hepatocellular carcinoma: from daily practice to future trends," *Liver Cancer*, vol. 2, no. 1, pp. 16–24, 2013.

[14] M. Donadon, G. Costa, and G. Torzilli, "State of the art of intraoperative ultrasound in liver surgery: current use for staging and resection guidance," *Ultraschall in der Medizin*, vol. 35, no. 6, pp. 500–511, 2014.

[15] R. T.-P. Poon, S.-T. Fan, C.-M. Lo et al., "Improving survival results after resection of hepatocellular carcinoma: a prospective study of 377 patients over 10 years," *Annals of Surgery*, vol. 234, no. 1, pp. 63–70, 2001.

[16] M. Shoup, M. Gonen, M. D'Angelica et al., "Volumetric analysis predicts hepatic dysfunction in patients undergoing major liver resection," *Journal of Gastrointestinal Surgery*, vol. 7, no. 3, pp. 325–330, 2003.

[17] A. R. Gillams, "Radiofrequency ablation in the management of liver tumours," *European Journal of Surgical Oncology (EJSO)*, vol. 29, no. 1, pp. 9–16, 2003.

[18] M. Kudo, "Radiofrequency ablation for hepatocellular carcinoma: updated review in 2010," *Oncology*, vol. 78, no. Suppl 1, pp. 113–124, 2010.

[19] T. Minami, Y. Minami, H. Chishina et al., "Combination guidance of contrast-enhanced US and fusion imaging in radiofrequency ablation for hepatocellular carcinoma with poor conspicuity on contrast-enhanced US/fusion imaging," *Oncology*, vol. 87, no. s1, pp. 55–62, 2014.

[20] K. Sato, S. Tanaka, Y. Mitsunori et al., "Contrast-enhanced intraoperative ultrasonography for vascular imaging of hepatocellular carcinoma: clinical and biological significance," *Hepatology*, vol. 57, no. 4, pp. 1436–1447, 2013.

[21] J. B. Kruskal and R. A. Kane, "Intraoperative US of the liver: techniques and clinical applications," *Radiographics*, vol. 26, no. 4, pp. 1067–1084, 2006.

[22] A. Alzaraa, G. Gravante, W. Y. Chung et al., "Contrast-enhanced ultrasound in the preoperative, intraoperative and postoperative assessment of liver lesions," *Hepatology Research*, vol. 43, no. 8, pp. 809–819, 2013.

[23] E. Leen, P. Ceccotti, S. J. Moug et al., "Potential value of contrast-enhanced intraoperative ultrasonography during partial hepatectomy for metastases," *Annals of Surgery*, vol. 243, no. 2, pp. 236–240, 2006.

[24] I. Joo, "The role of intraoperative ultrasonography in the diagnosis and management of focal hepatic lesions," *Ultrasonography*, vol. 34, no. 4, pp. 246–257, 2015.

[25] P. R. Galle, A. Forner, and J. M. Llovet, "EASL clinical practice guidelines: management of hepatocellular carcinoma," *Journal of Hepatology*, vol. 69, no. 1, pp. 182–236, 2018.

[26] D. V. Sahani, S. P. Kalva, K. K. Tanabe et al., "Intraoperative US in patients undergoing surgery for liver neoplasms: comparison with MR imaging," *Radiology*, vol. 232, no. 3, pp. 810–814, 2004.

[27] S. Huf, N. Platz Batista da Silva, I. Wiesinger et al., "Analysis of liver tumors using preoperative and intraoperative contrast-enhanced ultrasound (CEUS/IOCEUS) by radiologists in comparison to magnetic resonance imaging and histopathology," *RöFo—Fortschritte auf dem Gebiet der Röntgenstrahlen und der bildgebenden Verfahren*, vol. 189, no. 5, pp. 431–440, 2017.

[28] S. Gaiani, N. Celli, F. Piscaglia et al., "Usefulness of contrast-enhanced perfusional sonography in the assessment of hepatocellular carcinoma hypervascular at spiral computed tomography," *Journal of Hepatology*, vol. 41, no. 3, pp. 421–426, 2004.

[29] C. F. Dietrich, W. Kratzer, D. Strobe et al., "Assessment of metastatic liver disease in patients with primary extrahepatic tumors by contrast-enhanced sonography versus CT and MRI," *World Journal of Gastroenterology*, vol. 12, no. 11, pp. 1699–1705, 2006.

[30] S. H. Morin, A. K. Lim, J. F. Cobbold, and S. D. Taylor-Robinson, "Use of second generation contrast-enhanced ultrasound in the assessment of focal liver lesions," *World Journal of Gastroenterology*, vol. 13, no. 45, pp. 5963–5970, 2007.

[31] S. Tanaka and S. Arii, "Current status and perspective of antiangiogenic therapy for cancer: hepatocellular carcinoma," *International Journal of Clinical Oncology*, vol. 11, no. 2, pp. 82–89, 2006.

[32] O.P.a.T. Network, "HRSA/OPTN. Policy 3.6 organ distribution: allocation of livers," 2017, https://optn.transplant.hrsa.gov/media/1200/optn_policies.pdf.

[33] K. M. Elsayes, A. Z. Kielar, M. M. Agrons et al., "Liver imaging reporting and data system: an expert consensus statement," *Journal of Hepatocellular Carcinoma*, vol. 4, pp. 29–39, 2017.

[34] M. Loss, J. Schneider, W. Uller et al., "Intraoperative high resolution linear contrast enhanced ultrasound (IOUS) for detection of microvascularization of malignant liver lesions before surgery or radiofrequeny ablation," *Clinical Hemorheology and Microcirculation*, vol. 50, no. 1-2, pp. 65–77, 2012.

[35] K. Seitz, D. Strobel, T. Bernatik et al., "Contrast-Enhanced Ultrasound (CEUS) for the characterization of focal liver lesions—prospective comparison in clinical practice: CEUS vs. CT (DEGUM multicenter trial). Parts of this manuscript were presented at the Ultrasound Dreilandertreffen 2008, Davos," *Ultraschall in der Medizin—European Journal of Ultrasound*, vol. 30, no. 4, pp. 383–389, 2009.

[36] D. Strobel, K. Seitz, W. Blank et al., "Contrast-enhanced ultrasound for the characterization of focal liver lesions—diagnostic accuracy in clinical practice (DEGUM multicenter trial)," *Ultraschall in der Medizin—European Journal of Ultrasound*, vol. 29, no. 5, pp. 499–505, 2008.

[37] G. Torzilli, F. Procopio, F. Botea et al., "One-stage ultrasonographically guided hepatectomy for multiple bilobar colorectal metastases: a feasible and effective alternative to the 2-stage approach," *Surgery*, vol. 146, no. 1, pp. 60–71, 2009.

[38] J.-E. Kim, Y.-s. Kim, H. Rhim et al., "Outcomes of patients with hepatocellular carcinoma referred for percutaneous radiofrequency ablation at a tertiary center: analysis focused on the feasibility with the use of ultrasonography guidance,"

European Journal of Radiology, vol. 79, no. 2, pp. e80–e84, 2011.

[39] N. P. B. da Silva, L. P. Beyer, M. C. Hottenrott et al., "Efficiency of contrast enhanced ultrasound for immediate assessment of ablation status after intraoperative radiofrequency ablation of hepatic malignancies," *Clinical Hemorheology and Microcirculation*, vol. 66, no. 4, pp. 357–368, 2017.

[40] P. Wiggermann, I. Zuber-Jerger, Y. Zausig et al., "Contrast-enhanced ultrasound improves real-time imaging of ablation region during radiofrequency ablation: preliminary results," *Clinical Hemorheology and Microcirculation*, vol. 49, no. 1–4, pp. 43–54, 2011.

[41] Y. Minami, M. Kudo, T. Kawasaki, H. Chung, C. Ogawa, and H. Shiozaki, "Treatment of hepatocellular carcinoma with percutaneous radiofrequency ablation:usefulness of contrast harmonic sonography for lesions poorly defined with B-mode sonography," *American Journal of Roentgenology*, vol. 183, no. 1, pp. 153–156, 2004.

[42] L. Solbiati, T. Ierace, M. Tonolini, and L. Cova, "Guidance and monitoring of radiofrequency liver tumor ablation with contrast-enhanced ultrasound," *European Journal of Radiology*, vol. 51, pp. S19–S23, 2004.

Hindawi
Journal of Oncology
Volume 2019, Article ID 3580379, 7 pages
https://doi.org/10.1155/2019/3580379

Research Article

Angiographic Findings in Patients with Hepatocellular Carcinoma Previously Treated Using Proton Beam Therapy

Hiroaki Takahashi,[1,2] **Kensaku Mori**,[1] **Yuta Sekino**,[3] **Toshiyuki Okumura**,[3] **Takashi Hiyama**,[4] **Kuniaki Fukuda**,[5] **Naoyuki Hasegawa**,[5] **Masafumi Sakai**,[1] **Shunsuke Kikuchi**,[1] **Yohei Takei**,[1] **Takashi Iizumi**,[3] **Hideyuki Sakurai**,[3] **and Manabu Minami**[1]

[1] *University of Tsukuba Hospital, Department of Diagnostic and Interventional Radiology, Ibaraki, Japan*
[2] *Ibaraki Prefectural Central Hospital, Department of Diagnostic Radiology, Ibaraki, Japan*
[3] *University of Tsukuba Hospital, Department of Radiation Oncology and Proton Medical Research Center, Ibaraki, Japan*
[4] *National Cancer Center Hospital East, Department of Diagnostic Radiology, Chiba, Japan*
[5] *University of Tsukuba Hospital, Department of Gastroenterology, Ibaraki, Japan*

Correspondence should be addressed to Hiroaki Takahashi; h.1982.takahashi@gmail.com

Received 15 April 2019; Revised 8 June 2019; Accepted 18 June 2019; Published 4 July 2019

Guest Editor: Tiago Bilhim

Given the growing interest in using proton beam therapy (PBT) for hepatocellular carcinoma (HCC), it is possible that transarterial chemoembolization (TACE) could be used for selected patients who have previously undergone PBT. However, these cases can be technically challenging to treat and require appropriate preparation. Thus, we aimed to identify angiographic findings in this setting. We retrospectively identified 31 patients (28 men and 3 women, mean age: 69 years, range: 43–84 years) who underwent hepatic angiography plus TACE or transarterial infusion chemotherapy (TAI) for HCC that recurred after PBT (July 2007 to June 2018). We discovered four angiographic findings, which we speculate were related to the previous PBT. 18 patients experienced recurrence in the irradiated field, and 13 patients experienced recurrence outside the irradiated field. 29 patients underwent TACE and only 2 patients underwent TAI. The mean number of previous PBT treatments was 1.3 ± 0.6 (range: 1–4). The median interval from the earliest PBT treatment to hepatic angiography was 559 days (range: 34–5,383 days), and the median interval from the latest PBT treatment to hepatic angiography was 464 days (range: 34–5,383 days). Abnormal staining of the irradiated liver parenchyma was observed in 22 patients, which obscured the angiographic tumor staining in 4 patients. Development of a tortuous tumor feeder vessel was observed in 13 patients. Development of an extrahepatic collateral pathway was observed in 7 patients. Development of an arterioportal or arteriovenous shunt was observed in 4 patients. Based on these findings, we conclude that PBT was associated with various angiographic findings during subsequent transarterial chemotherapy for recurrent HCC, and familiarity with these findings will be important in developing appropriate treatment plans.

1. Introduction

Hepatocellular carcinoma (HCC) is the most common primary cancer of the liver [1]. According to the NCCN guidelines, there are numerous strategies for treating HCC, including resection, transplantation, radiofrequency ablation, transarterial chemoembolization (TACE), radiotherapy (RT), and systemic therapy using sorafenib or lenvatinib [2]. All patients with HCC should be evaluated for potential curative therapies, including resection and transplantation [2]. Locoregional therapy, including ablation, TACE, and RT, is indicated for patients who are not candidates for curative therapy or indicated as a bridge therapy for patients who are candidates for transplantation [2].

Recent reports have described favorable clinical outcomes after proton beam therapy (PBT) for HCC, based on a 5-year overall survival rate of 24–48% [3, 4] and a 5-year local control rate of approximately 80% [3, 5]. Among the external

beam RT modalities, PBT may be superior to X-ray therapy based on excellent dose localization to the therapeutic target [1]. Furthermore, given the good outcomes after PBT for HCC, some patients may be eligible for TACE treatment of intrahepatic HCC metastasis, while repeated PBT, TACE, or systemic therapy may be feasible in cases of local recurrence after PBT. Moreover, PBT is effective for patients with HCC who also have portal vein tumor thrombus (PVTT) [6], and the efficacy of combined therapy of TACE and RT for HCC with PVTT has been reported [7, 8]. Therefore, given the growing interest in using PBT for HCC, it is possible that TACE could be used for selected patients who have previously undergone PBT.

The purpose of our study is to evaluate the angiographic findings from patients with HCC previously treated using PBT. We classified abnormal PBT-related angiographic findings and analyzed these factors' frequency, onset timing, and influence on technical difficulty.

2. Materials and Methods

This study's retrospective protocol was approved by our institutional review board. The requirement for informed consent was waived.

2.1. Patient Acquisition. We identified patients who underwent transarterial chemotherapy for HCC that recurred after PBT between July 2007 and June 2018. 37 patients fulfilled the inclusion criteria: (1) diagnosis of HCC was confirmed pathologically or clinically according to the accepted guidelines [9], (2) PBT was performed for HCC before the transarterial chemotherapy, and (3) TACE or transarterial infusion chemotherapy (TAI) was performed. However, 6 patients were excluded because hepatic resection (n=3) or radiofrequency ablation (n=3) had been performed before the transarterial chemotherapy. Thus, the present study included 31 patients (28 men and 3 women, mean age: 69 years, range: 43–84 years) who underwent TACE or TAI after PBT. The patients' records were reviewed to determine the type of transarterial chemotherapy, the number of previous PBT treatments, and the interval between the angiography and the previous PBT treatment(s).

2.2. Hepatic Angiography and Transarterial Chemotherapy. All patients routinely underwent digital subtraction angiography of the celiac trunk and/or superior mesenteric artery, as well as cone-beam computed tomography (CBCT) of the proper or common hepatic artery. Angiography of an extrahepatic artery was performed if the HCC was not observed using hepatic arteriography or CBCT. The TACE and TAI treatments involve a mixture of 4–10 mL of iodized oil (Lipiodol; Andre Guerbet, Aulnay-sous-Bois, France) and the chemotherapeutic agent (cisplatin up to 50 mg or epirubicin up to 50 mg and mitomycin C up to 10 mg). Gelatin sponge particles (Gelpart; Nihonkayaku, Japan) were also used during the TACE treatment. Both procedures were performed using 3–4-Fr shepherd hook catheters and microcatheters with a tip diameter of 1.7–1.9 Fr.

2.3. PBT Procedure. Treatment planning for PBT was performed as previously reported [3, 10]. The irradiation protocols were generally classified according to tumor location: (1) a total dose of 77.0 GyE in 35 fractions for tumors located <2 cm from a gastrointestinal organ, (2) a total dose of 72.6 GyE in 22 fractions for tumors located <2 cm from the porta hepatis, or (3) a total dose of 66.0 GyE in 10 fractions for peripheral tumors >2 cm from both the GI tract and porta hepatis. The protocols were adjusted in some cases to avoid excessive irradiation of the adjacent organs. All patients received PBT on 5 days per week.

2.4. Image Analysis. We analyzed the PBT-related angiographic findings in each case (based on their relationship to the PBT irradiation field) and categorized them into four types: (1) abnormal staining of the irradiated liver parenchyma, (2) development of tortuous tumor feeder vessels, (3) development of an extrahepatic collateral pathway to the liver, and (4) development of arterioportal (AP) or arteriovenous (AV) shunts. Intrahepatic and extrahepatic shunts observed in the PBT irradiation field were both included in the study. The four PBT-related angiographic findings were counted for each case, although findings that were not clearly related to the PBT irradiation field were not considered. The HCCs targeted during TACE or TAI were classified according to whether they were in or outside the previous PBT irradiation field. All characteristics were judged based on mutual agreement between two radiologists (HT: 8 years of experience, KM: 25 years of experience).

2.5. Statistical Analysis. Differences in the distributions of the angiographic findings were evaluated using the chi-squared test. All data were analyzed using R software (version 3.3.2). Differences were considered statistically significant at P-values of <0.05.

3. Results

Table 1 shows the 31 patients' characteristics. 18 patients experienced recurrence in the irradiated field and 13 patients experienced recurrence outside the irradiated field. Most patients underwent TACE (29 patients) and only 2 patients underwent TAI. The average age was 68.5 ± 9.8 years (range: 43–84 years). The mean number of previous PBT treatments was 1.3 ± 0.6 (range: 1–4). The median interval from the earliest PBT treatment to the angiography was 559 days (range: 34–5,383 days), and the median interval from the latest PBT treatment was 464 days (range: 34–5,383 days).

The relationships between the PBT-related angiographic findings and the HCC characteristics are summarized in Table 2. In the PBT irradiation fields, we identified four angiographic findings: (1) abnormal staining of the irradiated liver parenchyma, (2) development of a tortuous tumor feeder vessel, (3) development of an extrahepatic collateral pathway, and (4) development of AP or AV shunts. Abnormal staining of the irradiated liver parenchyma was observed in 22 patients, and the angiographic tumor staining was obscured by the abnormal parenchymal staining in 4 patients (Figure 1). In all 4 patients, the CBCT could identify the

Table 1: Patient characteristics.

Total patients	31
Procedure	
TACE	29 (93.5)
TAI	2 (6.5)
Male sex	28 (90.3)
Age at TACE or TAI, years	68.5 ± 9.8 (43–84)
Child-Pugh	
A	28 (90.3)
B	3 (9.7)
C	0 (0)
Previous PBT treatments	
1	25 (80.6)
2	5 (16.1)
3	0 (0)
4	1 (3.2)
Diameter of HCC treated using PBT, mm	37.5 ± 26.6 (8-122)
Median follow-up time after earliest PBT, days	559 (34–5,383)
Median follow-up time after latest PBT, days	464 (34–5,383)
Targeted HCCs in TACE or TAI	
Irradiated HCCs targeted	18
Irradiated HCCs not targeted	13
PBT-related findings	
Abnormal staining of irradiated liver parenchyma	22 (71.0)
Development of tortuous tumor feeder	13 (41.9)
Development of extrahepatic collateral pathway	7 (22.6)
Development of AP/AV shunt	4 (12.9)

Data are reported as number (percentage), median (range) or mean ± standard deviation.
TACE: transarterial chemoembolization, TAI: transcatheter arterial infusion, PBT: proton beam therapy, HCC: hepatocellular carcinoma, AP/AV: arterio-portal or arteriovenous.

Table 2: The prevalence of PBT-related angiographic findings at the initial hepatic angiography according to HCC targeting.

Angiographic findings	Total (n=31)	Irradiated HCCs targeted during TACE or TAI (n=18)	Irradiated HCCs NOT targeted during TACE or TAI (n=13)	*P*
Abnormal staining of irradiated liver parenchyma	22 (71%)	14 (78%)	8 (62%)	0.326
Development of tortuous tumor feeder	13 (42%)	13 (72%)	0 (0%)	<0.001
Development of extrahepatic collateral pathway	7 (23%)	5 (28%)	2 (15%)	0.415
Development of AP/AV shunt	4 (13%)	4 (22%)	0 (0%)	0.069

The chi-squared test was used to calculate p-values. Irradiated HCCs refer to the TACE/TAI-targeted tumors being within the PBT irradiation field.
TACE: transarterial chemoembolization, TAI: transcatheter arterial infusion, PBT: proton beam therapy, HCC: hepatocellular carcinoma, AP/AV: arterio-portal or arteriovenous.

tumors and their feeding arteries. Among the 22 patients with abnormal parenchymal staining, the median interval from the earliest PBT treatment to the angiography was 629 days (range: 109–3,163 days) and the median time from the latest PBT treatment was 466.5 days (range: 109–3,163 days) (Table 3). Development of a tortuous tumor feeder vessel was observed in 13 patients, and in all cases the HCCs had recurred in the PBT irradiation field (Figures 1 and 2, Table 2). Among these 13 patients, the median interval from the earliest PBT treatment to the angiography was 911 days (range: 381–2,938 days), and the median interval from the latest PBT treatment was 559 days (range: 381–2,938 days) (Table 3). Development of an extrahepatic collateral pathway was observed in 7 patients, which involved the right inferior phrenic artery (6 patients) (Figure 3) or the omental artery (1 patient), and all collateral pathways fed the irradiated HCC or/and irradiated liver parenchyma. All the 7 patients only underwent a single PBT treatment,

Table 3: Relationship between PBT-related angiographic findings and the elapsed time after PBT treatment.

	All patients		Single PBT treatment (n=25)		Multiple PBT treatments (n=6)		
	Follow-up after first PBT, days	Follow-up after last PBT, days	N	Follow-up after PBT, days	N	Follow-up after first PBT, days	Follow-up after last PBT, days
Abnormal staining of irradiated liver parenchyma (n=22)	629 (109–3,163)	466.5 (109–3,163)	17	477 (109–3,163)	5	225 (464–720)	877 (1,274–1,950)
Development of tortuous tumor feeder (n=13)	911 (381–2,938)	559 (381–2,938)	9	699 (381–2,938)	4	466.5 (441–720)	1,284.5 (911–1,950)
Development of extrahepatic collateral pathway (n=7)	917 (418–31,63)	917 (418–3,163)	7	917 (418–3,163)	0	N/A	N/A
Development of AP/AV shunt (n=4)	588 (397–1,443)	588 (397–1,443)	4	588 (397–1,443)	0	N/A	N/A

Data are reported as median (range).
TACE: transarterial chemoembolization, TAI: transcatheter arterial infusion, PBT: proton beam therapy, HCC: hepatocellular carcinoma, AP/AV: arterio-portal or arteriovenous.

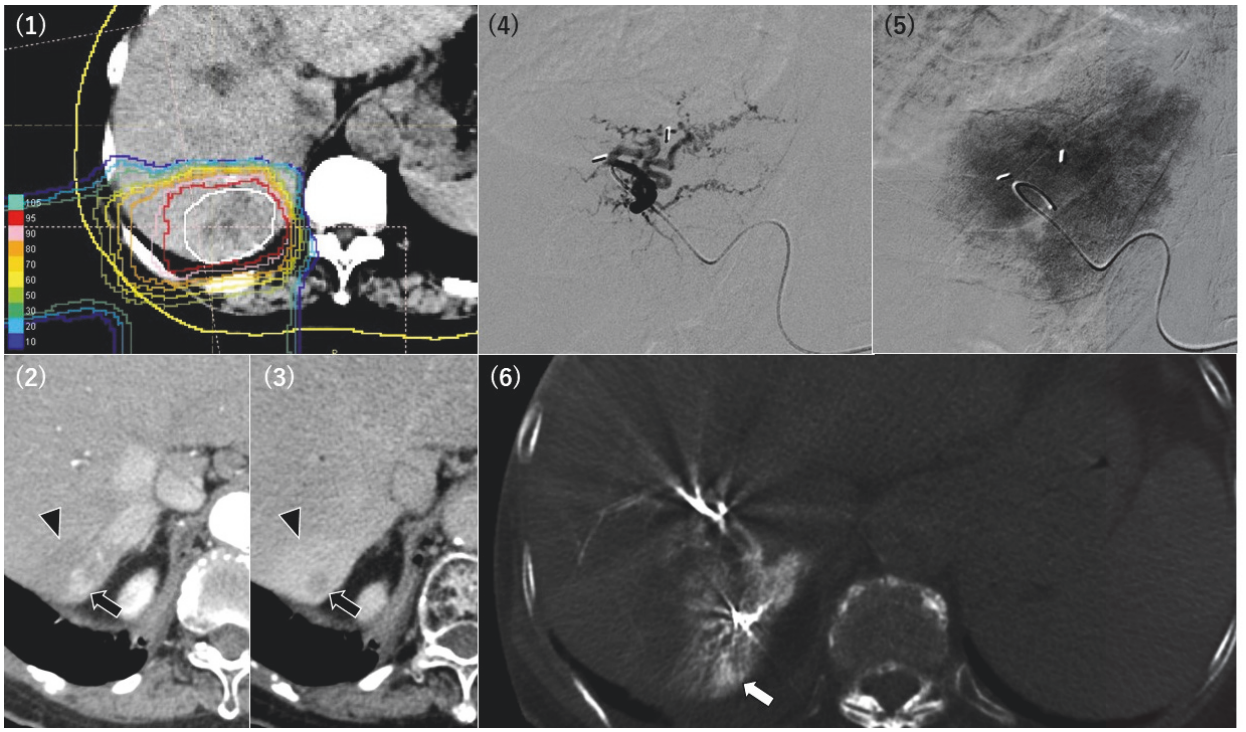

Figure 1: A 70-year-old woman underwent her first and second proton beam therapy (PBT) treatment for hepatocellular carcinoma (HCC) in S7 43 months (1) and 16 months (not shown) before the angiography, respectively. Dynamic computed tomography before the transarterial chemoembolization revealed local recurrence of the PBT-treated HCC, with early enhancement at the hepatic arterial phase and washout at the equilibrium phase (arrow). The surrounding irradiated parenchyma exhibited delayed enhancement (arrowhead) (2,3). A tortuous tumor feeder was noted during the procedure (4), although enhancement of the recurrent HCC was obscured by the abnormal staining of the irradiated liver parenchyma (5). Cone-beam computed tomography clearly showed that the selected artery fed the recurrent tumor (white arrow) (6).

and the median intervals from the PBT treatments to the angiography were both 917 days (range: 418–3,163 days) (Table 3). Development of AP or AV shunts was observed in 4 patients, which involved an AP shunt (2 patients), an AV shunt to the hepatic vein (1 patient), and an AV shunt to the pulmonary vein (1 patient) (Figure 3). All the 4 patients only underwent a single PBT treatment, and the median intervals from the earliest and latest PBT treatments to the angiography were both 588 days (range: 397–1,443 days) (Table 3).

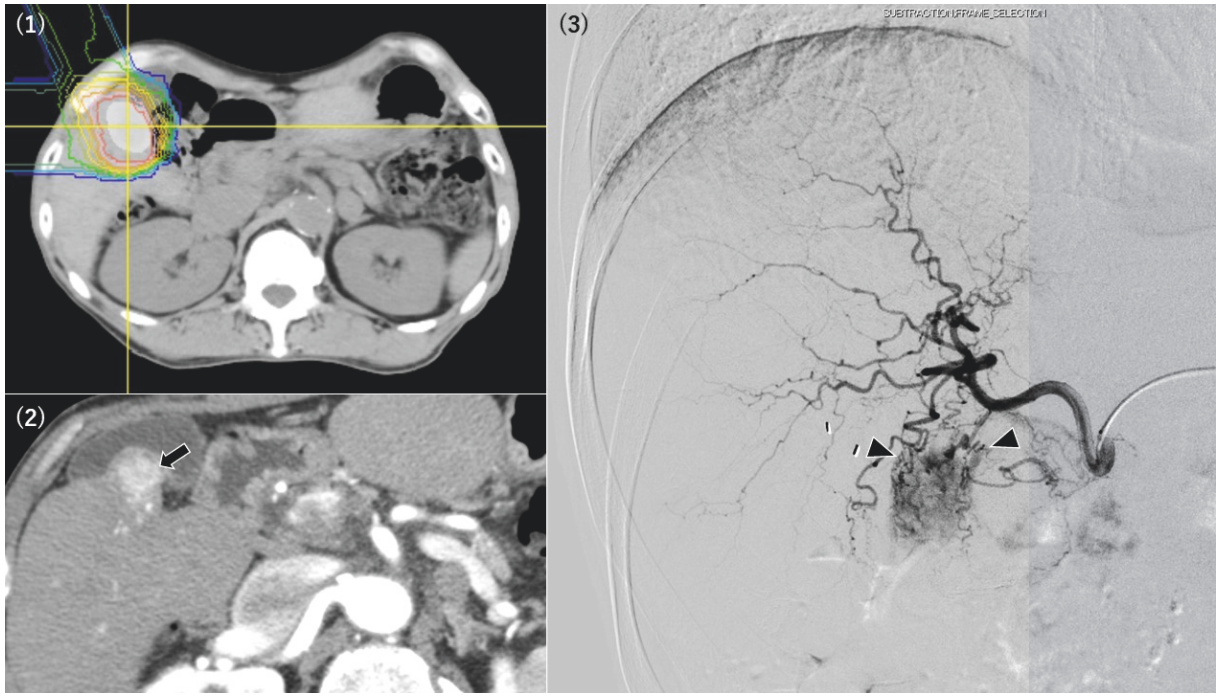

Figure 2: A 55-year-old man underwent proton beam therapy (PBT) for hepatocellular carcinoma (HCC) in S5 29 months before the angiography procedure (1). Dynamic computed tomography revealed local recurrence of the PBT-treated HCC (arrow) at the hepatic arterial phase (2). The recurrent HCC exhibited clear tumor staining during the procedure, with several tortuous vessels feeding the lesion (arrowhead), which made it technically difficult to perform selective catheterization (3).

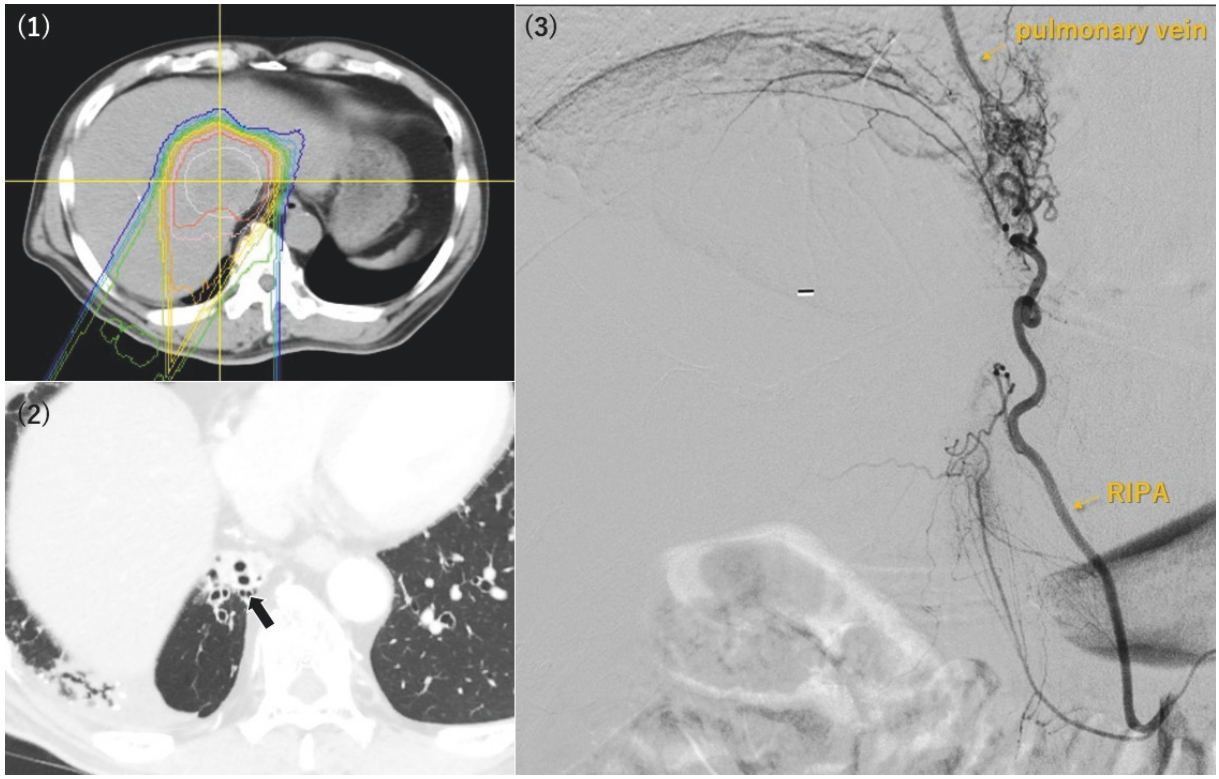

Figure 3: A 66-year-old man underwent his first proton beam therapy (PBT) treatment for hepatocellular carcinoma (HCC) in S8/1 48 months before the angiography procedure (1). Computed tomography revealed radiation-induced pneumonitis in the medial side of the right lower lung (2). An extrahepatic collateral pathway (via right inferior phrenic artery, RIPA) and an arteriovenous shunt for the pulmonary vein were noted during the procedure (3). The location of the arteriovenous shunt corresponded to the site of the radiation-induced pneumonitis.

4. Discussion

The present study identified four angiographic findings that were observed during transarterial chemotherapy, which was performed for HCCs that recurred after PBT. Interestingly, these four findings seem to appear at different intervals after the PBT. Among patients who underwent a single PBT treatment, the earliest finding was abnormal staining of the liver parenchyma (median interval: 477 days), the development of AV or AP shunts occurred later (median interval: 588 days), the development of tortuous feeder vessels occurred even later (median interval: 699 days), and the development of extrahepatic collateral pathways was the latest finding (median interval: 917 days).

Abnormal staining of irradiated liver parenchyma was the most common PBT-related angiographic finding in our study (22 out of 31 cases, 71%), which appeared as an area with dense and prolonged staining. Irradiated hepatic parenchyma after PBT can be observed as low-attenuation areas on noncontrast CT or areas with early and prolonged enhancement on dynamic CT [11]. During angiography-assisted CT, irradiated parenchyma exhibits decreased attenuation on CT arterial portography and increased attenuation on CT arteriography, which is the result of an arterial-predominant blood supply to the irradiated parenchyma (caused by radiation-induced venoocclusive disease) [11–13]. Prolonged enhancement of the irradiated parenchyma is related to contrast agent retention in the fibrous tissue [14]. Furthermore, a previous study demonstrated that the earliest disappearance of radiation-induced hepatic injury on imaging was observed 42 months after the PBT [11–13], which suggests that the irradiated parenchyma might have diminished arterial supply that persists long after the PBT treatment. These previously reported results agree with our findings, as we found early and prolonged abnormal staining of the irradiated parenchyma during angiography, which occurred at a relatively short interval after PBT. Moreover, we found that the irradiated liver parenchyma appeared as a pseudo-lesion in some cases and obscured the tumor staining in other cases. When the abnormal parenchymal staining obscured the tumor staining, CBCT was useful for detecting the tumor and its feeder vessels [15, 16].

Development of tortuous tumor feeder vessels was another PBT-related angiographic finding in the present study, and this characteristic was exclusively observed when the TACE or TAI targeted HCCs in the PBT irradiated field. Therefore, development of tortuous tumor feeder is likely to be associated with PBT-treated HCCs local recurrence. In addition, a previous report has described the local control rates of PBT-treated HCC (1-year: 98%, 3-year: 87%, 5-year: 81%) [3], which seems to be aligned with the mid-to-late development of tortuous tumor feeder vessels. According to our clinical experience, we speculate that selective catheterization becomes technically difficult when these vessels are present. Therefore, careful planning and attention are necessary when treating HCCs in the PBT irradiated field.

The present study revealed that extrahepatic collateral development could occur after PBT. In this context, previous reports have indicated that repeated transcatheter intervention could cause hepatic artery occlusion and the development of extrahepatic collaterals [17–19]. In our study, the right inferior phrenic artery or omental artery was developed to supply the irradiated liver parenchyma, without obstruction of any hepatic arteries. Thus, it is possible that extrahepatic collateral development after PBT might be the result of diaphragm or omentum irradiation. Furthermore, embolization of the adjacent organs should be avoided for patients who require embolization through an extrahepatic collateral feeder vessel [17]. Therefore, it is important to identify any extrahepatic collateral arteries using the pretreatment CT when planning TACE or TAI for patients with HCC that were previously treated using PBT.

Attention should also be paid to the development of AP and AV shunts, although it was less frequent than the other findings in patients with PBT-treated HCC. Nevertheless, TACE for HCC with AP or AV shunts can increase the risk of life-threatening complications, such as lung damage and pulmonary embolism [18, 20]. Lipiodol-related cerebral embolism is also known to occur in cases with artery-pulmonary vein shunts [21]. Thus, efflux of the embolic agent into the shunts should be avoided [20, 22], which might be achieved via prophylactic embolization of the AP shunt before TACE [22, 23]. Balloon-assisted TACE might also be useful when treating cases with AP shunts [22, 24].

The present study has several limitations. First, we did not evaluate angiographic findings before PBT, which raises the possibility that some of the angiographic findings were present before PBT (especially extrahepatic collateral pathways or AP and AV shunts). Second, the intervals between PBT and transarterial chemotherapy varied in each case. Thus, in order to accurately assess the onset period for each finding, it would be preferable to perform angiography at defined intervals after PBT. Third, the relationship between the radiation dose and angiographic findings could not be analyzed, as some of patients underwent multiple PBT treatments. Thus, well-designed prospective studies are needed to address these limitations and validate our findings.

5. Conclusions

In conclusion, PBT was associated with various angiographic findings that were observed during transarterial chemotherapy for HCC recurrence. Irradiated liver parenchyma appeared as a pseudo-lesion during angiography or obscured the tumor staining in some cases. In addition, tortuous tumor feeder vessels, extrahepatic collateral pathways, and AV and AP shunts were also observed. Familiarity with these angiographic findings may help radiologists develop appropriate treatment plans for patients with PBT-treated HCC recurrence.

Abbreviations

RT: Radiotherapy
PBT: Proton beam therapy
TACE: Transarterial chemoembolization
TAI: Transarterial infusion chemotherapy
AP: Arterioportal
AV: Arteriovenous

CBCT: Cone-beam CT
HCC: Hepatocellular carcinoma.

Data Availability

The data used to support the findings of this study are available from the corresponding author upon request.

Disclosure

This work was done at University of Tsukuba Hospital, Department of Diagnostic and Interventional Radiology, 1-1-1, Tennoudai, Tsukuba, Ibaraki, 305-8575, Japan.

Conflicts of Interest

The authors declare that there is no conflict of interest regarding the publication of this paper.

References

[1] G. S. Yoo, J. I. Yu, and H. C. Park, "Proton therapy for hepatocellular carcinoma: Current knowledges and future perspectives," *World Journal of Gastroenterology*, vol. 24, no. 28, pp. 3090–3100, 2018.

[2] A. B. Benson, T. A. Abrams, E. Ben-Josef et al., "NCCN clinical practice guidelines in oncology: hepatobiliary cancers, Version 1.2019," *Journal of the National Comprehensive Cancer Network*, 2019.

[3] M. Mizumoto, T. Okumura, T. Hashimoto et al., "Proton beam therapy for hepatocellular carcinoma: a comparison of three treatment protocols," *International Journal of Radiation Oncology • Biology • Physics*, vol. 81, no. 4, pp. 1039–1045, 2011.

[4] T. Chiba, K. Tokuuye, Y. Matsuzaki et al., "Proton beam therapy for hepatocellular carcinoma: a retrospective review of 162 patients," *Clinical Cancer Research*, vol. 11, no. 10, pp. 3799–3805, 2005.

[5] H. Sakurai, H. Ishikawa, and T. Okumura, "Proton beam therapy in Japan: current and future status," *Japanese Journal of Clinical Oncology*, vol. 46, no. 10, pp. 885–892, 2016.

[6] S. Sugahara, H. Nakayama, K. Fukuda et al., "Proton-beam therapy for hepatocellular carcinoma associated with portal vein tumor thrombosis," *Strahlentherapie und Onkologie*, vol. 185, no. 12, pp. 782–788, 2009.

[7] B. G. Jun, S. G. Kim, Y. D. Kim et al., "Combined therapy of transarterial chemoembolization and stereotactic body radiation therapy versus transarterial chemoembolization for </=5cm hepatocellular carcinoma: propensity score matching analysis," *PLoS One*, vol. 13, no. 10, Article ID e0206381, 2018.

[8] X. L. Li, W. X. Guo, X. D. Hong et al., "Efficacy of the treatment of transarterial chemoembolization combined with radiotherapy for hepatocellular carcinoma with portal vein tumor thrombus: a propensity score analysis," *Hepatology Research*, vol. 46, no. 11, pp. 1088–1098, 2016.

[9] European Association for the Study of the Liver and European Organisation for Research and Treatment of Cancer, "EASL-EORTC clinical practice guidelines: management of hepatocellular carcinoma," *Journal of Hepatology*, vol. 56, no. 4, pp. 908–943, 2012.

[10] K. Fukuda, T. Okumura, M. Abei et al., "Long-term outcomes of proton beam therapy in patients with previously untreated hepatocellular carcinoma," *Cancer Science*, vol. 108, no. 3, pp. 497–503, 2017.

[11] T. Ahmadi, Y. Itai, H. Onaya, H. Yoshioka, T. Okumura, and Y. Akine, "CT evaluation of hepatic injury following proton beam irradiation: appearance, enhancement, and 3D size reduction pattern," *Journal of Computer Assisted Tomography*, vol. 23, no. 5, pp. 655–663, 1999.

[12] G. B. Reed Jr. and A. J. Cox Jr., "The human liver after radiation injury. A form of veno-occlusive disease," *The American Journal of Pathology*, vol. 48, no. 4, pp. 597–611, 1966.

[13] L. F. Fajardo and T. V. Colby, "Pathogenesis of veno-occlusive liver disease after radiation," *Archives of Pathology & Laboratory Medicine*, vol. 104, no. 11, pp. 584–588, 1980.

[14] S. Takamatsu, K. Kozaka, S. Kobayashi et al., "Pathology and images of radiation-induced hepatitis: a review article," *Japanese Journal of Radiology*, vol. 36, no. 4, pp. 241–256, 2018.

[15] S. Miyayama, M. Yamashiro, Y. Hattori et al., "Efficacy of cone-beam computed tomography during transcatheter arterial chemoembolization for hepatocellular carcinoma," *Japanese Journal of Radiology*, vol. 29, no. 6, pp. 371–377, 2011.

[16] S. Miyayama, M. Yamashiro, M. Okuda et al., "Usefulness of cone-beam computed tomography during ultraselective transcatheter arterial chemoembolization for small hepatocellular carcinomas that cannot be demonstrated on angiography," *CardioVascular and Interventional Radiology*, vol. 32, no. 2, pp. 255–264, 2009.

[17] C. S. Soo, V. P. Chuang, S. Wallace, C. Charnsangavej, and H. Carrasco, "Treatment of hepatic neoplasm through extrahepatic collaterals," *Radiology*, vol. 147, no. 1, pp. 45–49, 1983.

[18] J. Xia, Z. Ren, S. Ye et al., "Study of severe and rare complications of transarterial chemoembolization (TACE) for liver cancer," *European Journal of Radiology*, vol. 59, no. 3, pp. 407–412, 2006.

[19] C. Charnsangavej, V. P. Chuang, S. Wallace, C. S. Soo, and T. Bowers, "Angiographic classification of hepatic arterial collaterals.," *Radiology*, vol. 144, no. 3, pp. 485–494, 1982.

[20] H. Ngan and W. Peh, "Arteriovenous shunting in hepatocellular carcinoma: Its prevalence and clinical significance," *Clinical Radiology*, vol. 52, no. 1, pp. 36–40, 1997.

[21] T. Karapanayiotides, J. Goulis, A. Theodorou, A. Anastasiou, G. Georgiadis, and G. Ilonidis, "Lipiodol brain embolism during hepatic transcatheter arterial chemoembolization," *Journal of Neurology*, vol. 256, no. 7, pp. 1171–1173, 2009.

[22] T. Senokuchi, Y. Baba, S. Hayashi, and M. Nakajo, "Embolization of hepatic arteriovenous shunt with absolute ethanol in a patient with hepatocellular carcinoma," *CardioVascular and Interventional Radiology*, vol. 34, no. Supplement 2, pp. S154–S156, 2011.

[23] H. Wu, W. Zhao, J. Zhang, J. Han, and S. Liu, "Clinical characteristics of hepatic Arterioportal shunts associated with hepatocellular carcinoma," *BMC Gastroenterology*, vol. 18, no. 1, p. 174, 2018.

[24] S. Hoshiai, K. Mori, T. Ishiguro et al., "Balloon-assisted chemoembolization using a micro-balloon catheter alongside a microcatheter for a hepatocellular carcinoma with a prominent arterioportal shunt: a case report," *CardioVascular and Interventional Radiology*, vol. 40, no. 4, pp. 625–628, 2017.